DETERMINISTIC MODELING OF BROMIDE TRACER TRANSPORT DURING THE TRACER/TIME-LAPSE RADAR IMAGING TEST AT THE BOISE HYDROGEOPHYSICAL RESEARCH SITE IN AUGUST, 20011

by

Gregory Nelson

A thesis

submitted in partial fulfillment

of the requirements for the degree of

Master of Science in Geophysics

Boise State University

December, 2007

The thesis presented by Gregory Nelson entitled "Deterministic Modeling of Bromide Tracer Transport During the Tracer/Time-Lapse Radar Imaging Test at the Boise Hydrogeophysical Research Site in August, 2001" is hereby approved:

Warren Barrash Advisor	Date
Tom Clemo Committee Member	Date
Shawn G. Benner Committee Member	Date
John R. Pelton Graduate Dean	Date

ACKNOWLEDGMENTS

Nothing I have accomplished could have been possible without the love and support of my family. My parents have always been encouraging and allowed me to explore anything that I'm interested in. The love of my life, Heather, has been with me through all of the time I've spent at Boise State. Through it all she even feigned interest and understanding. This work could not have been accomplished without the support of Heather and the rest of my family.

This project could not have been accomplished without the enthusiasm and support of Warren Barrash, my Advisor. Warren has a knack for pulling the best work out of you. The same can be said of both of my other committee members: Tom Clemo and Shawn Benner. Ideas, thoughts, and reviews made by Tim Johnson, Dave Hyndman, and Bwalya Balama were very helpful during the progression of this work. A special thanks must go out to all those who actualized the TTLT in August of 2001.

Work presented here was supported by EPA Grant X-97008501-0. Cooperative arrangements with the Idaho Transportation Department, the U.S. Bureau of Reclamation, and Ada County allow development and use of the BHRS.

This material is based upon work supported by the National Science Foundation under Grant No. 0321233 (Beowulf Cluster).

ABSTRACT

Contaminant transport and remediation strategies are based on knowledge of site specific parameters and states (e.g., hydraulic conductivity, porosity, hydraulic gradient, plume density). Often little is known in detail about these parameters or states and their spatial distributions. This uncertainty can introduce inaccuracies and errors in transport predictions. This thesis is a deterministic approach to reducing this uncertainty for transport of bromide, a conservative tracer, in a heterogeneous unconfined fluvial aquifer in a natural environment through a series of numerical simulations of the tracer test conducted at the Boise Hydrogeophysical Research Site (BHRS) in 2001. In particular, the investigation progresses from initial one-dimensional analytical modeling to three-dimensional numerical modeling that examines the influences of boundary conditions, heterogeneity (including consideration of hydraulic conductivity, porosity, and dispersivity), plume density effects, and evapotranspiration on bromide breakthrough behavior that was measured at multiple levels in a sampling well ~4 m down-gradient from the tracer injection well.

Analytical modeling provided initial estimates of average hydraulic conductivity and longitudinal dispersivity. Two approaches were used to numerically model the flow during the tracer test: (1) uniform gradient (simple boundaries) approach; and (2) complex boundaries approach. The uniform gradient approach included boundaries that defined a uniform regional hydraulic gradient through the BHRS. The complex

boundaries approach included the river as a groundwater divide, and general head and constant head boundaries calculated from a larger flow model of the gravel bar upon which the BHRS lies. Irrespective of which boundary flow approach was used, the same transport approach was used. The software codes used for this modeling are MODFLOW 2000 for groundwater flow, SEAWAT 2000 for including density effects in the flow model, and MT3DMS for solute transport. The goodness of fit for a given set of model conditions was evaluated by comparing visual matches of model and observed head changes in well B3 (injection well) and in the C wells (a ring of six wells ~5 m outside the injection and pumping wells), and matches of model and observed breakthrough summary statistics such as Time to Peak and Peak Concentration.

Findings from this modeling progression include: (1) improvements to fitting the breakthrough data resulted from including boundary conditions such as adding leakage through the bed of the Boise River which is given specified heads at a groundwater divide boundary, and also using general head boundaries on other sides of the gravel bar; (2) although the BHRS has a noticeable evapotranspiration signal (~2.5 cm daily fluctuation in the water table), simulations with and without evapotranspiration show that evapotranspiration is not important for transport during this tracer test; (3) plume density effects were expected to be significant for the conditions of this tracer test based on calculations of Barth et al.'s (2001) dimensionless α_2 parameter for the BHRS and for the tracer test, and this was confirmed by comparison of simulations with and without variable density flow; (4) using homogeneous hydrogeologic properties throughout the BHRS is not sufficient to match observed tracer behavior measured during the tracer test;

(5) heterogeneity (e.g. layers; contact geometry; distinct zonation within layering; variable distributions of hydraulic conductivity, porosity, or hydraulic conductivity and porosity) significantly affects simulated transport behavior and as more known heterogeneity is included, simulated breakthrough behavior matches observed behavior more closely; (6) by defining well bores in the simulations, more water flux from a sand channel in the upper part of the system and less water flux from the direction of the tracer plume is observed by later tracer breakthrough in the sampling well; (7) as expected, larger dispersivity results in more spreading of the tracer plume; (8) a uniform increase in effective porosity will cause later breakthrough; and (9) increasing vertical hydraulic conductivity anisotropy does not improve matches between simulated and observed breakthrough.

By accounting for more complexity (heterogeneity) in the hydrogeologic properties of the BHRS, improvements are made to matching observed tracer breakthrough with simulated breakthrough. This thesis is a first pass at hydrologic modeling upon which more follow-up or further development will be conducted.

TABLE OF CONTENTS

LIST OF FIGURES

LIST OF TABLES

1 INTRODUCTION

Contaminant transport predictions and remediation strategies are determined based upon knowledge of magnitude and distribution of parameters and states (e.g., hydraulic conductivity, porosity, hydraulic gradient, plume density). Often little is known in detail about these parameters and their spatial distributions. This uncertainty introduces inaccuracies and errors in transport predictions. This thesis follows a deterministic approach to reducing this uncertainty for transport of bromide, a conservative tracer, in a heterogeneous coarse-grained fluvial aquifer through a series of numerical simulations of a tracer test conducted at the Boise Hydrogeophysical Research Site (BHRS) in 2001.

Over the past several decades many tracer tests have been conducted to examine groundwater flow and solute transport theories and their applicability to contaminant transport in real aquifers. In particular, a number of well-studied tracer tests have been conducted in unconsolidated sedimentary aquifers, including (a) natural gradient tests in the relatively homogeneous systems at Borden (Mackay et al., 1986; Freyberg, 1986; Roberts et al., 1986; Curtis et al., 1986; Sudicky, 1986) and Cape Cod (LeBlanc et al., 1991; Garabedian et al., 1991; Hess et al., 1992), and in the highly heterogeneous aquifer system of the Macrodispersion Experiment – MADE – at Columbus, Mississippi (Boggs et al., 1992; Adams and Gelhar, 1992; Rehfeldt et al., 1992; and Boggs and Adams,

1992), and (b) forced gradient tests such as at Mobile (Molz et al., 1986) and Georgetown (Mas-Pla et al., 1992).

The Borden natural gradient tracer test's approach and a preliminary analysis of the plume path were presented by Mackay et al. (1986) who also described how horizontal spreading was more pronounced then vertical spreading. Freyberg (1986) computed zeroth-, first-, and second-order spatial moments for the conservative tracers (chloride and bromide) and used these to show applicability of stochastic transport theory (Dagan, 1984) until a change in behavior occurs due to large-scale heterogeneity after nearly three years into the experiment. The five organic tracers used in the Borden experiment were analyzed by Roberts et al. (1986) and were modeled including classical advection, dispersion, sorption (retardation), and transformation solute transport and fate behavior for the two years prior to the change in behavior due to the large-scale heterogeneity effect. Curtis et al. (1986) conducted laboratory experiments to show that the reactive and retarded plumes could be described using the linear, reversible, equilibrium sorption model. Sudicky (1986) used site hydraulic conductivity geostatistics to predict the dispersion observed in the Borden tracer test which was also consistent with stochastic transport theory (Gelhar and Axness, 1983; Dagan, 1984).

LeBlanc et al. (1991) described the tracer test in the stratified sand and gravel aquifer at Cape Cod in a manner similar to that of Mackay et al. (1986) for the Borden test, and they conducted the initial analysis of the plume movement. LeBlanc et al. (1991) noted the vertical displacement of the plume in the early portion of the tracer test due to recharge and density-induced sinking. The bromide tracer of the Cape Cod

experiment appeared to act conservatively compared to the other tracers. Garabedian et al. (1991) calculated the spatial moments of the Cape Cod tracers in much the same way as Freyberg (1986) did for the Borden experiment. Using hydraulic conductvity geostatistics, Hess et al. (1992) accurately predicted the observed macrodispersivities of the Cape Cod test.

Both the Borden and the Cape Cod tracer tests were benchmark experiments in that they showed that stochastic transport theories could be used to describe solute transport in relatively homogeneous real aquifers. They showed that a plume could be characterized and described using spatial moments. These tests verified many common assumptions used in modeling groundwater flow and contaminant fate and transport.

The Cape Cod and Borden tests were conducted at relatively homogeneous sites, but the fluvial hydrogeologic system at the MADE site is highly heterogeneous. Boggs et al. (1992) describe and give a brief overview of this test which was designed to verify that the same stochastic transport theories applied to the Borden and Cape Cod tests could apply to highly heterogeneous sites. The MADE test showed that plumes are very sensitive to heterogeneities in hydraulic conductivity and in flow velocities. Adams and Gelhar (1992) calculated spatial moments on the MADE plumes which showed systematic mass loss. Like Sudicky (1986) and Hess et al. (1992), Rehfeldt et al. (1992) used hydraulic conductivity geostatistics to estimate dispersivities. Boggs and Adams (1992) showed that the mass losses observed in the MADE experiment were most likely due to adsorption and sampling bias towards high hydraulic conductivity zones, but that

if these issues could be accounted for, the same fundamental flow and transport principles and theories could be applied to highly heterogeneous sites.

Molz et al. (1986) describe the forced gradient tracer test conducted at Mobile, Alabama in a hydrogeologic system of fluvial terrace deposits consisting of layered sands, clayey sands, sandy clays, and clays. They showed that the tracer test could be accurately simulated without knowledge of the test results and without calibration. Another forced gradient test was conducted by Mas-Pla et al. (1992) who used one-dimensional (1D) and two-dimensional (2D) flow and transport models that were developed based on tracer sampling from one sampling well. Mas-Pla et al. (1992) found that the 1D and 2D models would inadequately predict breakthrough at a second sampling well and that three-dimensional (3D) models would be needed.

Many of these tests were subsequently modeled to predict tracer (i.e., contaminant) breakthrough. Brusseau and Srivastava (1997) were able to numerically model the Borden test. Modeling by Zhang et al. (1998) showed the importance of heterogeneity and of variable density flow on transport at Cape Cod. Barlebo et al. (2004) were able to show that even in the highly heterogeneous MADE site, classical advection/dispersion processes can explain tracer transport. Molz et al. (1986), Huyakorn et al. (1986), Güven et al. (1992), and Peng et al. (2000) all were able to successfully predict tracer breakthrough at the Mobile site; and specifically Peng et al. (2000) show that “industry available” numerical modeling codes such as MODFLOW and MT3DMS can be used to predict tracer breakthrough. Mas-Pla et al. (1992) found that they could match breakthrough from one of two observation wells by using a layer-cake

hydrogeology in their simulations, but they were unable to match breakthrough in both observation wells using 2D layer-cake modeling indicating that a 3D characterization of the aquifer heterogeneity is needed to match observed breakthrough in both observation wells.

The modeling described above shows varied results with most tests being adequately modeled for the tracer plume path and dispersion – indicating the capability of these models to match elements of site heterogeneity significant to transport. Ptak et al. (2004) emphasize the importance of heterogeneity on tracer transport behavior, even in aquifers considered to be "homogeneous." Indeed, in a two-well tracer test somewhat similar to the one of this study, Molz et al. (1986), Huyakorn et al. (1986), and Mas-Pla et al. (1992) suggest that a 3D characterization of hydraulic conductivity is needed to match breakthrough in an observation well between the injection and pumping wells. Kapoor and Gelhar (1994) also suggest that a 3D characterization of hydraulic conductivity is needed to model transport behavior in many natural aquifers.

Hydraulic conductivity to a large degree controls flow and transport of tracers/contaminants in the subsurface as indicated above. Heterogeneity of hydraulic conductivity will therefore largely control plume migration in natural gradient tests or natural systems. A highly heterogeneous site, like the MADE site, lends itself to having preferential flow paths where most transport occurs. A major obstacle in any contaminant transport problem is determining the spatial distribution and heterogeneous nature of hydraulic conductivity (Sudicky and Huyakorn, 1991). Because transport is largely dependent upon this heterogeneity, the degree to which simulations in this study

predict tracer breakthrough is also a measure of how well the simulations capture the heterogeneity and heterogeneity scale of the tracer test.

In summary, previously conducted tracer tests have shown that models based on the advection-dispersion equations can adequately describe conservative tracer migration. Furthermore they have shown that horizontal plume spreading is greater than lateral or vertical spreading, and that density-induced sinking can be significant in some cases. Lastly, better characterization of the 3D distribution of hydrologic parameters (particularly hydraulic conductivity) will result in better simulation of observed behavior with a given numerical model, all else being equal.

This thesis is a first pass at estimating the 3D distribution of hydraulic conductivity at the BHRS from forward modeling of head, injection/pumping, and tracer data. Results from this work can be used as the foundation for future modeling, perhaps with stochastic or inverse methods and perhaps including use of geophysical data such as time-lapse data from the tracer/time-lapse imaging test (TTLT) of 2001, to more fully characterize the 3D distribution of hydraulic conductivity at the BHRS.

1.1 Goals and Objectives

The goal of this thesis is to develop a numerical flow and transport model of the BHRS and the bromide tracer test actualized there in 2001. Recognizing that the aquifer at the BHRS is heterogeneous (e.g., Barrash and Clemo, 2002) and is influenced by hydrologic stresses and boundary conditions, objectives of this thesis are to: (1) progressively examine parameter distributions and hydrologic boundaries and stresses to

determine which hydrogeologic properties of the BHRS are significant in modeling transport of the TTLT, and quantify these improvements through transport summary statistics (e.g., Scheibe and Chien, 2003). Doing this will provide the framework and starting point for future work in modeling of groundwater flow and solute transport at the BHRS.

Simulations were run to determine which hydrogeologic properties – and spatial distribution of the properties – of the BHRS are significant in modeling the bromide tracer transport of the TTLT. To quantify improvements to the modeling, metrics were developed comparing observations taken during the TTLT and calculations made from simulations. The simulations were developed progressively from a simple homogeneous model, to multilayer, patchy models. This thesis demonstrates how more detail affects simulations and can improve the fit between observed and simulated measurements of changes in head and in breakthrough behavior.

2 TRACER/TIME-LAPSE RADAR IMAGING TEST

In this chapter I briefly describe the hydrogeologic setting and design features of the BHRS that are relevant to the TTLT. Then I describe the TTLT with enough detail to provide the basis for model development and testing which is the main focus of this thesis.

2.1 Boise Hydrogeophysical Research Site

The BHRS lies alongside the Boise River ~15 km southeast of Boise, Idaho and ~5 km downstream from Lucky Peak Dam. The BHRS is developed in a cobble, gravel, and sand fluvial unconfined aquifer in a gravel bar alongside the Boise River. This gravel bar is in the bottomland of the Boise River which includes the river bed and flood plain (see Figure 1); the bottomland is the most recent feature developed in a series of Quaternary to Recent depositional and erosional events marked by a succession of terraces incised into the Boise River Valley by the Boise River. The Boise River Valley lies in the Western Snake River Plain.

All of these terraces include pebble-to-cobble gravel deposits with a coarse sand matrix (Othberg, 1994); and the terrace deposits are all similar to the deposits of the BHRS (Reboulet and Barrash, 1999; Reboulet and Barrash 2000; Reboulet, 2003; Reboulet and Barrash 2003; Barrash and Reboulet, 2004; Othberg, 1994). Figure 1 shows a cross section (modified from Othberg, 1994) of the Boise River Valley near the

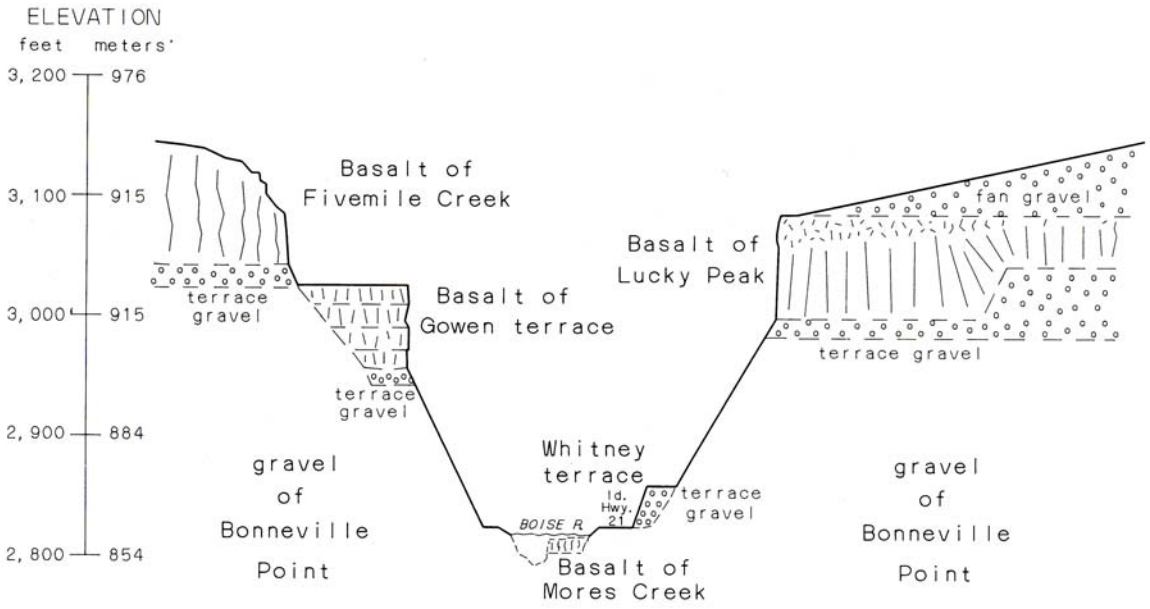

Figure 1: Cross section of the Boise River Valley near Lucky Peak Dam (near the BHRS). Modified from Othberg (1994). The BHRS is developed in a gravel bar of the bottomland of the Boise River Valley. The bottomland includes the riverbed and flood plain.

BHRS and Lucky Peak Dam. The relative terrace age generally decreases with decreasing elevation as the ancestral Boise River incised to a given level, created a terrace, and then incised to the next terrace level.

Figure 2 is a photomap of the BHRS which shows the location of the 18 wells at the site: five boundary wells (X wells) and two concentric circles, each of six wells (C and B wells), around well A1. It is difficult to determine sedimentary facies directly from drill or core samples in subsurface coarse unconsolidated fluvial deposits similar to those of the BHRS. However, analysis of porosity logs (Barrash and Clemo, 2000; 2002), geophysical measurements (Peretti et al., 1999; Peterson et al., 1999; Knoll and Clement, 1999; Clement et al., 1999; Clement et al., 2006), and grain size distributions of core taken from the 18 wells at the BHRS (Reboulet, 2003; Barrash and Reboulet, 2004)

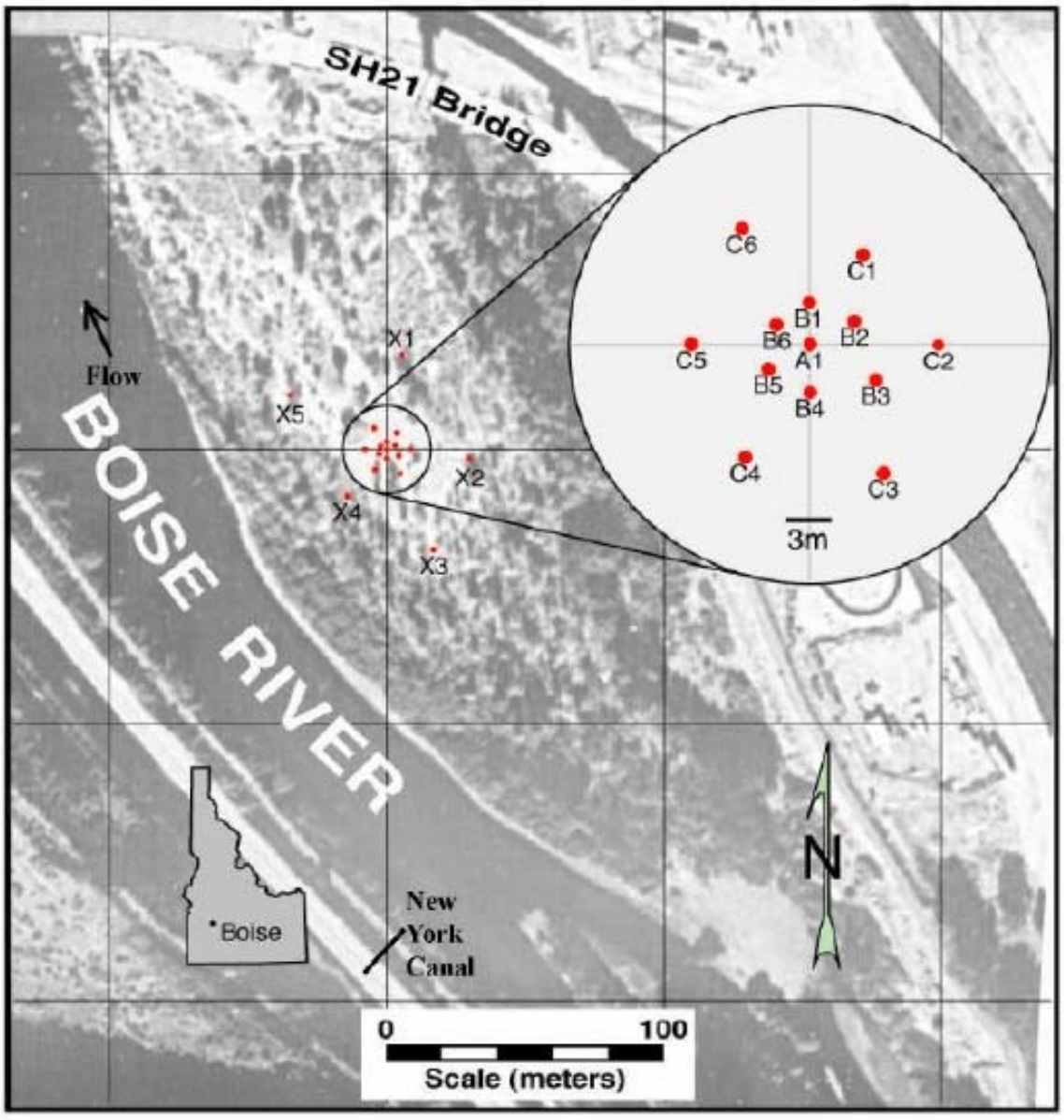

Figure 2: Photomap of the Boise Hydrogeophysical Research Site (BHRS). The BHRS is located ~15 km southeast of downtown Boise, Idaho and ~5 km downstream from the Lucky Peak dam. The locations of the 18 wells at the BHRS are shown in the inset (modified from Barrash and Clemo, 2002).

resulted in the identification of five stratigraphic/hydrostratigraphic units that are traceable across the

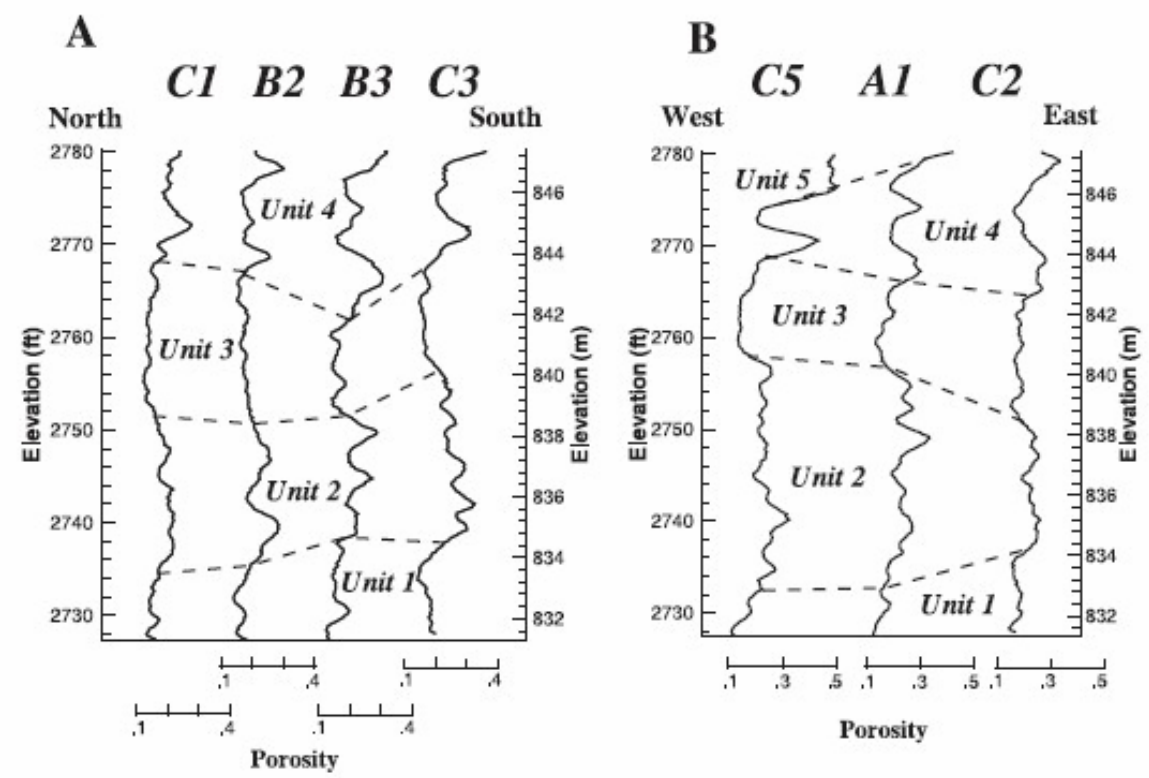

Figure 3: Cross sections showing stratigraphy at the BHRS (see Figure 2 for locations of the wells). The units were determined through porosity and log analysis, grain size distribution analysis, and geophysical measurements (after Barrash and Clemo 2000, 2002).

central region of the BHRS. These five units can be seen in porosity log cross sections from the BHRS (Figure 3). In particular, Unit 5 is a high porosity sand channel that thickens toward the Boise River and pinches out in the middle of the well field, and Units 1 through 4 are conglomeratic with gravel and cobble framework grains, and sand to pebble matrix in the interstices between the framework grains. Of these four conglomeratic units, Units 2 and 4 have relatively higher and more variable porosity while Units 1 and 3 have relatively lower and less variable porosity. Table 1 lists the porosity statistics from Barrash and Clemo (2002) for the five units.

Table 1: Porosity statistics for the hydrogeologic units at the BHRS (Barrash and Clemo, 2002).

	Porosity (mean)	Porosity (variance)	Number of values
Unit 5	0.452	0.00302	118
Unit 4	0.224	0.00251	853
Unit 3	0.172	0.00059	716
Unit 2	0.240	0.00142	1161
Unit 1	0.180	0.00050	476

2.2 TTLT Objectives

The objectives of the TTLT were to (Barrash et al., 2002):

1. Conduct time-lapse radar tomography during a controlled tracer test to demonstrate the ability of this method to detect the presence of, and also temporal and spatial variations in, a tracer plume through cross-sectional and longitudinal planes of imaging;

2. Quantify attenuation magnitudes and differences in terms of concentration magnitudes and differences at a central location along the path of the plume where a well that is in line with two of the time-lapse radar imaging planes will be instrumented for multilevel sampling for tracer concentration;

3. Assess issues of resolution and uncertainty associated with the time needed for collecting the tomographic data compared with the flow rate of plume passage through the imaging plane;

4. Identify operational and equipment features that can be modified to improve efficiency of field data collection and subsequent image generation and interpretation; and

5. Provide a data set for hydrologic modeling to estimate the 3D distribution of permeability from head, injection/pumping, tracer, and time-lapse geophysical data.

This thesis deals primarily with the fifth objective: using the tracer test to estimate 3D distributions of hydraulic conductivity in the central well field of the BHRS.

2.3 TTLT: Design and Chronology

Details of the TTLT are given in reports by Barrash et al. (2002) and Hausrath et al. (2002); test design and chronology features relevant to modeling groundwater flow and tracer transport during the TTLT are given here. The TTLT was designed largely as a natural gradient test between a pulse (or slug) injection well (B3) and a highly discretized monitoring well (A1) approximately 4 m from B3. The TTLT also included extraction at a low pumping rate (~5 gpm) through well B6 (about 3 m from A1, Figure 2) to: (a) assure plume passage through observation well A1; (b) remove tracer from the system and support quantification of tracer recovery; and (c) minimize the influence of pumping on the test between wells B3 and A1.

Two tracers believed to be chemically conservative (potassium bromide [a salt] and sodium fluoroscein or uranine [an organic dye]) were injected simultaneously so the test could examine tracer evolution with chemical sampling and with radar imaging in a naturally heterogeneous medium, and so the two tracers could provide checks on the conservative behavior expectation (Käss, 1998). It is believed that the bromide tracer did behave conservatively, and that it provided a successful target of varying electrical conductivity for time-lapse radar tomographic imaging (e.g., Goldstein et al., 2003; Johnson et al., 2005; Johnson et al., 2007) as the plume moved through the system.

However, the uranine exhibited significant reactive behavior (Hausrath et al., 2002) and will not be considered in the test modeling here.

Approximately 1000 gal (3785 L) of water with the tracers in solution were injected as a discrete "slug" over a short period of time (33.3 min) into well B3 with an initial plume design diameter of about 2 m in Unit 2. Injection occurred over a 4 m interval centered on the contact between Units 2 and 3 (Figures 3-5) to enhance the opportunity to observe plume shape evolution due to heterogeneity at one or several scales because these hydrostratigraphic units have different hydraulic conductivity and porosity magnitudes and spatial structures, and because the contact between these units is not flat but has some topography (Barrash et al. 2002). Figure 4 is a schematic diagram of the injection, pumping, and sampling zones in the B wells and in well A1. Figure 5 is another schematic diagram of the B wells and of well A1 showing planes for time-lapse radar tomograms, sampling locations, and injection and pumping zones of the TTLT.

About 35 min after injection ended, pumping at ~5 gpm (0.315 L/s) began at well B6 over a 4 m interval equal in elevation to that used for injection. Figure 6 shows the pumping and injection rates in wells B3 and B6 and Table 2 lists the timing of injection and pumping events during the TTLT. Pumping from well B6 was continuous during the test except for interruptions by brief power failures, pump failure, and cross hole radar tomography in the longitudinal direction of plume transport. With this injection and pumping scheme and site gradient configuration (Figure 7), it was anticipated that the plume would remain within the ring of B wells.

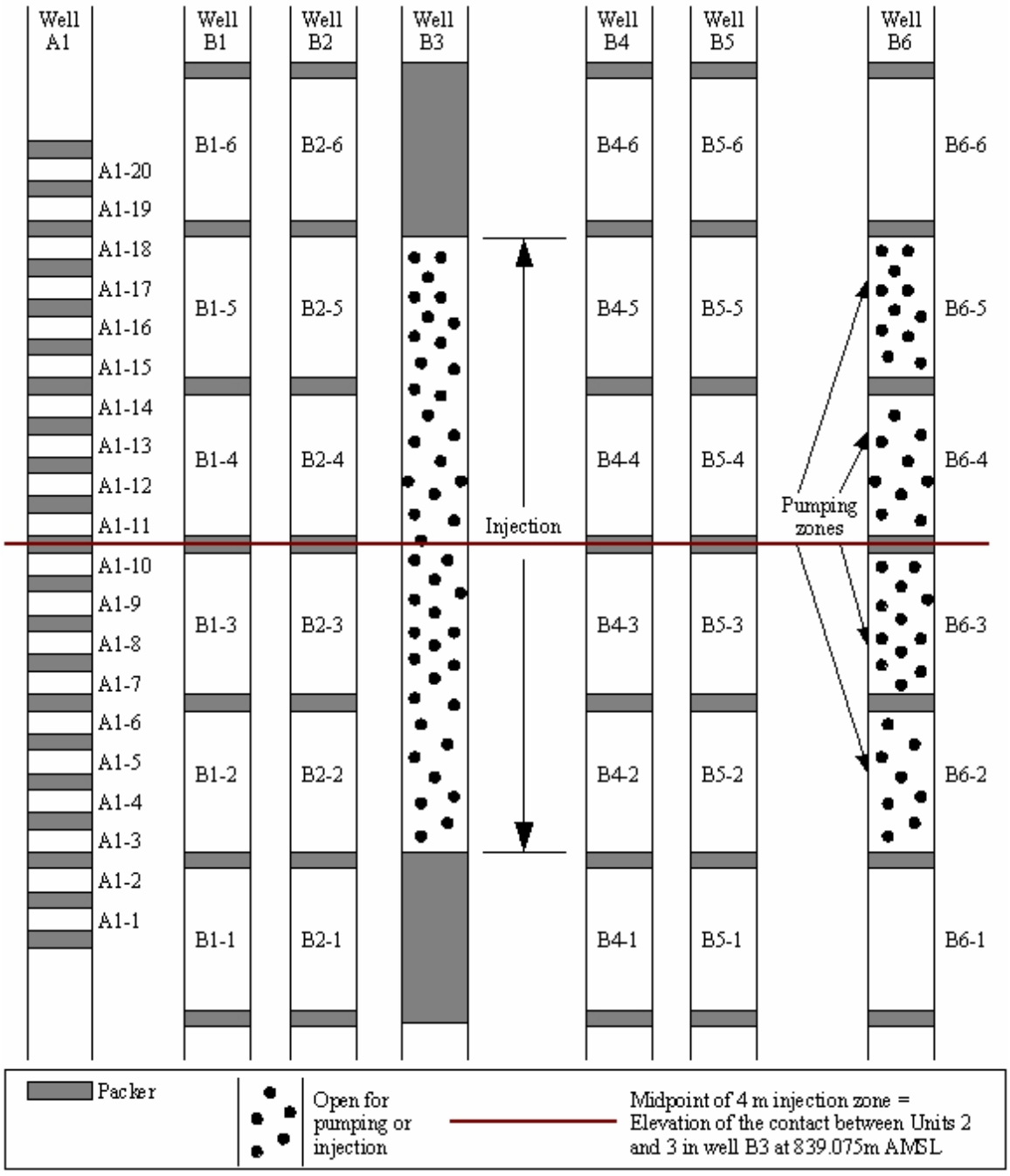

Figure 4: Schematic diagram of the sampling locations in well A1 and in the B wells (modified from Barrash et al., 2002).

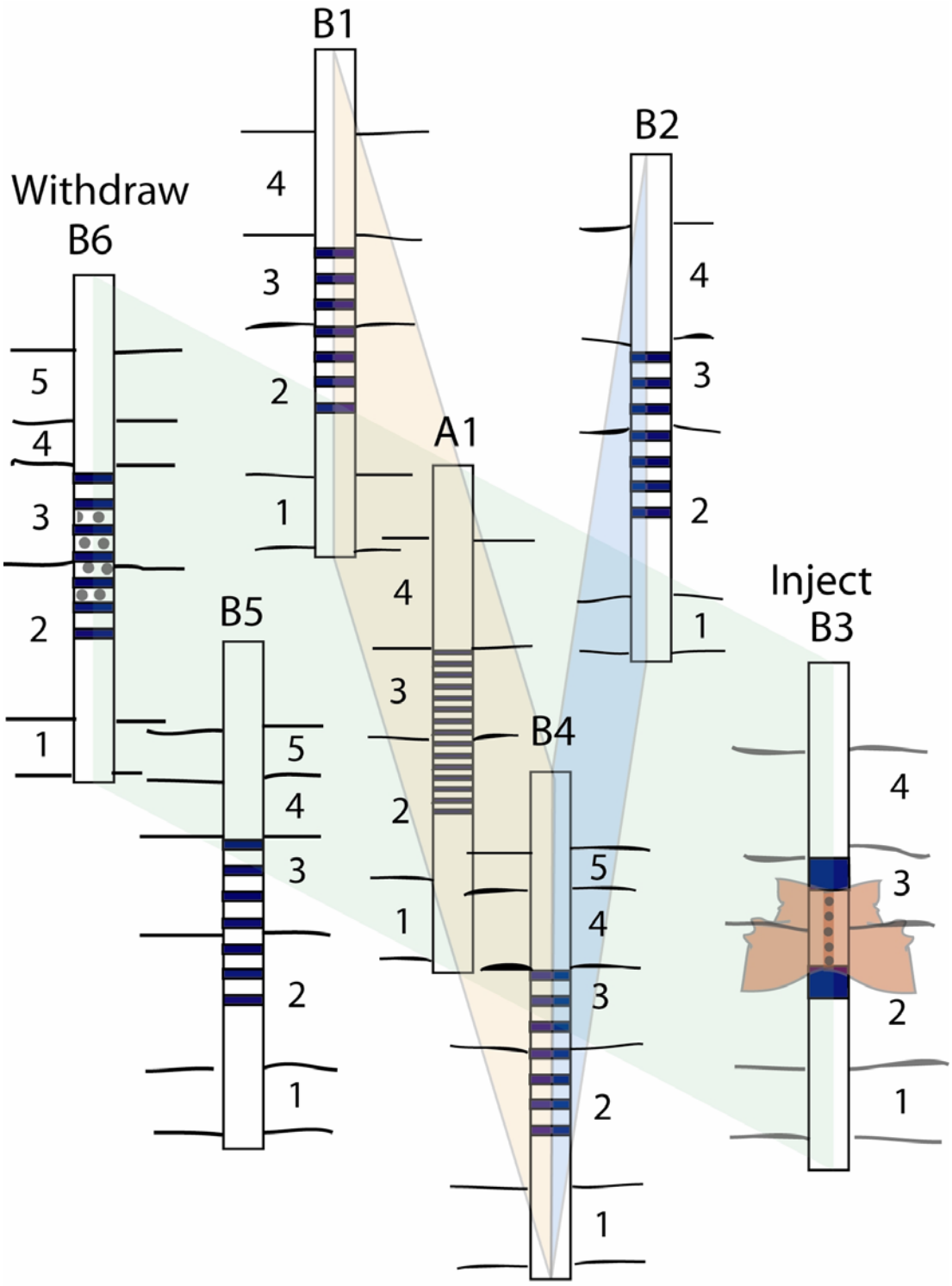

Figure 5: Schematic diagram of well A1 and the B wells showing the injection and pumping zones, sampling zones, and radar tomogram planes. The hydrostratigraphic unit contacts within each well are also roughly shown (Barrash et al., 2002).

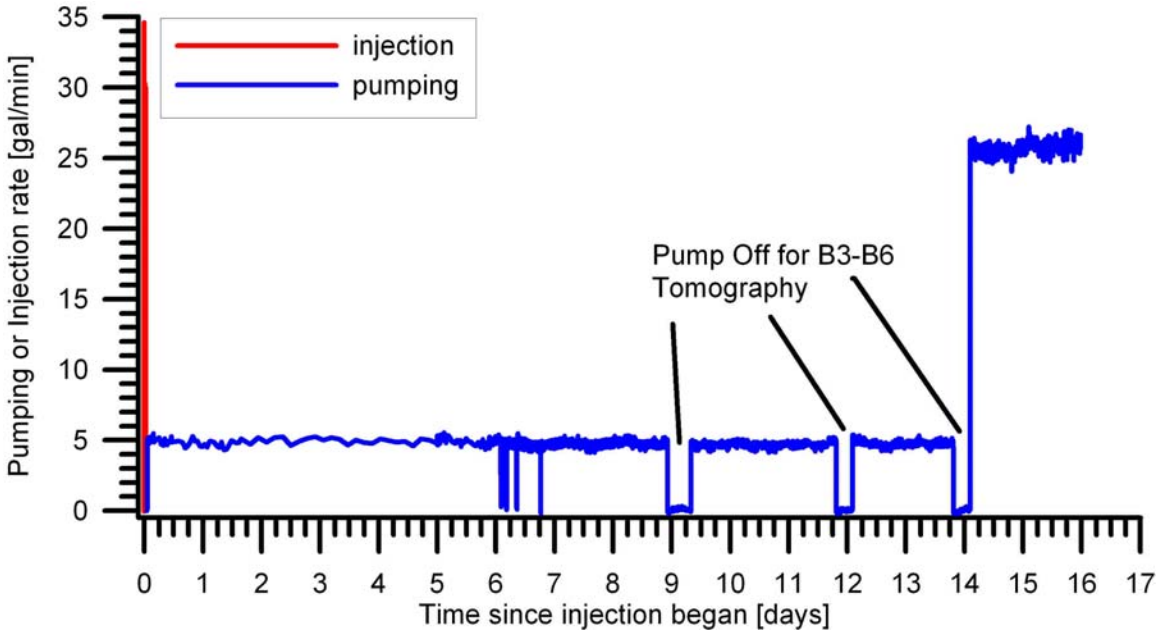

Figure 6: The pumping and injection rates during the TTLT (modified from Barrash et al., 2002).

Table 2: Pumping and injection events during the TTLT (Barrash et al., 2002).

Date and time	Time since injection began [days]	Event
8/1/01 11:40	0.0000	Begin injection in well B3 at ~29.5 gal/min.
8/1/01 12:13	0.0229	Stop injection in well B3.
8/1/01 12:48	0.0472	Start pumping in well B6 at ~5 gal/min.
8/2/01 8:30	0.8681	Decrease pumping in well B6 from 5.35 gal/min to 5 gal/min.
8/7/01 13:43	6.0854	Pumping stopped in well B6 due to pump failure.
8/7/01 14:00	6.0972	Resume pumping in well B6 at 5 gal/min.
8/7/01 20:10	6.3542	Pumping stopped in well B6 due to power failure.
8/7/01 20:17	6.3590	Resume pumping in well B6 at 5 gal/min.
8/10/01 10:00	8.9306	Stop pumping in well B6 for B3-B6 radar tomography.
8/10/01 19:30	9.3264	Resume pumping in well B6 at 5 gal/min.
8/13/01 7:10	11.8125	Stop pumping in well B6 for B3-B6 radar tomography.
8/13/01 13:45	12.0868	Resume pumping in well B6 at 5 gal/min.
8/15/01 7:00	13.8056	Stop pumping in well B6 for B3-B6 radar tomography.
8/15/01 14:00	14.0972	Resume pumping in well B6 at 26 gal/min.

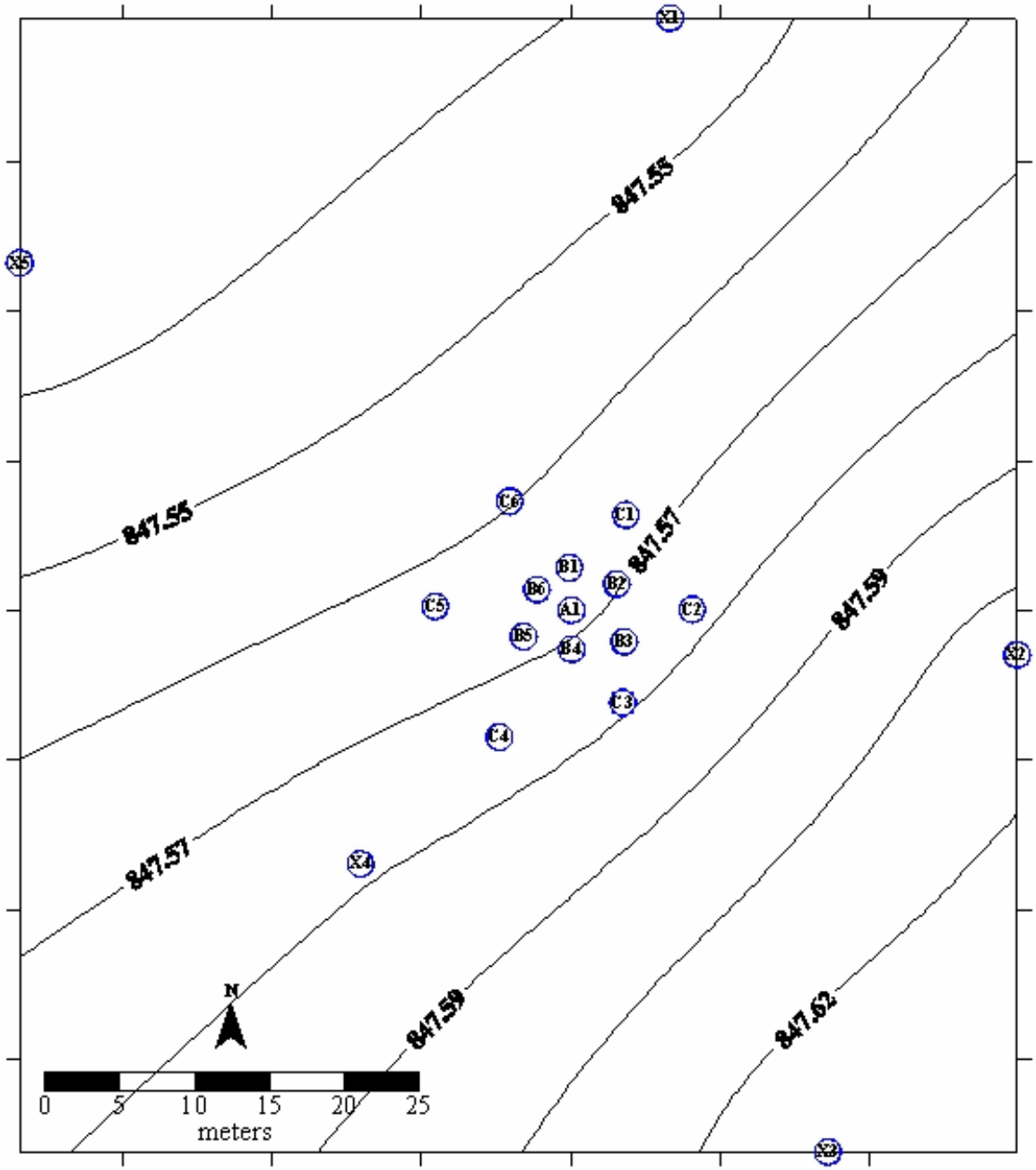

Figure 7: Water level contours at the BHRS during the summer months. Contours are meters above sea level. The Boise River is to the southwest and flows northwest at the margin of the BHRS (Barrash et al., 2002).

During the TTLT water chemistry samples were collected about every four hours in well A1, the B wells, and the discharge line, and from the injection line about every 1 min during injection. Well A1 contained a port and packer system isolating 20, 0.25 m sampling zones with 21 packers which spanned the injection interval in well B3; the center of the 11th packer in well A1 was at the same elevation as the middle of the injection zone in well B3 (Figure 4). The sampling zones are labeled with a prefix (the well name) and then with the sampling zone number (e.g., 1 for the lowest zone in a given well and increasing zone numbers up the well). For example the third sampling location from the bottom in well B2 would be labeled B2-3. Wells B1, B2, B4, B5, and B6 were implemented with a port and packer system that isolated six, 1 m sampling zones with seven packers. The elevation of the middle of the 4th packer is at the same elevation as the middle of the injection zone in well B3 (Figure 4). The 4 m injection zone in well B3 was isolated using inflatable packers. Appendix A lists the times at which water chemistry samples were collected, the sample event number, the number of samples collected, and the number of QC samples collected.

In addition to flow rate and water chemistry measurements, head measurements were taken in all wells and in the Boise River adjacent to the BHRS before, during, and after the TTLT. Strain-gauge transducers were placed in the C wells, X wells, and Boise River for head measurements there, and fiber optic transducers were threaded through access tubes to measure head in some of the sampling zones in well A1 and in the B wells. Because of drift in many of the fiber-optic transducers used in sampling zones in

the B wells and in well A1, head changes (Δh) could not be measured reliably for some of these zones.

2.4 Water Chemistry, Injection/Pumping Rate, and Head Data from the TTLT

The concentration of potassium bromide (here-after referred to as bromide or the bromide tracer) was measured via electrical conductivity of the fluid. Hausrath et al. (2002) developed the conversion between fluid electrical conductivity and bromide concentration as:

$$Bromide = \left(C_{25} - C_{background}\right) * 0.9255 + 0 \quad (1)$$

where bromide units are ppm and electrical conductivity units are μS/cm. $C_{background}$ was approximately 206.4 μS/cm based on 94 samples collected before tracer injection. C_{25} is the fluid electrical conductivity at 25º C. Water sample electrical conductivity was converted to fluid electrical conductivity for 25º C through:

$$C_{25} = \frac{C_m}{\left(1 + 0.02\left(T_m - 25\right)\right)} \quad (2)$$

where C_m is the actual measured conductivity and T_m is the sample temperature at time of measurement C_m (Hausrath et al., 2002).

The uranine concentration was measured via fluorescence which was analyzed in a Turner Designs AU-10 fluorometer that was calibrated for uranine concentration (Hausrath et al., 2002).

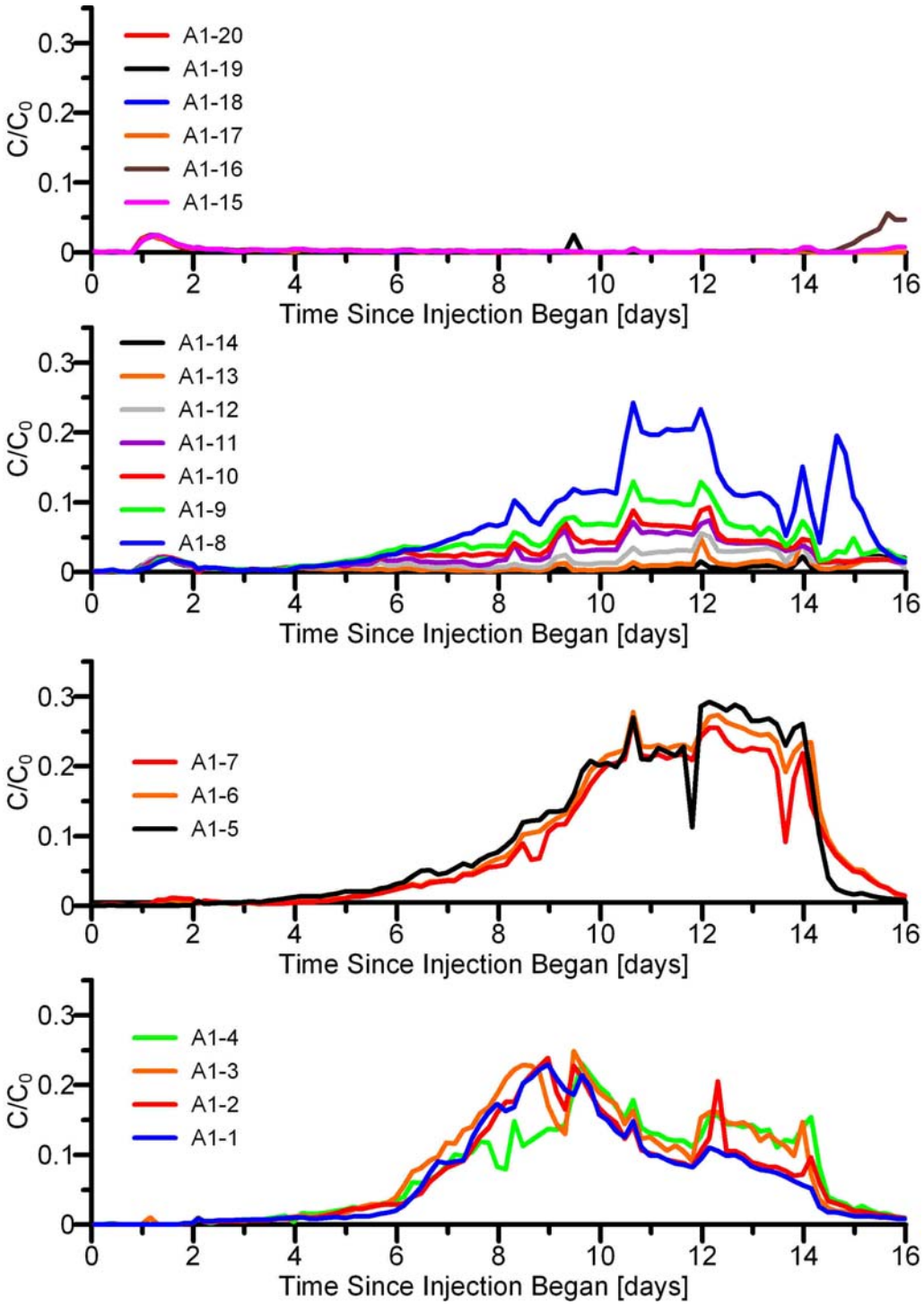

Figure 8: Observed bromide breakthrough curves (adjusted for outliers) measured in the sampling zones of well A1 during the TTLT. Breakthrough curves are grouped by similar behavior in adjacent sampling zones (modified from Hausrath et al., 2002).

Figure 8 is a plot of the bromide breakthrough curves from the TTLT in well A1 normalized to bromide injection concentration in well A1. Breakthrough curves from the 20 zones in A1 are divided into four groups based on similarities (Barrash et al., 2002; Hausrath et al., 2002); the lowest sampling zones (A1-1 through A1-4) show relatively high breakthrough concentrations with peak concentrations occurring about nine days into the test; the high breakthrough magnitudes in these sampling zones strongly suggest that tracer also passes below the sampling zones. The next higher three sampling zones (A1-5 through A1-7) also show relatively high bromide breakthrough concentrations with what appears to be two peaks – one around day 11 and a second around day 12. This second peak is also seen in the lower sampling zones (A1-1 through A1-4) but has lower magnitude there. The upper sampling zones (A1-8 through A1-20) show breakthrough magnitude decreasing to background levels by sampling zone A1-14. These upper breakthrough curves peak at around day 11. This complex breakthrough behavior is generally consistent with topography on contacts and contrasts in hydraulic conductivity between Units 2 and 3 as included in pre-test modeling (Barrash et al., 2002) and may be important in explaining flow behavior.

This two lobed, or two peak breakthrough behavior was also noticed in the analysis of geophysical radar tomograms (Johnson, 2007; Goldstein, 2005). Although the author acknowledges this two-peaked breakthrough, it is beyond the scope of this thesis to try and account for the multiple peaks in the modeling. It is however suggested that subsequent modeling of the tracer test (perhaps modeling done with incorporation of geophysical radar tomograms) account for this two-lobe tracer plume.

Figure 9 shows uranine breakthrough curves normalized to uranine injection concentration. Because no breakthrough or barely recognizable breakthrough was measured for either of the tracers in the sampling zones of wells B1, B2, B4, and B5 (Hausrath et al. 2002), the breakthrough curves for these sampling zones are not shown here but are included on the CD accompanying this thesis for completeness. The breakthrough curves measured in wells B3 and B6, and the tracer concentrations in the discharge line are also included on the CD. By comparing Figures 8 and 9, it is clear that uranine breakthrough is significantly retarded in time and reduced in magnitude, and the vertical pattern of breakthrough is different compared to that of the bromide breakthrough curves. Because of uranine's non-conservative behavior compared to bromide, it is not considered further in this study.

Changes in head values in the C wells, in various sampling zones of the B wells, in various sampling zones in well A1, and in the X wells were also measured during the test. Figure 10 shows the changes in head of the C wells, and the changes of head of the other transducers in other wells and sampling locations are provided on the CD accompanying this thesis. Daily fluctuations of 0.5 to 2.5 cm are seen in the changes of head of Figure 10. These fluctuations are due to evapotranspiration as determined from unpublished monitoring data (Barrash et al., 2002). The river stage of the Boise River was also monitored during the TTLT and changes in river stage are shown in Figure 11; because of disturbances to the transducer in the river (fisherman bumps), the river stage data were corrected (Barrash et al., 2002). Both the uncorrected and the corrected changes in river stage are plotted in Figure 11. Discharges from Lucky Peak Dam to the

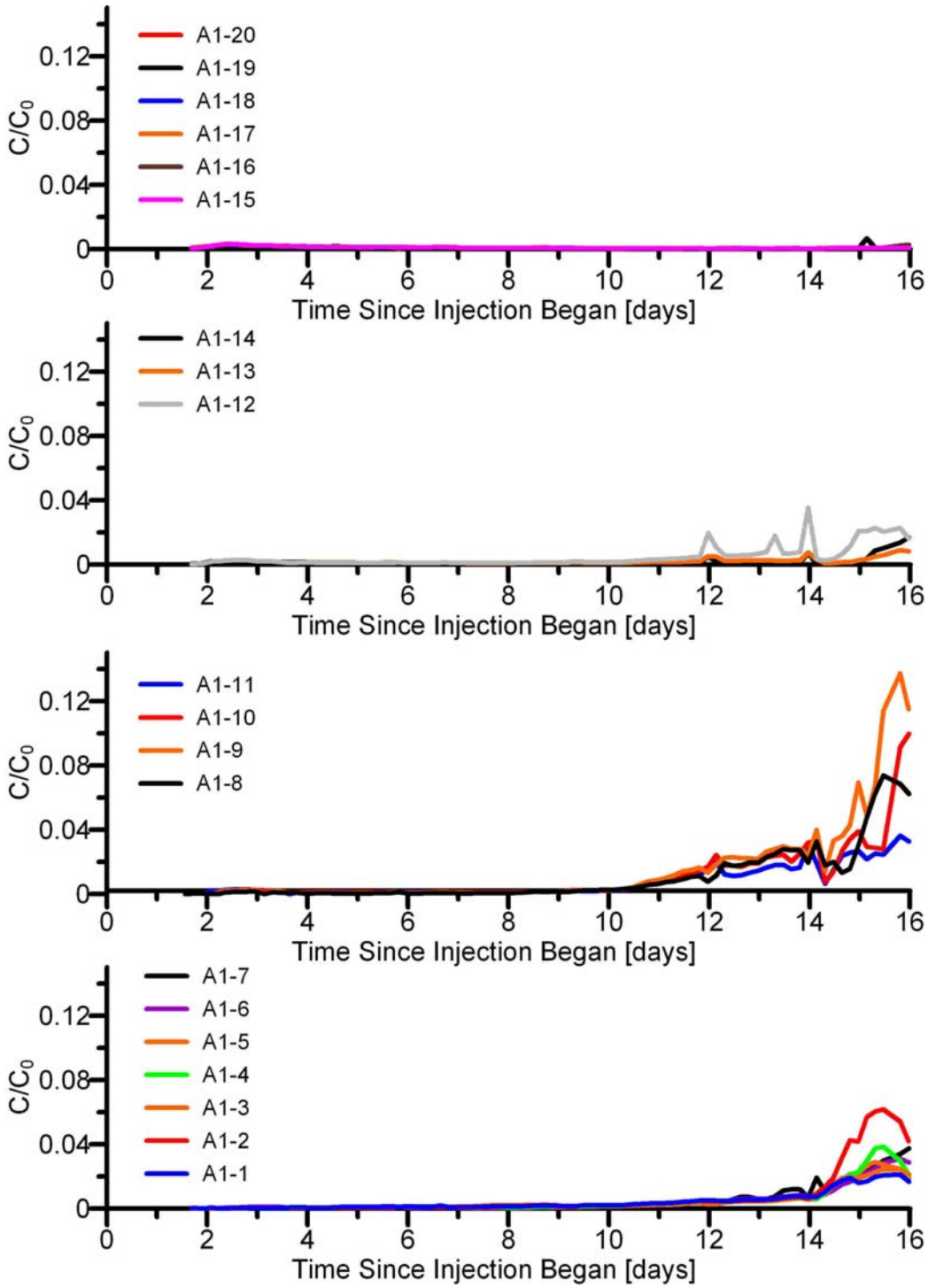

Figure 9: Observed uranine breakthrough curves measured in the sampling zones of well A1 during the TTLT. Breakthrough curves are grouped by similar behavior in adjacent sampling zones (modified from Hausrath et al., 2002).

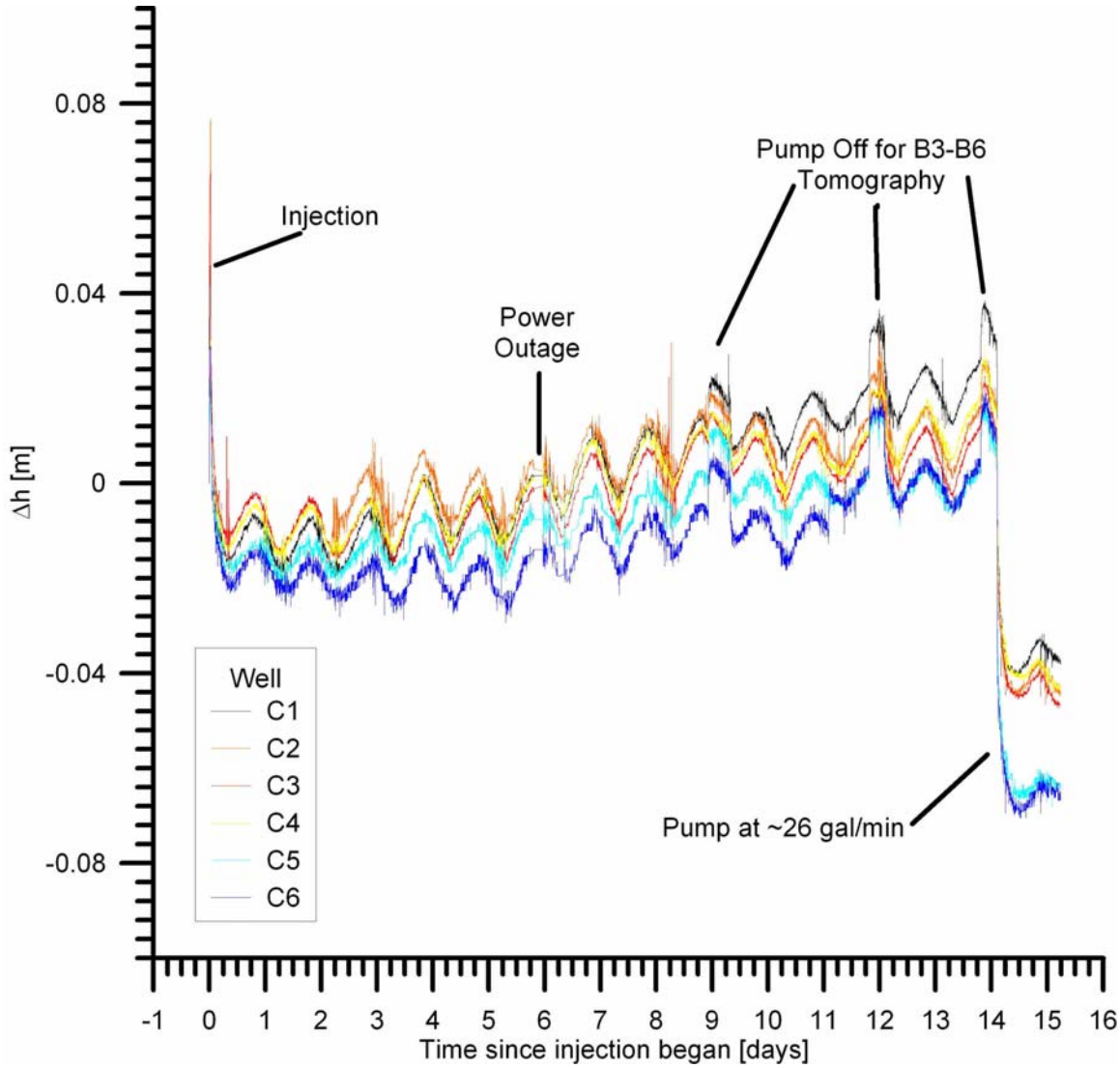

Figure 10: Observed head changes in the C wells during the TTLT (modified from Barrash et al., 2002).

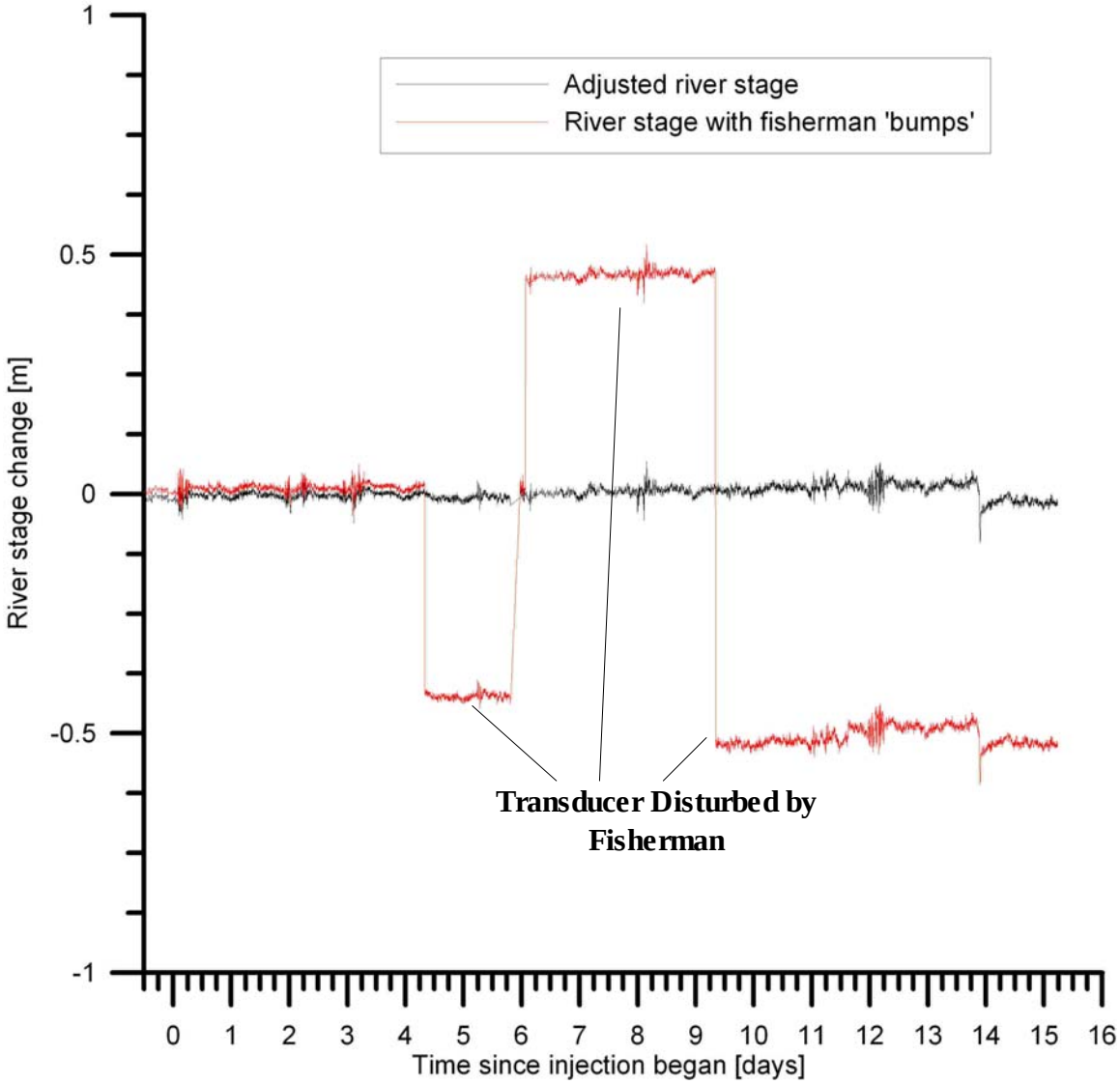

Figure 11: Adjusted and unadjusted measured change in river stage as measured during the TTLT. The displacements in the unadjusted plot are due to the transducer being bumped. (Modified from Barrash et al., 2002.)

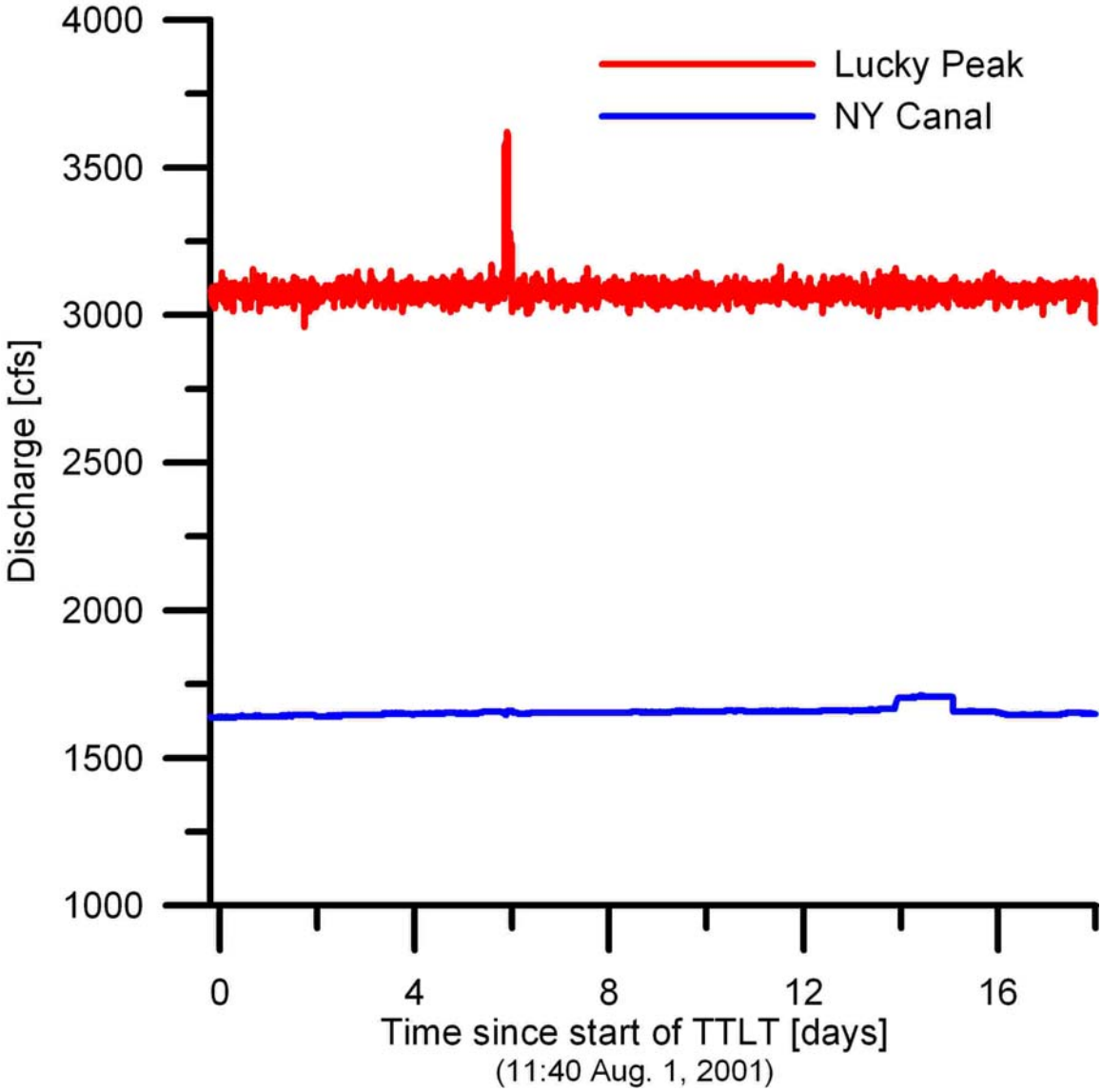

Figure 12: Discharge at Lucky Peak Dam and diversion of the New York Canal near the BHRS. (Modified from Barrash et al., 2002.).

Boise River and into the New York Canal at the Diversion Dam just upstream of the BHRS were recorded by the Bureau of Reclamation and are shown in Figure 12 and indicate that the Boise River flow rates during the TTLT in the reach by the BHRS included minor variations.

2.5 Project Scope

One goal of this thesis is to determine hydrogeologic properties of the BHRS that are significant in modeling the TTLT. A number of characteristics or issues associated with the BHRS and/or TTLT were identified before or during the modeling, and were evaluated for the BHRS through simulations. Below is a list of the issues or characteristics that are evaluated in this thesis (also see Table 3). Also listed below – with open circles – and in Table 3 are brief explanations of the results of the evaluation of each characteristic or issue.

- Analytic modeling of the breakthrough curves measured in the sampling zones of well A1 yields estimates of hydraulic conductivity and dispersivity.
    - The hydraulic conductivity estimates are sensitive to estimates of hydraulic gradient.
- There is a noticeable evapotranspiration signal – the water table fluctuates 0.5-2.5 cm daily (Figure 10). Does evapotranspiration influence transport during the TTLT?
    - Two simulations, one including evapotranspiration, and one without were compared to show that evapotranspiration is not significant for bromide

transport during the TTLT. Evapotranspiration does influence transport but not significantly for the TTLT.

- When there is a positive density contrast between a tracer or contaminant plume and the ambient groundwater (tracer or contaminant plume is more dense then the ambient groundwater), there is a tendency for the plume to sink. Barth et al. (2001) show that the tendency to sink is dependent upon the variability in hydraulic gradient, the hydraulic conductivity, and the density difference between the plume and the ambient groundwater. During the TTLT are the density contrasts significant enough to affect transport?
    - Using Barth et al.'s criterion to evaluate the tendency for variable density flow during the TTLT, and through simulations, the bromide tracer shows downward movement due to the contrast between the denser bromide plume and the less-dense ambient groundwater.
- Using homogeneous hydrogeologic properties throughout a given system is often the most that can be done with limited time and data; how much of the transport behavior can be described using homogeneous hydrogeologic properties?
    - Using average estimates of hydrogeologic properties at the BHRS, simulations show that simulated breakthrough generally occurred early, and breakthrough magnitudes were high in most cases. Using homogeneous properties throughout the system is not sufficient to capture bromide transport behavior during the TTLT.

- Do boundary conditions to the flow system influence transport significantly? The Boise River bounds one side of the BHRS and its influence on bromide transport during the TTLT can be investigated through simulation.
    - The Boise River induces a relative gradient away from it that essentially shifts the bromide tracer northeastward so it does not pass directly through well A1. If the center of the tracer plume does not pass through well A1, then the breakthrough magnitudes measured in the sampling zones of well A1 will be less because a lower-concentration side portion of the plume is being sampled.
- Will layering influence transport? Contrasts in hydrogeologic properties between layers will introduce heterogeneity into the system which may affect transport.
    - As more heterogeneity - through layering - is included in simulations, data matching improves.
- The wells at the BHRS are fully screened. This could introduce local high vertical hydraulic conductivity flow paths. Do these high vertical hydraulic conductivity flow paths significantly influence flux to the pumping well and/or the distribution from the injection well? For example, the fully screened well bore in well B6 could result in more flux from the relative high hydraulic conductivity sand channel at the top of the system to the vicinity of the pumping zone. This would result in less flux from the direction of the bromide plume which would be seen as later breakthrough in the sampling zones of well A1.

- This effect is seen when well bores are included in the simulations, but simulated breakthrough is not slowed enough by this effect to significantly improve matches to observed breakthrough.

- Dispersivity is a measure of the tendency of a plume to spread. A larger dispersivity will result in a broader breakthrough curve with smaller magnitude. How do estimates of dispersivity influence transport?
  - Estimates of the dispersivity are taken from analysis of the measured breakthrough curves. This analysis yields a range of values which are used in simulations to show effects of dispersivity on breakthrough and, as expected, a larger dispersivity results in more spreading of the plume.
- In most simulations of this study, much of the simulated breakthrough in the sampling zones of well A1 is early compared to measured values. Advective transport is inversely proportional to effective porosity. Will increasing effective porosity slow advective transport enough to improve the breakthrough match?
  - Effective porosity was increased to see if this would cause later breakthrough in the sampling zones of well A1. A uniform increase in effective porosity will slow the tracer plume, but not sufficiently to match observed breakthrough.
- High vertical hydraulic conductivity anisotropy (K_H/K_V) will tend to dampen variable density flow, and affect distribution of flux to the pumping interval from above and below. Fox (2006) and Barrash et al. (2006) estimate vertical hydraulic conductivity anisotropy from analysis of pumping tests at the BHRS to generally

be ~1 but locally range to ~2. How would including vertical hydraulic conductivity anisotropy influence transport?

- Increasing the hydraulic conductivity anisotropy to reasonable values above 1 does not significantly influence transport during the TTLT.

- Despite including layering, bore holes, and increasing effective porosity, some simulated breakthrough curves from the sampling zones of well A1 show early breakthrough. As increasing heterogeneity through adding layering shows the most improvement in matching measured breakthrough, a greater characterization of the hydraulic conductivity heterogeneity and the porosity heterogeneity could improve the match between simulated and measured breakthrough. One way to examine this heterogeneity is through stochastic simulations.
  - One hydraulic conductivity realization and one porosity realization were created to show the potential this method has in examining how the heterogeneity at the BHRS contributes to transport during the TTLT.

Table 3: Characteristics and issues investigated.

Complexity	***Comment***	***Result***
Semi-Analytical Fitting of the Breakthrough Curves	Semi-analytical analysis of the breakthrough curves measured in well A1.	Yields estimates of dispersivity and hydraulic conductivity. Hydraulic conductivity estimates are sensitive to hydraulic gradient estimates.

Complexity	***Layering***	***Comment***	***Result***
Evapotranspiration	None	Simulations with and without evapotranspiration to show effect of evapotranspiration on transport.	Evapotranspiration does not influence bromide transport during the TTLT.
Variable Density Flow	Two layers	Evaluation of the tracer test to estimate whether there is significant variable density flow. Comparisons of simulations that do, and do not account for variable density flow.	Variable density flow is significant to bromide transport during the TTLT.
Homogeneous Hydrogeologic Properties Throughout the Model	None	Simplest model with homogeneous hydrogeologic properties throughout the model, and a uniform, regional hydraulic gradient. Hydrogeologic properties simulated: the average of Units 2 and 3, Unit 2, and Unit 3.	Using average hydrogeologic properties yields early simulated breakthrough and high breakthrough magnitudes.
Boundaries	None	Effects of the river boundary on transport.	By adding the river boundary, a relative gradient away from the river is induced through the BHRS and causes the center of the bromide tracer plume to pass ~1 m to the side of well A1 resulting in lower breakthrough magnitudes simulated in the sampling zones of well A1.

Table 3: (Continued) Characteristics and issues investigated.

Complexity	***Layering***	***Comment***	***Result***
Layering	None, two layers, three layers, 5 layers, and many layers.	Layering: Homogeneous hydrogeologic properties of the average of Units 2 and 3 throughout; Units 2 and 3 from Barrash and Clemo (2002); two different three layer models as determined by semi-analytical analysis of the breakthrough curves measured in well A1; Five layers – Units 1 through 5 from Barrash and Clemo (2002); Many layers – Units 1, 3, 4, 5, from Barrash and Clemo (2002) and Unit 2 from Barrash and Clemo (2002) subdivided into smaller lenses.	By adding layering, the hydrogeologic property heterogeneity is better characterized and improvements to matching the observed breakthrough is seen.
Well Bores	Five layers corresponding to the 5 Units from Barrash and Clemo (2002).	Simulations with no well bores, well bores defined only in the pumping and injecting zones (with packers), and well bores defined for the entire vertical screen extent of the pumping and injection wells.	By including well bores, flux from the high K sand channel (Unit 5) to the pumping interval in well B6 is increased and the flux to the pumping interval from the plume is less causing later breakthrough in well A1. However, this later breakthrough is still earlier than measured breakthrough in several sampling zones.

Table 3: (Continued) Characteristics and issues investigated.

Complexity	***Layering***	***Comment***	***Result***
Dispersivity	5 Layers and many layers	Analysis of the breakthrough curves measured in well A1 indicates that the longitudinal dispersivity varies between 0.1 and 0.2 m. Simulations with longitudinal dispersivity of 0.1 and of 0.2.	By increasing the dispersivity, the breakthrough curves are broader and have slightly less magnitudes.
Porosity	None and five layers corresponding to the 5 Units from Barrash and Clemo (2002).	Investigate the effects of increasing the porosity either uniformly by up to 30% or by up to 2 times standard deviation calculated by Barrash et al. (2002).	The increasing of effective porosity will cause later breakthrough. But the later breakthrough is not sufficient to match observed in several sampling zones.
Vertical Hydraulic Conductivity Anisotropy	A many layered case where Unit 2 is subdivided into many lenses.	Vertical anisotropy is varied from 1 to 4.	Increasing the vertical hydraulic conductivity anisotropy above the 1 (calculated value from Barrash et al. 2006) does not influence transport greatly.
Hydraulic Conductivity and Porosity Varying Throughout the Well Field	Five layers corresponding to the 5 Units from Barrash and Clemo (2002).	The hydraulic conductivity and porosity vary within each layer, but each layer has distinct geostatistics.	By capturing the hydraulic conductivity heterogeneity and porosity heterogeneity can improve matches of simulated to observed breakthrough.

3 FLOW AND TRANSPORT MODELING METHODS

The approach to flow and transport modeling used in this thesis is given in this chapter. The overall idea was to begin with simple representations of the hydrogeological system and progressively add hydrologic complexities while measuring quality of simulated matches to observed tracer breakthrough behavior to recognize improvement associated with a given change to the modeled system.

This chapter begins with one-dimensional semi-analytical analysis of the breakthrough curves measured in well A1 to check or confirm the need for numerical modeling and to generate average flow (hydraulic conductivity) and transport (longitudinal dispersivity or α_L) values. Next the numerical modeling codes used for flow (including variable-density flow) and transport are identified with statements of the governing equations of flow and transport used in these codes. The chapter continues with information on the approach to numerical modeling used in this thesis - including: (a) an explanation of the simulation environment and utilities; (b) descriptions of the three models used in this effort (uniform gradient or simple boundaries flow model, more-detailed complex boundaries flow model, and transport model) and (c) the relationships between these models. This chapter concludes with a description of the transport summary statistics used to determine how well a given simulation's transport behavior matches that of the observed bromide behavior during the TTLT and other simulations.

3.1 Semi-Analytical Analysis of Bromide Breakthrough Curves

Käss (1998) describes a process developed by Sauty (1977) to determine the effective flow velocity (seepage velocity) and dispersion coefficients (i.e. dispersivities) using the Peclet number (*Pe*):

$$Pe = \frac{x}{\alpha_l} \tag{3}$$

Dispersivity (α_l) has the units of length and is a measure of how the tracer plume spreads in relation to the length scale of the problem (x). A smaller dispersivity value corresponds to a tracer plume that does not spread very much – that is, the plume would be dominated by advective transport. The length scale of the problem at hand is just over 4 m (the distance from the injection well, B3, to the sampling well, A1). From Gelhar et al. (1992) the longitudinal dispersivity would fall within the range of 0.02 m to 1 m based on scale considerations and reported values in the literature. This gives a range of Peclet numbers from 4 to 200. The method developed by Sauty (1977) uses curve fitting of the normalized measured concentration curve to normalized concentration type curves generated with different Peclet numbers using:

$$c_r = \frac{A}{\sqrt{t_r}} \cdot e^{-\frac{Pe}{r \cdot t_r}(1-t_r)^2} \tag{4}$$

where c_r is the type concentration, Pe is the Peclet number, t_r is the time of the type curve, and A is the normalizing factor:

$$A = \frac{1}{c_{r,max}} \tag{5}$$

Figure 13 shows a number of these type curves for Peclet numbers which include the 4-200 range estimate for the BHRS: 1, 3, 10, 30, 100, and 300.

A breakthrough curve can be overlain by type curves until a match is found. A dispersivity is calculated by using equation 3 with the distance x between the injection well (B3) and the sampling well (A1), and the Peclet number of the matching type curve.

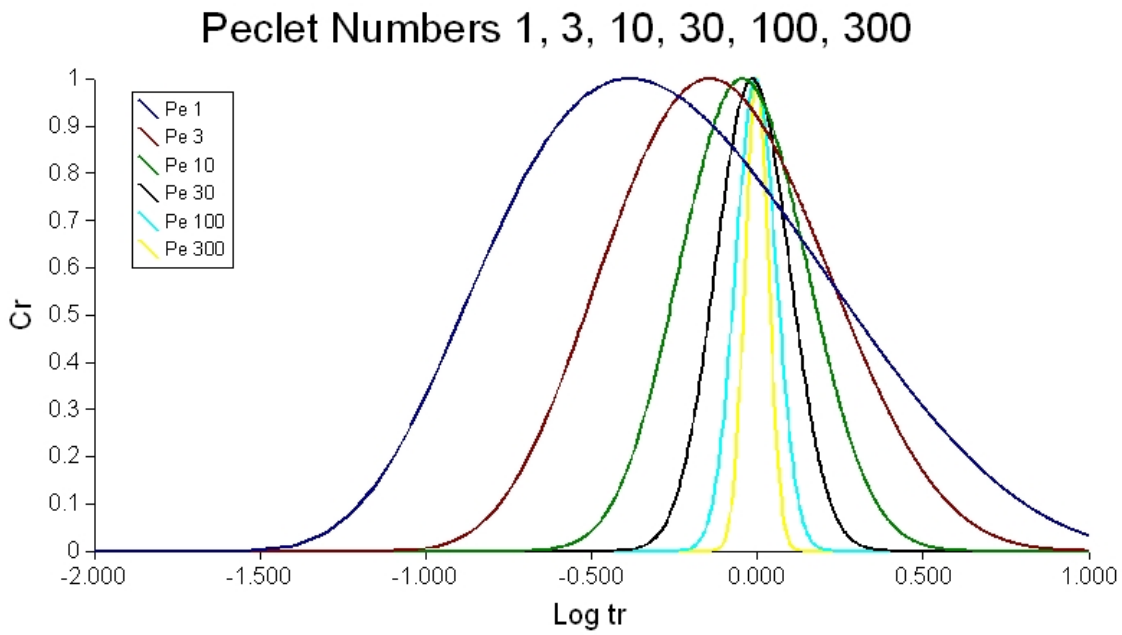

Figure 13: Normalized type curves using six Peclet numbers (1, 3, 10, 30, 100, and 300) which include the 4-200 range expected at the BHRS.

The effective flow velocity (v_a) is determined through:

$$v_a = \frac{x}{t_k} \tag{6}$$

where t_k is the time associated with the effective flow velocity and is determined as:

$$\log t_k = \log t_{max} - \log t_{r,max} \tag{7}.$$

where t_{max} is the time of peak of the observed breakthrough curve and $t_{r,max}$ is the time of the peak of the type curve. Using the estimated effective flow velocity, hydraulic conductivity can be calculated by assuming a uniform hydraulic gradient and effective porosity:

$$K = \frac{v_a \cdot \eta}{i} \tag{8}$$

where η is porosity, and i is the hydraulic gradient.

An analysis similar to that described by Käss (1998) and Sauty (1977) was conducted with the breakthrough curves measured in sampling zones of well A1. Leven et al. (2002) also conducted a similar analysis of the TTLT breakthrough curves and obtained estimates of about 0.1 m for α_l. It is worth noting that Käss (1998) and Sauty (1977) developed this model for 1D flow, but with pumping at 5 gpm from well B6, the TTLT is radially convergent overall. However, considering the low pumping rate, unconfined conditions, and relatively high hydraulic conductivity aquifer, the test was largely natural gradient between injection well B3 and monitoring well A1. With this in mind, the analysis of breakthrough curves from the sampling zones of well A1 are estimates dependent upon the hydraulic gradients used in the analysis. Table 4 shows the various inputs (hydraulic gradient, time to peak, etc.) and results used in analyzing the breakthrough curves. The breakthrough curves from the sampling zones in well A1 matched different type curves (different Peclet numbers) and the change in plume position and geometry from injection indicate that tracer transport during the TTLT cannot be adequately modeled with one 1D treatment.

Table 4: Values used in the 1D semi-analytical modeling of the bromide breakthrough curves with the Sauty (1977) method and the estimated longitudinal dispersivities and hydraulic conductivities.

Sampling Zone	Pe	T_k [d]	v_a [m/day]	α_l [m]	t_{max} [days]	Gradient (i)	Porosity	K [m/s]
A1-1	45	9.33	0.44	0.09	9.14	0	0.26	0.000330
A1-2	50	9.33	0.44	0.08	9.14	0	0.25	0.000322
A1-3	40	9.33	0.44	0.10	9.14	0	0.25	0.000316
A1-4	40	9.99	0.41	0.10	9.79	0	0.25	0.000298
A1-5	45	11.88	0.35	0.09	11.64	0	0.26	0.000265
A1-6	40	12.22	0.34	0.10	11.97	0	0.27	0.000260
A1-7	40	12.40	0.33	0.10	12.15	0	0.24	0.000231
A1-8	40	11.71	0.35	0.10	11.47	0	0.21	0.000213
A1-9	35	11.83	0.35	0.12	11.47	0	0.21	0.000207
A1-10	35	11.66	0.35	0.12	11.31	0	0.20	0.000208
A1-11	35	11.83	0.35	0.12	11.47	0	0.19	0.000196
A1-12	40	12.90	0.32	0.10	12.64	0	0.20	0.000186
A1-1	45	9.33	0.44	0.09	9.14	0.02	0.26	0.000003
A1-2	50	9.33	0.44	0.08	9.14	0.02	0.25	0.000003
A1-3	40	9.33	0.44	0.10	9.14	0.02	0.25	0.000003
A1-4	40	9.99	0.41	0.10	9.79	0.02	0.25	0.000003
A1-5	45	11.88	0.35	0.09	11.64	0.02	0.26	0.000003
A1-6	40	12.22	0.34	0.10	11.97	0.02	0.27	0.000003
A1-7	40	12.40	0.33	0.10	12.15	0.02	0.24	0.000003
A1-8	40	11.71	0.35	0.10	11.47	0.02	0.21	0.000002
A1-9	35	11.83	0.35	0.12	11.47	0.02	0.21	0.000002
A1-10	35	11.66	0.35	0.12	11.31	0.02	0.20	0.000002
A1-11	35	11.83	0.35	0.12	11.47	0.02	0.19	0.000002
A1-12	40	12.90	0.32	0.10	12.64	0.02	0.20	0.000002

3.2 Numerical Modeling Codes and Governing Equations for Three-Dimensional Flow and Transport

Recognizing the need for 3D treatment of flow and transport for the TTLT, the finite difference codes MODFLOW 2000 (Harbaugh et al., 2000), MT3DMS (Zheng and Wang, 1999), and SEAWAT 2000 (Langevin et al., 2003) were selected because they are well-documented public-domain codes with the capabilities to numerically simulate the complexities listed in Table 3. SEAWAT 2000 can account for variable density flow (i.e., possible influence of relatively high concentrations of tracer during the TTLT – see preliminary analysis in section 3.2.3) while MODFLOW 2000 and MT3DMS do not. SEAWAT 2000 accounts for variable density flow by using freshwater equivalent-heads, whereas MODFLOW 2000 uses heads. SEAWAT 2000 is a modification and combination of MODFLOW 2000 and MT3DMS where the heads are transformed into freshwater heads using concentrations calculated in MT3DMS prior to solving the flow equation.

3.2.1 Governing Flow and Transport Equations

MODFLOW 2000 and SEAWAT 2000 each solve slightly different governing equations of flow. MODFLOW 2000 solves:

$$\frac{\partial}{\partial x}\left(K_{xx}\frac{\partial h}{\partial x}\right)+\frac{\partial}{\partial y}\left(K_{yy}\frac{\partial h}{\partial y}\right)+\frac{\partial}{\partial z}\left(K_{zz}\frac{\partial h}{\partial z}\right)+W=S_s\frac{\partial h}{\partial t} \qquad (9)$$

where K_{xx}, K_{yy}, K_{zz} are the hydraulic conductivities along the x, y, and z coordinate axes which are assumed to be parallel to the major axes of hydraulic conductivity (L/T); h is the potentiometric head (L); W is the volumetric flux per unit volume representing

sources and/or sinks of water where W is positive for flow into the groundwater system (L^3/T); S_s is the specific storage of the aquifer (1/L); and t is time (Harbaugh et al., 2000). SEAWAT 2000 solves:

$$\frac{\partial}{\partial \alpha}\left(\rho K_{f\alpha}\left[\frac{\partial h_f}{\partial \alpha}+\frac{\rho-\rho_f}{\rho_f}\frac{\partial Z}{\partial \alpha}\right]\right)+\frac{\partial}{\partial \beta}\left(\rho K_{f\beta}\left[\frac{\partial h_f}{\partial \beta}+\frac{\rho-\rho_f}{\rho_f}\frac{\partial Z}{\partial \beta}\right]\right)$$
$$+\frac{\partial}{\partial \gamma}\left(\rho K_{f\gamma}\left[\frac{\partial h_f}{\partial \gamma}+\frac{\rho-\rho_f}{\rho_f}\frac{\partial Z}{\partial \gamma}\right]\right)=\rho S_f\frac{\partial h_f}{\partial t}+\theta\frac{\partial \rho}{\partial C}\frac{\partial C}{\partial t}-\overline{\rho} q_s \quad (10)$$

where $K_{f\alpha}$, $K_{f\beta}$, $K_{f\gamma}$ are the freshwater equivalent hydraulic conductivities aligned along the major axes (α, β, γ) of hydraulic conductivity; ρ is the density of the groundwater (M/L^3); ρ_f is the density of freshwater (M/L^3); $\overline{\rho}$ is the density of the water entering through sources or leaving through sinks (M/L^3); q_s is the volumetric flow rate per unit volume of aquifer representing sources and/or sinks (T^{-1}); h_f is the equivalent freshwater head (L); θ is effective porosity; z represents the vertical direction; C is the solute concentration (M/L^3); and S_f is the freshwater equivalent specific storage (1/L) (Langevin et al., 2003).

MODFLOW 2000 solves an equation that conserves volume whereas SEAWAT 2000 solves an equation that conserves mass (Guo and Langevin, 2002). SEAWAT 2000 solves the flow equation in terms of equivalent freshwater head which is defined as the elevation above some datum, z, plus the pressure head (i.e., pressure at the point of calculation divided by the density of the fluid and by the gravity acceleration constant). Once freshwater heads are calculated for the current time step, the flow equation for the next time step is solved. For the current time step, SEAWAT 2000 uses the concentration distribution of the previous time step.

3.2.2 Governing Transport Equation

The governing equation for transport in a porous media is (Zheng and Bennett 1995):

$$R\frac{\partial C}{\partial t}=\nabla\cdot(D\cdot\nabla C)-\nabla\cdot(vC)+\frac{q_s}{\theta}C_s-\lambda\left(C+\frac{\rho_b}{\theta}\overline{C}\right) \quad (11).$$

Where R is the retardation factor:

$$R=1+\frac{\rho_b}{\theta}\frac{\partial\overline{C}}{\partial C} \quad (12)$$

and C is the dissolved concentration [M/L^3], $\overline{C}$ is the sorbed concentration [M/M] which is a function of C and a sorption isotherm, D is the dispersion coefficient tensor [L^2/T], q_s is the flow rate of a fluid source or sink per unit aquifer volume [T^{-1}], C_s is the concentration of the source or sink [M/L^3], λ is the reaction rate constant – assuming first-order irreversible rate reactions, ρ_b is the bulk density of the porous media [M/L^3], and v is the seepage velocity [L/T] which relates the transport governing equation to the flow governing equation through:

$$v=\frac{-K_f}{\theta}\nabla h \quad (13).$$

The same governing transport equation (11) is solved in both MT3DMS and SEAWAT 2000 with the exception that the seepage velocity used in SEAWAT 2000 uses freshwater head (h_f) instead of head (h).

3.2.3 Preliminary Analysis of Significance of Variable Density Flow for the TTLT

Variable density flow has been a topic of recent research investigation (List, 1965; Schincariol and Schwartz, 1990; Oostrom et al., 1992a, 1992b; Paschke and Hoopes, 1984; Schincariol et al., 1994, 1997; Zhang et al., 1998; Barth et al., 2001; Simmons et al., 2001). Much of the discussion in the literature has been on the development of free-convection flow instabilities and on determination of stable verses unstable criteria (List, 1965; Oostrom et al., 1992a; Schincariol et al., 1994, 1997; Barth et al., 2001; Simmons et al., 2001). A flow instability is manifest for a dense plume in less-dense ambient groundwater as finger-like lobes that extend downward. List (1965) analytically defined several dimensionless numbers that distinguished between stable and unstable flow conditions. He concluded that boundaries between two miscible fluids of differing densities were always unstable, but due to the magnitude and wavelength of the instability, it could be considered quasi-stable. Oostrom et al. (1992a) defined other stability criteria for homogeneous media through experiment. Schincariol et al. (1997) considered parameters that determine the stability of stratified flows in variable density systems by furthering List's analytical treatment; they found that permeability, density contrasts (between the tracer or contaminant plume and the ambient groundwater), and dispersion tend to influence the stability of variable density flow. Conditions of low to medium permeability, small density contrasts, and large dispersion lead towards stability while a higher permeability, large density contrasts, and small dispersion will lead to the development and propagation of instabilities (Schincariol et al., 1997).

Oostrom et al. (1992a) experimentally determined a dimensionless parameter for homogeneous porous media, π_1:

$$\pi_1 = \frac{\left(K_{sat}\,\rho_{rel}\right)}{q_x} \tag{14}$$

where K_{sat} is the saturated hydraulic conductivity, ρ_{rel} is the relative density contrast between the dense fluid and the ambient groundwater $\left(\Delta\rho/\rho_0\right)$, and q_x is the average seepage velocity. If π_1 is ≤ 0.3, it indicates stability. Beginning with Oostrom's π_1, Barth et al. (2001) developed a criterion for heterogeneous media:

$$\alpha_2 = \frac{\left(\rho_{rel}\right)}{J_1 - 2\,\sigma_{j1}} \tag{15}$$

where J_1 is the overall hydraulic gradient and σ_{j1} is the standard deviation of the natural gradient. In this regard, the variance of hydraulic gradient is calculated using the hydraulic conductivity spatial statistics:

$$\sigma_{j1}^2 = \frac{\sigma_f^2 J_1^2}{4\pi} \int_1^{-1} \int_0^{2\pi} \frac{-u^4}{\left(u^2\left(1-u^2\right)\left(\sin^2\theta + r^2\cos^2\theta\right)\right)^2}\, d\theta\, du \tag{16}$$

where σ_f^2 is the hydraulic conductivity variance, r is the ratio of the longitudinal hydraulic conductivity correlation length to the vertical hydraulic conductivity correlation length, and u and θ are both variables of integration. As with Oostrom's π_1, α_2 must be $\leq$ 0.3 to indicate stability. Using appropriate values for the BHRS and the TTLT, α_2 was calculated to determine if variable density flow is significant during the TTLT. The α_2 results (listed in the top 8 rows of Table 5) indicate instabilities will arise and variable density flow will need to be included in simulations of the TTLT. Also listed in Table 5 are results of α_2 values determined with mean hydraulic gradients of 0.02 (bottom 2

rows). These α_2 values (from the bottom 2 rows of Table 5) are less then the critical 0.3, but the mean hydraulic gradients are too high for the TTLT between the injection well (B3) and the monitoring well (A1).

Evidence of variable density flow is also seen in the breakthrough curves measured in well A1. In Figure 8, the lower sampling zones (A1-1 through A1-4) show substantial breakthrough and the top of the plume in A1 (A1-14) is below the top of the injection interval in B3 by about 1 m – indicating significant downward movement of the bromide tracer between well B3 and well A1. Numerical modeling runs also examine this question (see section 4.2 below).

Table 5: Results of evaluating the TTLT for the α_2 parameter from Barth et al. (2001). Calculations of α_2 for various correlation lengths and hydraulic gradients of the TTLT. The bottom two rows are α_2 calculations where the mean hydraulic gradient was raised until an α_2 value less than 0.3 was reached.

Horizontal Correlation Length [m]	Vertical Correlation Length [m]	Mean Hydraulic Gradient	Estimated Variance of the Hydraulic Gradient	Lower 95% Hydraulic Gradient	Upper 95% Hydraulic Gradient	α_2
10	1.8	0.001	2.04E-08	0.00071	0.00129	10.59
10	1.8	0.003	1.83E-07	0.00214	0.00386	3.53
10	1.8	0.01	7.33E-07	0.00429	0.00771	1.76
10	1.8	0.01	2.04E-06	0.00715	0.01285	1.06
3	1.0	0.001	2.04E-08	0.00071	0.00129	10.59
3	1.0	0.003	1.83E-07	0.0021	0.0039	3.53
3	1.0	0.01	7.33E-07	0.0043	0.0077	1.76
3	1.0	0.01	2.04E-06	0.0071	0.0129	1.06
10	1.8	0.04	3.26E-05	0.0286	0.0514	0.26
3	1.8	0.04	3.26E-05	0.0286	0.0514	0.26

3.2.4 MODFLOW 2000, MT3DMS, and SEAWAT 2000 Packages

The SEAWAT 2000, MODFLOW 2000, and MT3DMS programs are divided into packages. Each package is a capability or module of the program that may be used depending on the modeling problem. For example, in modeling a pumping test where a river passes through a site and influences the hydrogeologic system, the Well package would be used to describe pumping and the River package would be used to describe the river. Because SEAWAT 2000 is a combination and modification of MODFLOW 2000 and MT3DMS, the packages or modules used in SEAWAT 2000 are the same packages of MODFLOW 2000 and MT3DMS. Table 6 lists the packages that are used in at least one simulation of this study.

3.3 Simulation Environment and Utilities

As noted above, the numerical modeling effort included both a simple uniform gradient (simple boundaries) flow model and a more-detailed complex boundaries flow model and a transport model. This section describes the mechanics of model set-up, information transfer between flow and transport models, model operation, management of output, and analysis and plotting of statistical characteristics of output.

Simulations were run according to the flow chart shown in Figure 14. Thoma et al. (2007) document the simulation process and the reader is referred to that report for a detailed discussion of modeling steps; following is a brief summary of the simulation steps. The first step is development of the input files for the simulations, and this is the most difficult step. The input files for the different modeling packages were created

Table 6: MODFLOW 2000, MT3DMS, and SEAWAT 2000 packages used in at least one simulation. For a complete description of the packages see Zheng (2005), Zheng and Wang (1999), Harbaugh et al. (2000), and Langevin et al. (2003).

MODFLOW 2000, MT3DMS, or SEAWAT 2000 package	Description/purpose
Discretization	Spatial and temporal discretization of the modeling domain.
Layer Property Flow	These packages define the hydrogeologic properties of the model.
Hydrogeologic Unif Flow	
Basic	This package defines the active cells in the finite difference grid of the flow model.
Well	Defines the well cells and the pumping/injection rates of the model
Evapotranspiration	Defines the evapotranspiration cells of the model.
Output Control	Defines when flow and head values will be saved/printed to file or standard output.
Observation	Defines when the heads will be saved during the simulation.
General Head Boundary	Defines the general head boundary cells of the model.
Constant-Head Boundary	Defines the constant head boundary cells of the model.
River	Defines the river cells of the model.
Preconditioned Conjugate-Gradient	These two packages solve the system of finite difference flow equations.
Geometric Multigrid Solver	
Basic Transport	Defines the active transport cells in the model and the porosity in each cell of the model.
Advection	Defines how advection is treated in the model.
Dispersion	Defines the dispersion of the model.
Source and Sink Mixing	Defines the sources and sinks within the model.
Generalized Conjugate Gradient	This is the transport solver package.
Transport Observation	This defines when the concentrations of selected cells are saved during the simulation.
Variable Density Flow	This package defines the relationship of the concentration to the density of the fluid
Horizontal Flow Barrier	This package defines horizontal barriers to flow between cells.

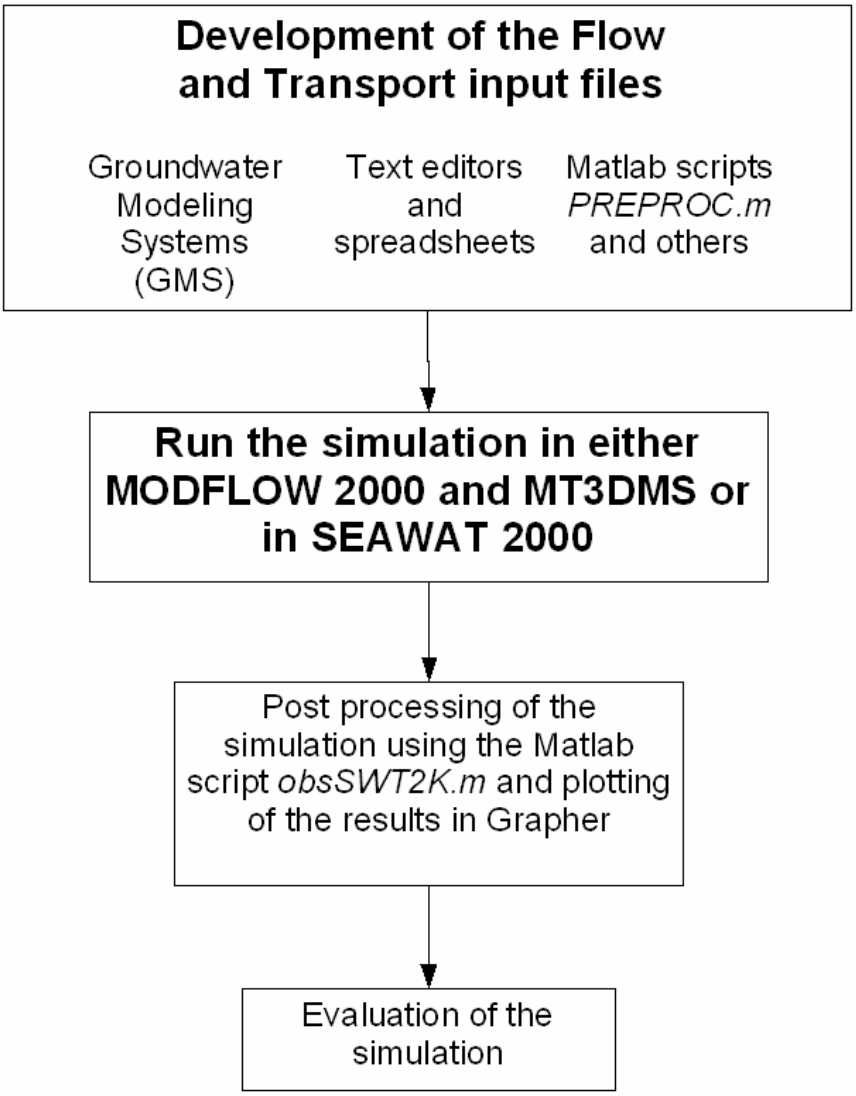

Figure 14: Flow chart of the development and analysis of each simulation.

using Groundwater Modeling Systems (GMS), text editors, spreadsheet programs, and Matlab scripts. The Matlab script PREPROC.m (included on the CD with its documentation) is a custom utility, developed as part of this thesis research, that has been used to generate many of the simulation input files. Also simulations were run and post-processed using the Matlab script obsSWT2K.m (included on the CD). Plots of simulated and observed breakthrough, simulated and observed head changes in the C wells and in well B3, plume slices, and summary transport statistics were created using the Matlab script obsSWT2K.m and Grapher for analysis of results from a given simulation.

3.4 Descriptions of Flow Approaches

In this section the two basic flow approaches will be described: their development, and essential features (model structure). The two flow model approaches are the uniform gradient (simple boundaries) flow modeling approach and the complex boundaries flow modeling approach. The uniform gradient approach was developed to investigate what transport behavior could be described through a simple conceptual model of the BHRS. Subsequent to developing this approach, more complexities were added to the modeling: the Boise River, and specified head boundaries developed from a larger more regional model. The two flow approaches were developed as a natural progression of increasing complexity in the modeling from the simpler uniform gradient approach to the complex boundaries flow approach.

3.4.1 Uniform Gradient (Simple Boundaries) Flow Modeling Approach

Figure 7 shows the water level contours at the BHRS during the summer months. From this map, a background site hydraulic gradient can be estimated as ~0.00125 m/m in a direction of approximately N45°W. Using this hydraulic gradient, a modeling domain for the BHRS was designed as seen in Figure 15. Boundaries to this model are no-flow boundaries parallel to flow and constant head boundaries perpendicular to flow. The steady state solution of this model – with homogeneous hydrogeologic properties and without pumping, injection, or other stresses – yields a planar potentiometric surface with hydraulic gradient ~0.00125 m/m in a direction approximately N45°W across the entire BHRS which is used to provide initial heads for simulations using this framework.

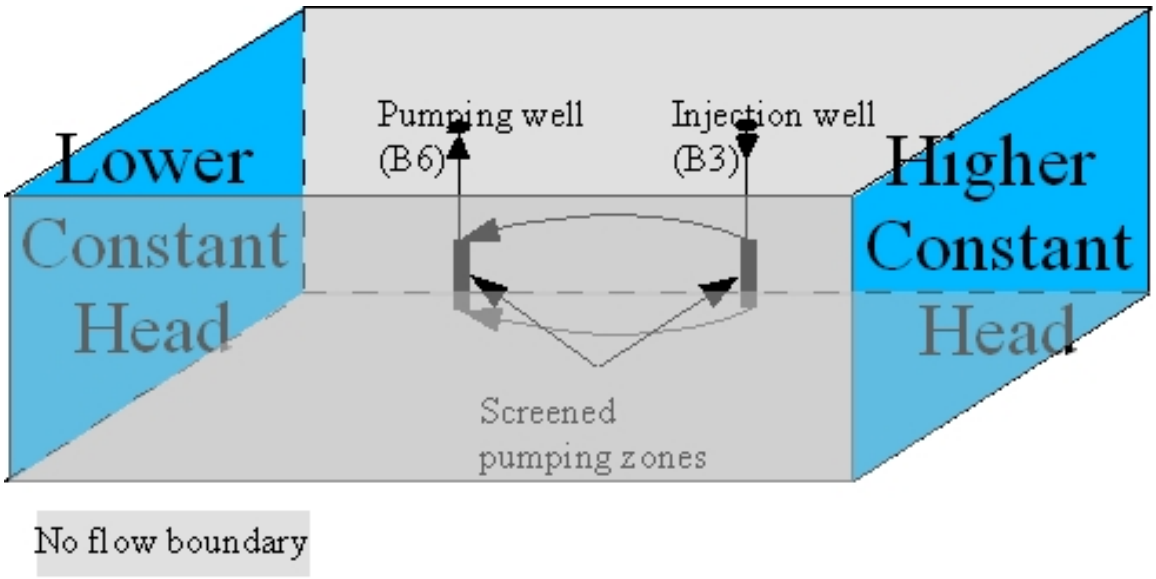

Figure 15: Conceptual model for the uniform gradient (simple boundaries) flow approach showing constant head boundaries, no flow boundaries, and injection and pumping wells.

3.4.1.1 Grid Cell Discretization

Maximum model cell discretization in the central well field of the BHRS was calculated using:

$$Pe = \frac{x_g}{\alpha_L} \quad (17)$$

where Pe is the grid Peclet number (unitless), x_g is the grid cell size (L), and α_L is the longitudinal dispersivity (L). To reduce numerical dispersion Zheng and Bennett (1995) suggest a grid Peclet number ≤ 2. Using some preliminary estimates of the longitudinal dispersivity determined from the semi-analytical analysis of the breakthrough curves, a maximum grid cell size was determined to be 0.2 m. This grid spacing was used in the inner well field of the BHRS – within and around the C wells. Outside this finely gridded region the grid cell size increases progressively by an expansion factor of 1.43. The vertical discretization is 0.25 m per model layer over the sampling zones of well A1 and then increases progressively by an expansion factor of 1.2 above and below this zone. The grid discretization in the central well field (within the C wells) is the same as that used by Leven et al. (2002) based on a similar analysis. A copy of a MODFLOW 2000 discretization file is included in Appendix B. The spatial discretization yielded a finite difference grid of 40 layers, 120 rows, and 110 layers. Figure 16 shows a mapview of the grid used in this flow approach.

3.4.1.2 Time Discretization

Fifteen stress periods are used in this uniform hydraulic gradient flow approach. The first stress period is a steady state stress period used to get initial heads – there is no injection or withdrawal in this stress period. The remaining 14 stress periods coincide with injection, pumping, or no-stress times during the TTLT as listed in Table 2. Each stress period is further divided into expanding time steps. The first time step of a given

stress period is small with subsequent time steps either 1.2 or 1.5 times larger then the previous time step (depending on the stress period). A copy of a MODFLOW 2000 discretization file showing time discretization is included in Appendix B.

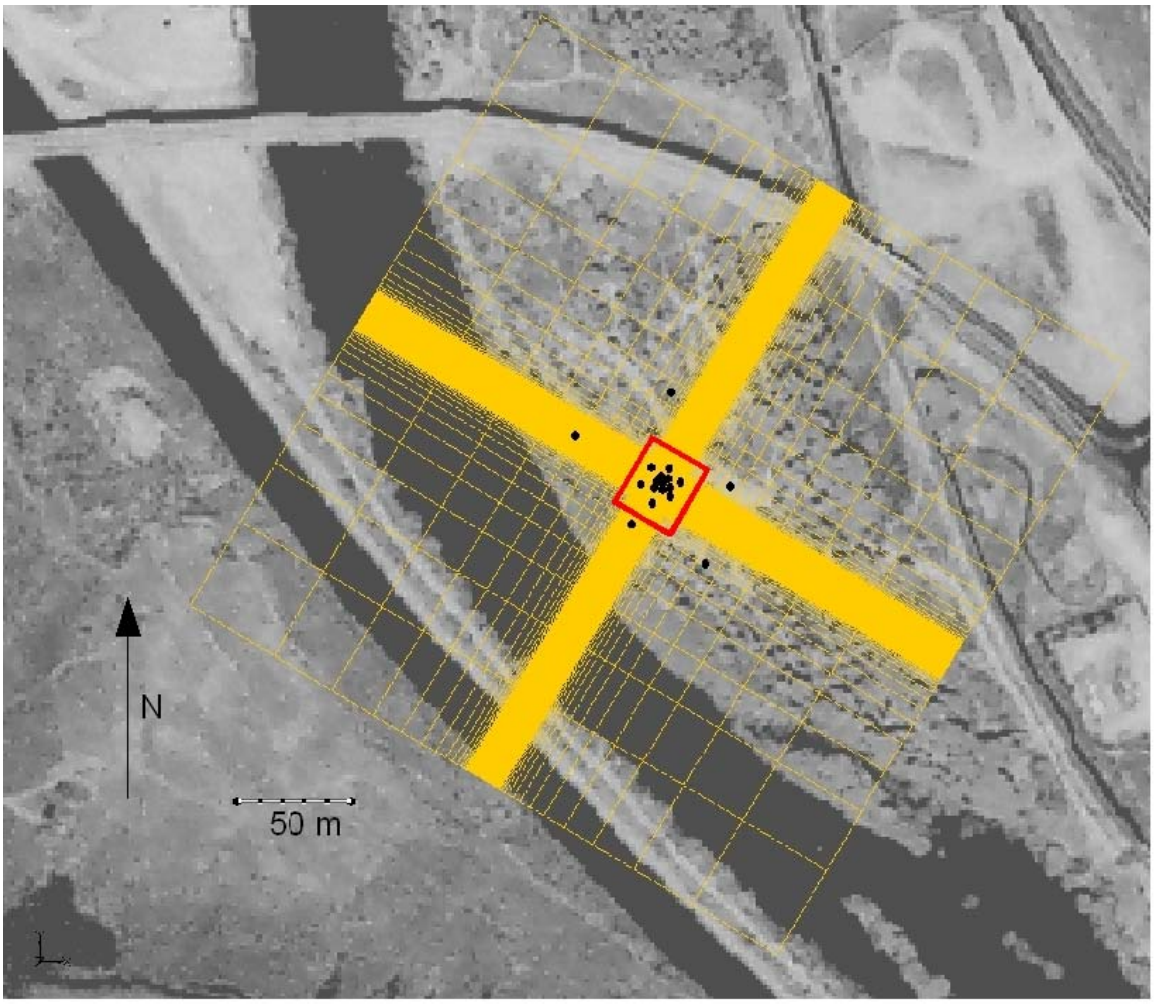

Figure 16: Uniform gradient flow approach modeling grid with satellite image showing gravel bar with BHRS and Boise River. The red box indicates the cells that are active in the transport model.

3.4.1.3 Boundary Conditions

As described above (beginning of section 3.4.1) and seen in Figures 15 and 16, the northwest and southeast sides of this grid contain constant head cells and the northeast and southwest sides of the grid contain no-flow cells; this configuration, when run steady state as in the first stress period of this flow approach, produces a uniform hydraulic gradient of 0.00125 m/m across the site in the direction of N45°W.

3.4.1.4 Flow Model Characteristics

This uniform hydraulic gradient flow approach was used with various hydrostratigraphic configurations ranging from: homogeneous hydrogeologic properties throughout the flow field to several layered hydrostratigraphies with each hydrostratigraphic layer having homogeneous hydrogeologic properties throughout the layer, but varying from layer to layer. The various hydrostratigraphies were implemented through the use of the Layer Property Flow (LPF) package or the Hydrogeologic Unit Flow (HUF) package of MODFLOW 2000/SEAWAT 2000. The LPF package was used for simulations where the modeling domain was homogeneous and for the case where each model layer was considered as a separate hydrostratigraphic layer. Whenever layering was introduced in the simulations (other than the case mentioned above), each layer was defined using a hydrogeologic unit of the HUF package. Contacts between layers were determined based on kriging from porosity unit picks at wells (Clemo, unpublished).

Injection and pumping stresses are included in this flow approach as listed in Table 2 and seen in Figure 6. Injection and pumping were implemented through the use of the Well package. When injection and/or pumping occurred over several model layers, the injection/pumping for a given layer was determined based on the layer's thickness and its hydraulic conductivity:

$$Q_i = \frac{K_i b_i}{\sum K_i b_i} Q_{tot} \tag{18}$$

where Q_i is the pumping or injection rate of the well for layer i, K_i is the hydraulic conductivity of layer i, b_i is the layer thickness of layer i, and Q_{tot} is the total pumping or injection rate.

The aquifer at the BHRS is unconfined and has a thickness of 16-18 m which is the saturated thickness from the water table to the clay layer under the site (Barrash et al., 1999). The flow modeling domain extends about 140 m beyond the central well field (C wells) as seen in Figure 16. This modeling domain extends beyond the Boise River, but the river is not included in this flow approach.

3.4.2 Complex Boundaries Flow Modeling Approach

The complex boundaries flow approach uses the same grid cell discretization and time discretization (stress periods) as the uniform gradient (simple boundaries) flow modeling approach (see sections 3.4.1.1 and 3.4.1.2 respectively). This modeling approach incorporates more-complex boundaries: (a) the Boise River, assumed to be a groundwater divide; (b) no-flow boundaries; (c) constant head boundaries; and (d)

general head boundaries. The development of these boundaries will be discussed below. In particular, the constant head boundaries and general head boundaries were calculated from a MODFLOW 2000 flow model of the entire gravel bar that contains the BHRS. The river boundary will be discussed first followed by the large gravel bar model from which heads for the constant head boundaries and the general head boundaries were derived.

3.4.2.1 River as a Groundwater Divide

As noted above, the BHRS lies on a gravel bar adjacent to the Boise River. The Boise River is assumed to act as a groundwater divide; Figure 17 shows a cross section of an idealized river-as-a-groundwater divide where the river is a loosing river and so groundwater flow occurs down and away from the river.

The river boundary is implemented through the River and Flow packages of SEAWAT 2000. Boundary cells along the top of the modeling domain are assigned as river cells through the River package. These cells are assigned a riverbed conductance, river stage, and riverbed elevation. The riverbed conductance for a given river cell (i,j,k) is determined through:

$$C_{river} = L_{river;i,j,k} \cdot W_{river;i,j,k} \cdot RB_{thick;i,j,k} \cdot K_{riverbed} \qquad (19)$$

where C_{river} is the river conductance, $L_{river;i,j,k}$ is the length of the river within cell (i,j,k), $W_{river;i,j,k}$ is the width of the river within cell (i,j,k), $RB_{thick;i,j,k}$ is the riverbed thickness within cell (i,j,k), and $K_{riverbed}$ is the vertical hydraulic conductivity of the riverbed.

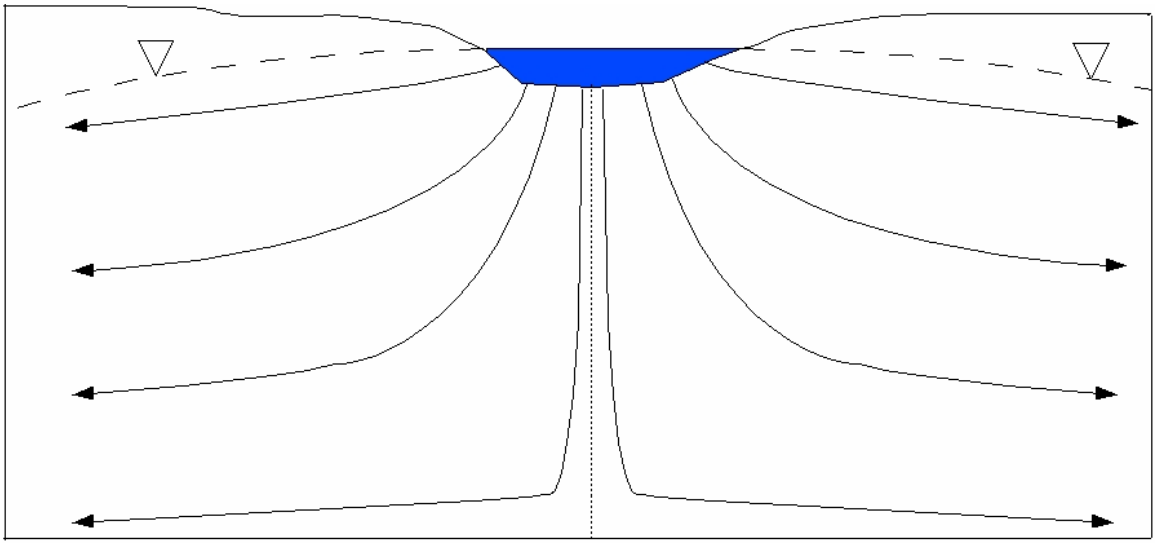

Figure 17: Idealized cross section of a river acting as a groundwater divide.

The riverbed sediments of the Boise River adjacent to the BHRS are cobbles and sands and it is assumed that there are few fines in the riverbed sediments. These riverbed sediments would have a high hydraulic conductivity based on the general lack of fines observed and the relatively rapid leakage response from the river under low induced gradients during pumping tests at the BHRS (Barrash, unpublished data). This assumption about the riverbed hydraulic conductivity yields large values for the riverbed conductances in the river cells and high connectivity between the river and the underlying aquifer.

The SEAWAT 2000 River package allows for river stages to vary from cell to cell and from stress period to stress period. The change in river stage was measured during the TTLT by a pressure transducer placed in the river. Figure 11 shows the change in river stage measured during the TTLT including both the uncorrected and the corrected "fisherman bump" changes in stage. The "fisherman bumps" were instances where the

transducers were bumped – presumably by fishermen – causing a step change in river stage. Figure 18 shows only the corrected change in stage measured in the river.

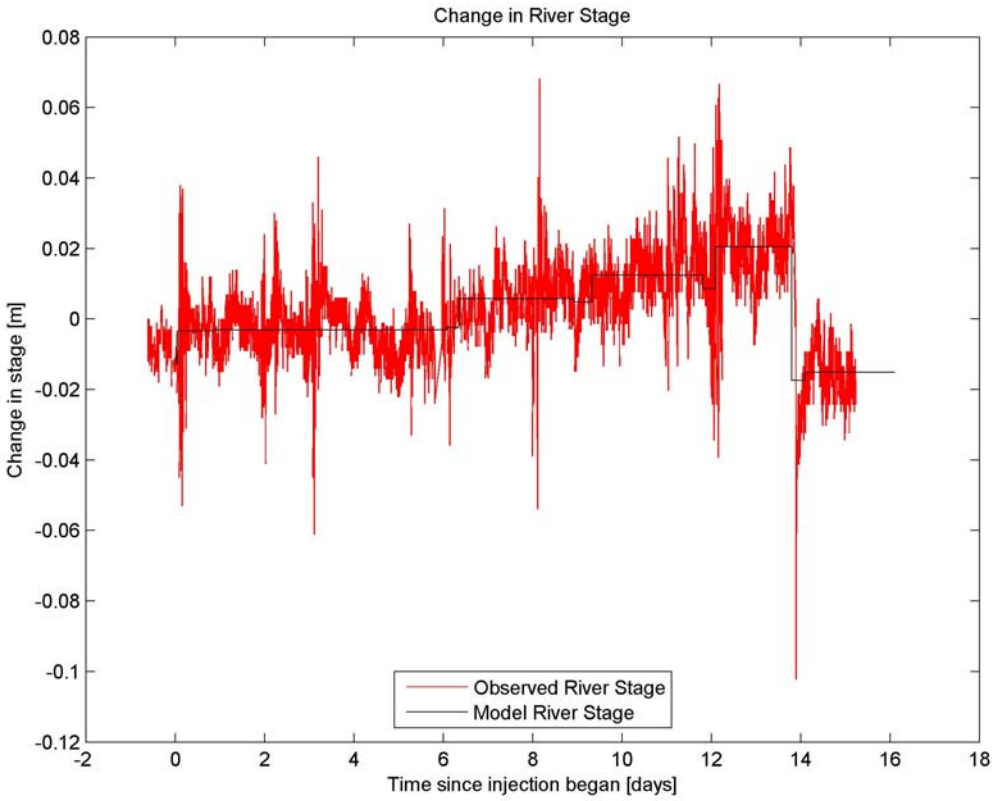

Figure 18: Adjusted change in river stage during the TTLT (see Figure 11). The black line indicates the value used in modeling for a given stress period.

The riverbed elevation in the River package of SEAWAT 2000 is set to ~1.5 meters below the initial river stage. Initial river stage was estimated by manually extrapolating water-level contours to points along the river. Because the modeling domain is finely discretized, the actual river extends beyond the cells along the boundary. The river extent is therefore implemented in the Flow package of SEAWAT 2000 – either with the HUF package or the LPF package. When the HUF package is used, a separate hydrogeologic unit is defined for the river with high hydaulic conductivity (10 m/s) and a

porosity and specific yield equal to 1. When the LPF package is used, the model cells that lie within the river are given the same high hydraulic conductivity (10 m/s), and porosity and specific yield equal to 1.

3.4.2.2 Gravel Bar Model

Figure 19 shows the extent of the MODFLOW 2000 gravel bar model. Boundaries for this model consist of the river along the southwest side, constant head boundary along the southeast side, and no flow boundaries along the northeast and northwest sides. The river was added as explained in the previous section and was assumed to be a groundwater divide: river defined through the River package and either the LPF or HUF package with the boundary cells below the river set as no-flow cells. The constant head boundaries changed from stress period to stress period – this change mimicked the change in river stage observed during the TTLT. The hydrogeologic properties for most of the modeling domain were the average of Units 2 and 3 and are described in section 3.6 – Model Parameterization. Unit 5 was also added to the gravel bar model.

Initial heads were determined by setting the boundary conditions and running the model in steady-state. Observed and calculated heads from the C and X wells from July 29, 2001 were compared as calibration of the model. Figure 20 shows the observed versus calculated heads in the C and X wells for the gravel bar model. Once calibrated, the simulation was run through the entire time of the TTLT with heads saved for use in

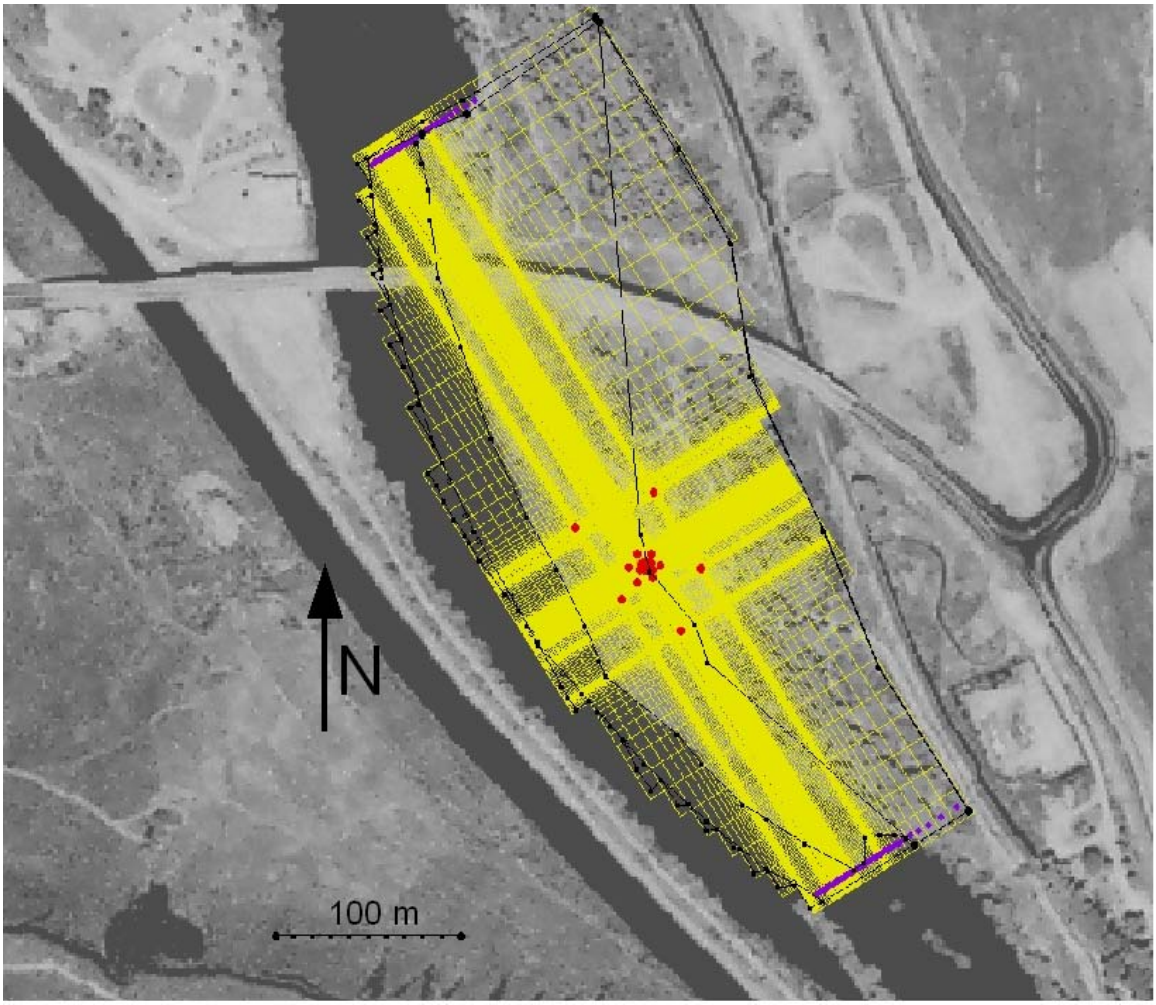

Figure 19: Satellite image of the BHRS and Boise River with an overlay of the Gravel Bar model. The wells of the BHRS are shown in red. The modeling grid is shown in yellow. The purple squares are the constant head cells.

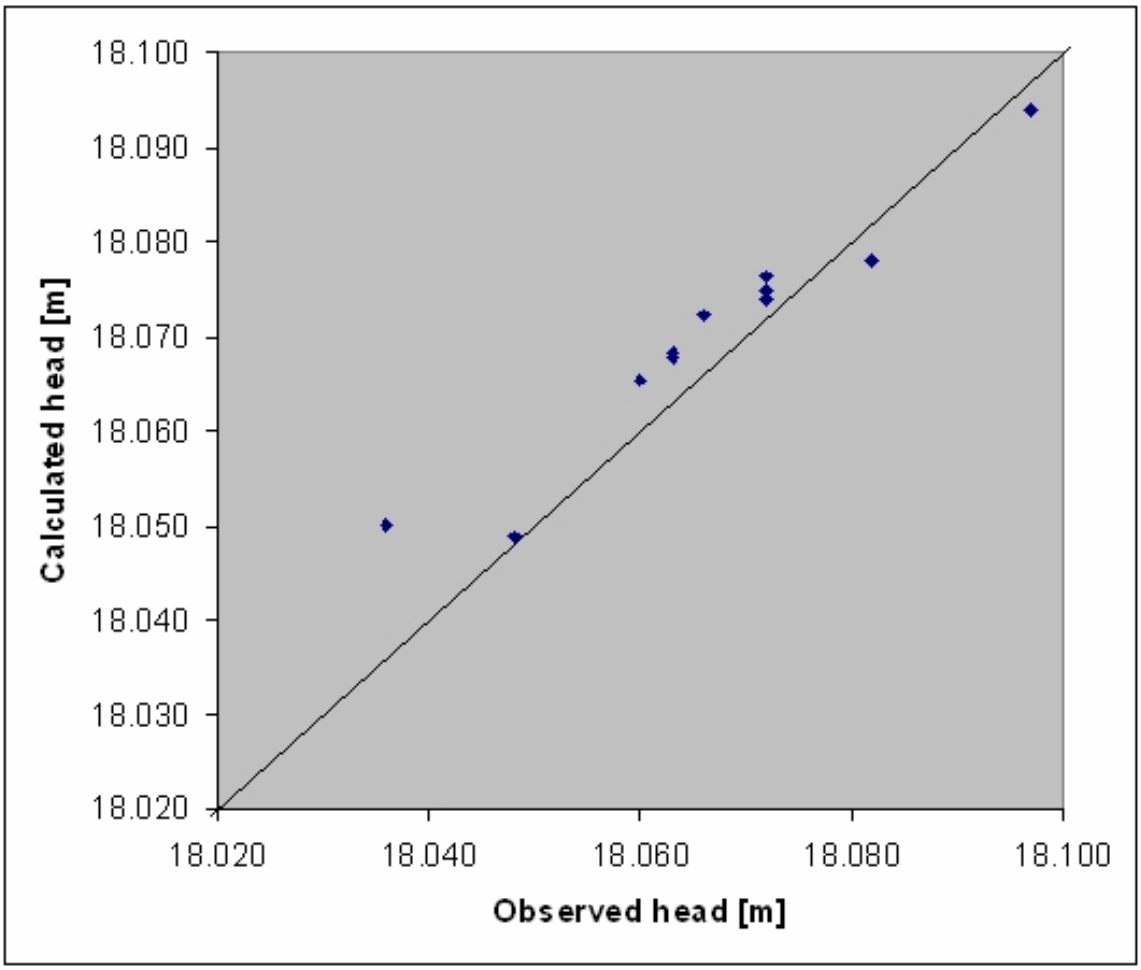

Figure 20: Observed vs. calculated heads in the C and X wells for July 29, 2001. Simulated heads are from the Gravel Bar model, and the observed heads were measured in the C and X wells on July 29, 2001.

general head boundaries and for constant head boundaries in the complex boundaries flow modeling approach.

3.4.2.3 Flow Model Characteristics in the Complex Boundaries Approach

The river was included in this flow approach. Constant heads and general head boundaries were also included and derived from the gravel bar model. Figure 21 shows the modeling grid of this approach with the boundaries as indicated in the figure; it should be noted that the same modeling grid was used in both the uniform gradient approach and the complex boundaries approach.

This flow approach was used with various hydrostratigraphies ranging from homogeneous hydrogeologic properties throughout the flow field, to several layered hydrostratigraphies with each layer having homogeneous hydrogeologic properties throughout the layer (but varying from layer to layer), and to a layered hydrostratigraphy with each layer's hydrogeologic properties varying within it according to its geostatistics. The various hydrostratigraphic configurations were implemented through the use of the LPF package and the HUF package of SEAWAT 2000.

Injection and pumping stresses (Table 2, Figure 6) were implemented through the use of the Well package.

The aquifer is unconfined with a saturated thickness between 21 m and 16 m depending on the simulation and the degree to which the topography of the basal clay is included (Barrash et al., 2002; Reboulet and Barrash, 2003; Reboulet 2003).

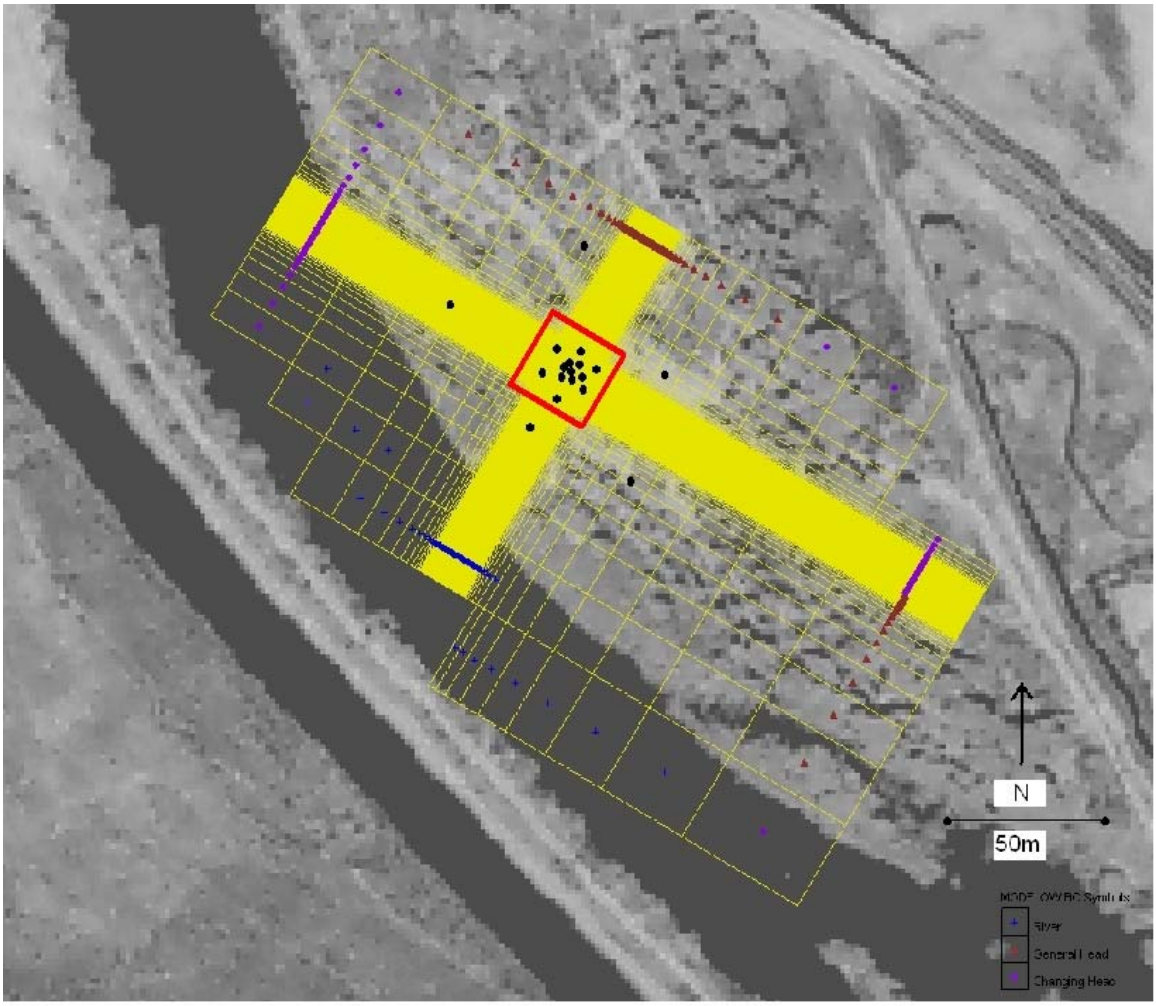

Figure 21: Complex boundaries flow modeling grid with satellite image showing gravel bar with BHRS and Boise River. The red box indicates the cells that are active in the transport model.

3.4.3 Injection (Well B3), Pumping (Well B6), and Sampling from Sampling Zones

Injection, pumping, and sampling in all of the wells was included in both of the flow approaches. Pumping and injection occurred from the packed off zones of wells B3 and B6 as shown in Figures 4 and 5. Injection and pumping rates are shown in Figure 6. The causes and lengths of pumping stoppage are listed in Table 2. All sampling zones

shown in Figure 4 were pumped at a rate of ~5 mL/min when not sampling and at ~30 mL/min during sampling events of the TTLT. To implement the sampling in the simulations, all sampling zones are pumped at a continuous 5 mL/min sampling rate throughout the test.

The sampling, pumping, and injection were all implemented in the simulations using the Well package in MODFLOW 2000/SEAWAT 2000. Because the injection, pumping, and some sampling zones extend over several model layers, pumping or injection rates are weighted according to the hydraulic conductivity and the vertical thickness of the cell using equation 18.

Boreholes can have a significant effect on flow and transport. To implement boreholes and packers within various simulations the hydrogeologic properties of the cells corresponding to a bore hole where changed to reflect the bore hole or packer; i.e. a higher vertical hydraulic conductivity, porosity, and specific yield were assigned to model cells with a bore hole and a lower vertical hydraulic conductivity, porosity, and specific yield were assigned to model cells with a packer in them.

3.5 Transport Modeling Approach

Irrespective of which flow approach was used, the same transport modeling approach was used. The transport modeling domain is within the central well field as seen by the red box in Figures 16 and 21.

3.6 Model Parameterization

3.6.1 Hydraulic Conductivity

Several methods were used to determine distributions of hydraulic conductivity for simulations. Among those is the semi-analytical method described above. Most of the others involve a subset and/or average of a data set of hydraulic conductivities derived from a modified form of the Kozeny-Carman empirical relationship (Kozeny, 1927; Carman, 1937):

$$K_{KC} = \frac{\rho g}{\mu} \cdot \frac{\theta^3 d_e^2}{180 \cdot (1-\theta)^2} \qquad (20).$$

where K_{KC} is the Kozeny-Carmen hydraulic conductivity, ρ is the density, g is the gravitational constant, μ is the dynamic viscosity at 15˚ C, θ is the porosity, and d_e is the effective grain size and is d_{10}. Equation 20 is modified such that the estimated K is multiplied by the fraction of the total volume that is matrix (P_m):

$$K = K_{KC} \cdot P_m \qquad (21);$$

because it is assumed that there is no flow through the cobbles or large grains. This reduces the estimated hydraulic conductivity values.

Grain size distribution (GSD) analyses on well core samples collected at the BHRS were run by Reboulet (2003). Porosity data were taken from porosity well logs at the BHRS. Hydraulic conductivity estimates in the wells were then calculated using equation 21 (Heinz et al., 2003; Hughes, 2005; Barrash et al., in prep.).

3.6.2 Porosity/Specific Yield

For many simulations run for this study, porosity and specific yield values were taken to be the porosity values reported by Barrash and Clemo (2002). Effective porosity and specific yield are taken to be the same as porosity values because the aquifer consists of coarse grained sediments with virtually no silt or clay. Porosity estimates for simulations with hydrostratigraphies different from the porosity units described by Barrash and Clemo (2002) were derived from a subset and/or averages of the porosity logs taken from wells at the BHRS.

3.6.3 Vertical Hydraulic Conductivity Anisotropy

Analysis of fully penetrating pumping tests conducted at the BHRS yield vertical hydraulic conductivity anisotropy at 1 or nearly at 1 (Fox, 2006). Five simulations were also run with vertical hydraulic conductivity anisotropy (K_H/K_V) varying from 1 to 4 to test the effect on transport.

3.6.4 Specific Storage

Analysis of fully penetrating pumping tests conducted at the BHRS yield specific storage estimates between wells B3, A1, and B6 of ~0.000045 m^{-1} (Fox, 2006). These values were used in the simulations. Similar values are reported in Bohling et al. (2007) for an unconsolidated sand with gravel aquifer.

3.6.5 Dispersivity and Dispersion

The longitudinal dispersivities used in the simulations were estimated from the analytical evaluation of the bromide breakthrough curves measured in A1 (see section 3.1) and were implemented using the dispersion package of MT3DMS/SEAWAT 2000. Transverse and vertical dispersivities were taken to be 10% and 1% of the longitudinal dispersivities, respectively (e.g. Domenico and Schwartz, 1998). For most simulations reported in this thesis, the dispersivities are homogeneous throughout the modeling domain.

3.7 Summary Transport Statistics Used to Determine "Goodness of Fit"

This thesis shows how additional information (i.e. increased complexity in the conceptual model) affects the match of model results to the observed field data. Because one statistic such as the sum of the squared residuals of the observed and simulated breakthrough curves might mask details (e.g., if breakthrough magnitudes are close, but timing is off, this will not be seen in a sum of squared residual metric) a set of transport summary statistics similar to those used by Scheibe and Chien (2003) have been adopted. In addition to these metrics, observed and calculated head changes in the C wells and in well B3 are plotted to see how observed and calculated head changes compare. Table 7 lists the calculated statistics for the breakthrough curves measured in sampling zones A1-1 through A1-12. Transport statistics from these sampling zones are calculated because it is only in these zones that detectable breakthrough is observed (Figure 8).

Table 7: Metrics calculated from the observed breakthrough curves of sampling zones A1-1 through A1-12. TCM is the Time to Center of Mass; PC is the normalized Peak Concentration; TP is the Time to Peak concentration; R 0.075 Q is the time to when the normalized concentration first rose above 7.5% of the injected concentration; F 0.075 Q is the time when the normalized concentration last fell below 7.5% of the injected concentration; M is the calculated Mass under the Breakthrough Curve; α_L is the calculated effective longitudinal dispersivity.

Summary Statistic							
Sampling Zone	TCM [days]	PC [g/l]	TP [days]	R 0.075 Q [days]	F 0.075 Q [days]	M [kg]	α_L [m]
A1-12	11.82	0.41	11.97	0.97	15.97	1.15	0.09
A1-11	11.41	0.55	12.14	0.97	15.97	1.77	0.11
A1-10	11.09	0.72	12.14	0.97	15.97	2.46	0.12
A1-9	11.54	0.95	10.64	1.31	15.97	3.04	0.11
A1-8	12.37	1.79	10.64	1.56	15.81	5.33	0.13
A1-7	12.05	1.95	10.64	5.81	15.64	6.47	0.11
A1-6	12.05	2.05	10.64	5.68	15.64	7.33	0.11
A1-5	11.48	2.15	12.14	5.14	14.64	7.52	0.12
A1-4	11.04	1.70	9.64	4.64	15.30	5.74	0.13
A1-3	10.37	1.84	9.47	5.14	14.80	6.45	0.13
A1-2	10.63	1.76	8.97	4.97	15.14	5.41	0.12
A1-1	10.25	1.70	8.97	5.68	14.64	5.26	0.13

The transport summary statistics are:

- Time to Center of Mass (TCM) represents the mean time that the bromide tracer takes to reach the sampling zone. This statistic is used to show the timing of the plume as it passes by well A1.
- Peak Concentration (PC) is the maximum concentration normalized by the injection concentration. This statistic is a measure of the relative magnitude of breakthrough.
- Time to Peak (TP) is the time from the beginning of injection in well B3 until the Peak Concentration was measured. This statistic shows the timing of the plume as

it passes by well A1 although this statistic is complicated by the presence of a second peak observed in many of the sampling zones.

- Time to the first concentration above 7.5 % of the injection concentration (R 0.075 Q) is the time at which the concentration first rises above 7.5% of the injection concentration. This statistic and the time where the concentration falls below 7.5% of the injection concentration show the overall spread of the tracer plume.
- Time where the concentration falls below 7.5 % of the injection concentration (F 0.075 Q) is the time at which the concentration falls below 7.5% of the injection concentration. This statistic and the time to the first concentration above 7.5% of the injection concentration show the overall spread of the tracer plume.
- Mass under the Breakthrough Curve (M) is the area under the breakthrough curve determined by integrating the measured concentrations over time. This statistic and the Peak Concentration statistic show the magnitude of breakthrough passing a given sampling zone.
- Estimated effective dispersivity (α_L) is the effective dispersivity as estimated by Sauty's (1977) 1D breakthrough curve analysis technique (see section 3.1). This statistic, along with the time to the first concentration above 7.5% of the injection concentration and the time where the concentration falls below 7.5% of the injection concentration show the spread of the plume.

4 RESULTS

This chapter presents results of the flow and transport simulations run to examine the effects of including various boundary, hydrologic, stratigraphic, and system stress conditions. Results are given as descriptions and as statistical metrics of the simulated breakthrough curves compared with statistical metrics from the measured breakthrough curves in the sampling zones of well A1 (Table 3). Table 8 lists the simulations that were conducted in this study along with the varying complexities within each simulation and the hydrogeologic properties for hydrostratigraphic subdivisions within the models (i.e., stratigraphic layers and/or lenses). More thorough descriptions of each of the simulations are given in Appendix C.

For all the simulations listed in Table 8, plots of observed and simulated breakthrough curves from the sampling zones in well A1 and plots of changes in head in well B3 and in the C wells are included on the CD accompanying this thesis.

4.1 Semi-Analytical Fitting of the Breakthrough Curves Measured in Well A1

As discussed in the previous chapter (section 3.1), the type curve fitting method described by Sauty (1977) and Käss (1998) was applied to the breakthrough curves measured in the sampling zones of well A1. Because only the bottom 12 sampling zones of well A1 (A1-1 through A1-12) showed significant breakthrough, only these 12 breakthrough curves were analyzed in this manner. Figure 22 shows the type curve fits

Table 8: Simulations run in this study, their hydrogeologic properties, and the various complexities included in each simulation.

Hydrogeologic Properties of the Simulations Run using the Uniform Gradient Flow Model approach						
Simulation Name	Layer	K [m/s]	Vertical K Anisotropy [VK/HK]	Porosity or Specific Yield	Longitudinal Dispersivity (α_L) [m]	Specific Storage [m^{-1}]
Unit 2-3 Ave	Homogeneous throughout the modeling domain	0.000305	1.0	0.213	0.10	0.000045
Unit 2	Homogeneous throughout the modeling domain	0.000394	1.0	0.240	0.10	0.000045
Unit 3	Homogeneous throughout the modeling domain	0.000107	1.0	0.172	0.10	0.000045
Unit 2-3	Unit2	0.000394	1.0	0.240	0.10	0.000045
	Unit3	0.000107	1.0	0.172	0.10	0.000045
Units 2a, 2b, and 3	Unti2a	0.0000759	1.0	0.244	0.10	0.000045
	Unit2b	0.0000502	1.0	0.210	0.10	0.000045
	Unit3	0.0000447	1.0	0.172	0.10	0.000045

Table 8: (Continued) Simulations run in this study, their hydrogeologic properties, and the various complexities included in each simulation.

Hydrogeologic Properties of the Simulations Run using the Uniform Gradient Flow Model approach						
Simulation Name	Layer	K [m/s]	Vertical K Anisotropy [VK/HK]	Porosity or Specific Yield	Longitudinal Dispersivity (α_L) [m]	Specific Storage [m^{-1}]
Many Horizontal Units	40 (Bottom)	0.0000579	1.0	0.187	0.09	0.000045
	39	0.0000575	1.0	0.185	0.09	0.000045
	38	0.0000590	1.0	0.190	0.09	0.000045
	37	0.0000572	1.0	0.184	0.09	0.000045
	36	0.0000564	1.0	0.182	0.09	0.000045
	35	0.0000615	1.0	0.198	0.09	0.000045
	34	0.0000695	1.0	0.224	0.09	0.000045
	33	0.0000759	1.0	0.244	0.09	0.000045
	32	0.0000729	1.0	0.235	0.09	0.000045
	31	0.0000741	1.0	0.239	0.09	0.000045
	30	0.0000772	1.0	0.249	0.09	0.000045
	29	0.0000802	1.0	0.258	0.09	0.000045
	28	0.0000781	1.0	0.251	0.08	0.000045
	27	0.0000767	1.0	0.247	0.10	0.000045
	26	0.0000723	1.0	0.250	0.10	0.000045
	25	0.0000642	1.0	0.263	0.09	0.000045
	24	0.0000631	1.0	0.266	0.10	0.000045
	23	0.0000560	1.0	0.240	0.10	0.000045
	22	0.0000518	1.0	0.209	0.10	0.000045
	21	0.0000502	1.0	0.205	0.12	0.000045

Table 8: (Continued) Simulations run in this study, their hydrogeologic properties, and the various complexities included in each simulation.

Hydrogeologic Properties of the Simulations Run using the Uniform Gradient Flow Model approach						
Simulation Name	Layer	K [m/s]	Vertical K Anisotropy [VK/HK]	Porosity or Specific Yield	Longitudinal Dispersivity (α_L) [m]	Specific Storage [m^{-1}]
Many Horizontal Units	20	0.0000504	1.0	0.203	0.12	0.000045
	19	0.0000477	1.0	0.195	0.12	0.000045
	18	0.0000452	1.0	0.201	0.10	0.000045
	17	0.0000505	1.0	0.211	0.11	0.000045
	16	0.0000467	1.0	0.198	0.11	0.000045
	15	0.0000430	1.0	0.184	0.11	0.000045
	14	0.0000421	1.0	0.178	0.11	0.000045
	13	0.0000414	1.0	0.176	0.11	0.000045
	12	0.0000397	1.0	0.169	0.11	0.000045
	11	0.0000374	1.0	0.159	0.11	0.000045
	10	0.0000380	1.0	0.162	0.11	0.000045
	9	0.0000408	1.0	0.173	0.11	0.000045
	8	0.0000460	1.0	0.195	0.11	0.000045
	7	0.0000457	1.0	0.194	0.11	0.000045
	6	0.0000468	1.0	0.199	0.11	0.000045
	5	0.0000513	1.0	0.218	0.11	0.000045
	4	0.0000491	1.0	0.209	0.11	0.000045
	3	0.0000447	1.0	0.190	0.11	0.000045
	2	0.0000495	1.0	0.210	0.11	0.000045
	1 (Top)	0.0000624	1.0	0.265	0.11	0.000045

Table 8: (Continued) Simulations run in this study, their hydrogeologic properties, and the various complexities included in each simulation.

Hydrogeologic Properties of the Simulations Run with More Complex Boundary Flow Model approach.						
Simulation Name	Layer	K [m/s]	Vertical K Anisotropy [VK/HK]	Porosity or Specific Yield	Longitudinal Dispersivity (α_L) [m]	Specific Storage [m^{-1}]
U23A	Homogeneous throughout the modeling domain	0.000305	1.0	0.213	0.10	0.000045
	Complexities*:	WB				
TwL	Unit 2	0.000373	1.0	0.240	0.10	0.000045
	Unit 3	0.000102	1.0	0.172	0.10	0.000045
	Complexities*:	WB				
ThL	Unit 2a	0.000280	1.0	0.244	0.10	0.000045
	Unit 2b	0.000235	1.0	0.251	0.10	0.000045
	Unit 3	0.000190	1.0	0.184	0.10	0.000045
	Complexities*:	WB				
ThLO	Unit 2a	0.0000759	1.0	0.244	0.10	0.000045
	Unit 2b	0.0000502	1.0	0.210	0.10	0.000045
	Unit 3	0.0000447	1.0	0.172	0.10	0.000045
	Complexities*:	WB				

Table 8: (Continued) Simulations run in this study, their hydrogeologic properties, and the various complexities included in each simulation.

Hydrogeologic Properties of the Simulations Run with More Complex Boundary Flow Model approach.						
Simulation Name	Layer	K [m/s]	Vertical K Anisotropy [VK/HK]	Porosity or Specific Yield	Longitudinal Dispersivity (α_L) [m]	Specific Storage [m^{-1}]
Five Layer simulations: FL, FLw, FLwsc, FLwS63, FLwS3, FLwS6, FLwa, FLwab1, FLwab2, FLpor1, FLpor2, and FLpor3.	Unit 1	0.000148	1.0	0.180	0.10	0.000045
	Unit 2	0.000373	1.0	0.240	0.10	0.000045
	Unit 3	0.000102	1.0	0.172	0.10	0.000045
	Unit 4	0.000292	1.0	0.224	0.10	0.000045
	Unit 5	0.000989	1.0	0.425	0.10	0.000045

Simulation Name	Description	Complexities*
FL	Five Layer simulation where each layer has homogeneous properties within but properties varying from layer to layer.	None
FLw	Five Layer simulation where each layer has homogeneous properties within but properties varying from layer to layer.	WB
FLwsc	Five Layer simulation where each layer has homogeneous properties within but properties varying from layer to layer.	WB, TWB
FLwa	Five Layer simulation where each layer has homogeneous properties within but properties varying from layer to layer.	WB, A

Table 8: (Continued) Simulations run in this study, their hydrogeologic properties, and the various complexities included in each simulation.

Hydrogeologic Properties of the Simulations Run with More Complex Boundary Flow Model approach.		
Simulation Name	Description	Complexities*
FLwab1	Five Layer simulation where each layer has homogeneous properties within but properties varying from layer to layer. The transport porosities for this simulation for each layer are those listed above plus the standard deviation reported by Barrash and Clemo (2002). The longitudinal dispersivities for this simulation are set to 0.2.	WB, A, θ_{σ}
FLwab2	Five Layer simulation where each layer has homogeneous properties within but properties varying from layer to layer. The transport porosities for this simulation for each layer are those listed above plus two times the standard deviation reported by Barrash and Clemo (2002). The longitudinal dispersivities for this simulation are set to 0.2.	WB, A, $\theta_{2\sigma}$
FLpor1	Five Layer simulation where each layer has homogeneous properties within but properties varying from layer to layer. The transport porosities for each layer in this simulation have been multiplied by 1.10.	WB
FLpor2	Five Layer simulation where each layer has homogeneous properties within but properties varying from layer to layer. The transport porosities for each layer in this simulation have been multiplied by 1.20.	WB
FLpor3	Five Layer simulation where each layer has homogeneous properties within but properties varying from layer to layer. The transport porosities for each layer in this simulation have been multiplied by 1.30.	WB

Table 8: (Continued) Simulations run in this study, their hydrogeologic properties, and the various complexities included in each simulation.

Hydrogeologic Properties of the Simulations Run with More Complex Boundary Flow Model approach.						
Simulation Name	Layer	K [m/s]	Vertical K Anisotropy [VK/HK]	Porosity or Specific Yield	Longitudinal Dispersivity (α_L) [m]	Specific Storage [m^{-1}]
Unit 2 Subdivided Simulations: same layering as the Five Layer system, except Unit 2 is broken up into many lenses. Simulations: MLhp, MLsb, MLsbS, MLsba2S, MLsbV15a2S, MLsbV2a2S, MLsbV3a2S, and MLsbV4a2S	Unit 1	0.000148	1.0	0.180	0.10	0.000045
	Unit 2a	0.000467	1.0	0.250	0.10	0.000045
	Unit 2b	0.000273	1.0	0.240	0.10	0.000045
	Unit 2c	0.000639	1.0	0.280	0.10	0.000045
	Unit 2d	0.000224	1.0	0.241	0.10	0.000045
	Unit 2e	0.000484	1.0	0.350	0.10	0.000045
	Unit 2f	0.000214	1.0	0.210	0.10	0.000045
	Unit 2g	0.000824	1.0	0.300	0.10	0.000045
	Unit 2h	0.000375	1.0	0.270	0.10	0.000045
	Unit 3	0.000102	1.0	0.172	0.10	0.000045
	Unit 4	0.000292	1.0	0.224	0.10	0.000045
	Unit 5	0.000989	1.0	0.425	0.10	0.000045

Table 8: (Continued) Simulations run in this study, their hydrogeologic properties, and the various complexities included in each simulation.

Simulation Name	Description	Complexities*
MLhp	Each unit or lens in this simulation has homogeneous hydrogeologic properties within the unit or lens, but the properties vary from unit to unit or lens to lens.	WB
MLsb	Each unit or lens in this simulation has homogeneous hydrogeologic properties within the unit or lens, but the properties vary from unit to unit or lens to lens.	WB, TWB
MLsbS	Each unit or lens in this simulation has homogeneous hydrogeologic properties within the unit or lens, but the properties vary from unit to unit or lens to lens.	WB, TWB, SB3, B6
MLsba2S	Each unit or lens in this simulation has homogeneous hydrogeologic properties within the unit or lens, but the properties vary from unit to unit or lens to lens.	WB, TWB, SB3, B6, A
MLsbV15a2S	Each unit or lens in this simulation has homogeneous hydrogeologic properties within the unit or lens, but the properties vary from unit to unit or lens to lens.	WB, TWB, SB3, B6, A, V1.5
MLsbV2a2S	Each unit or lens in this simulation has homogeneous hydrogeologic properties within the unit or lens, but the properties vary from unit to unit or lens to lens.	WB, TWB, SB3, B6, A, V2
MLsbV3a2S	Each unit or lens in this simulation has homogeneous hydrogeologic properties within the unit or lens, but the properties vary from unit to unit or lens to lens.	WB, TWB, SB3, B6, A, V3
MLsbV4a2S	Each unit or lens in this simulation has homogeneous hydrogeologic properties within the unit or lens, but the properties vary from unit to unit or lens to lens.	WB, TWB, SB3, B6, A, V4

Table 8: (Continued) Simulations run in this study, their hydrogeologic properties, and the various complexities included in each simulation.

Hydrogeologic Properties of the Simulations Run with More Complex Boundary Flow Model approach.						
Simulation Name	Layer	K [m/s]	Vertical K Anisotropy [VK/HK]	Porosity or Specific Yield	Longitudinal Dispersivity (α_L) [m]	Specific Storage [m^{-1}]
Distributed hydraulic conductivity and/or porosity: DK, DP, and DKP	Unit 1	Distributed	1.0	Distributed	0.10	0.000045
	Unit 2	Distributed	1.0	Distributed	0.10	0.000045
	Unit 3	Distributed	1.0	Distributed	0.10	0.000045
	Unit 4	Distributed	1.0	Distributed	0.10	0.000045
	Unit 5	Distributed	1.0	Distributed	0.10	0.000045

Simulation Name	Description	Complexities*
DP	Only porosity is distributed throughout each Unit. Hydraulic conductivity is that of the Five Layer simulations.	WB, TWB
DK	Only hydraulic conductivity is distributed throughout the each Unit. Porosity is that of the Five Layer simulations.	WB, TWB
DKP	Both hydraulic conductivity and porosity are distributed throughout each unit.	WB, TWB

Table 8: (Continued) Simulations run in this study, their hydrogeologic properties, and the various complexities included in each simulation.

*Complexities	
WB	Well bores and packers within the injection well (B3) and within the pumping well (B6). The well bore cells are defined as having a horizontal hydraulic conductivity of 0.0004 m/s and having a vertical hydraulic conductivity anisotropy of 0.00008. The porosity and specific yield of the well bore cells are defined as 0.587. The horizontal hydraulic conductivity of the packer cells are defined as 0.0004 m/s with a vertical hydraulic conductivity anisotropy of 1. The porosity of the packers are defined as 0.131. In most simulations the wellbores and packers are defined as Units within the Hydrogeologic Unit Flow package.
TWB	Well bores are defined throughout the entire vertical extent of wells: A1, B3, and B6. The horizontal hydraulic conductivity of the well bore cells are defined as 0.0004 m/s with vertical hydraulic conductivity anisotropy equal to 0.00008. The porosity and specific yield of these cells are defined as 0.587.
Swell	Barrash et al. (2006) document the existence of well bore skin at the BHRS. This complexity indicates that the Barrash et al. (2006) well skin values are implemented in the listed wells (subscript). The well bore skin is implemented through the Horizontal Flow Barrier package.
A	This complexity indicates that for the given simulation, the longitudinal dispersivities for the model were increased to 0.2 m.
$\theta_{i\sigma}$	The transport porosities are increased by i times the standard deviation of the porosities reported by Barrash and Clemo (2002).
VHK/VK	The vertical hydraulic conductivity anisotropy throughout the modeling domain is listed (subscript).

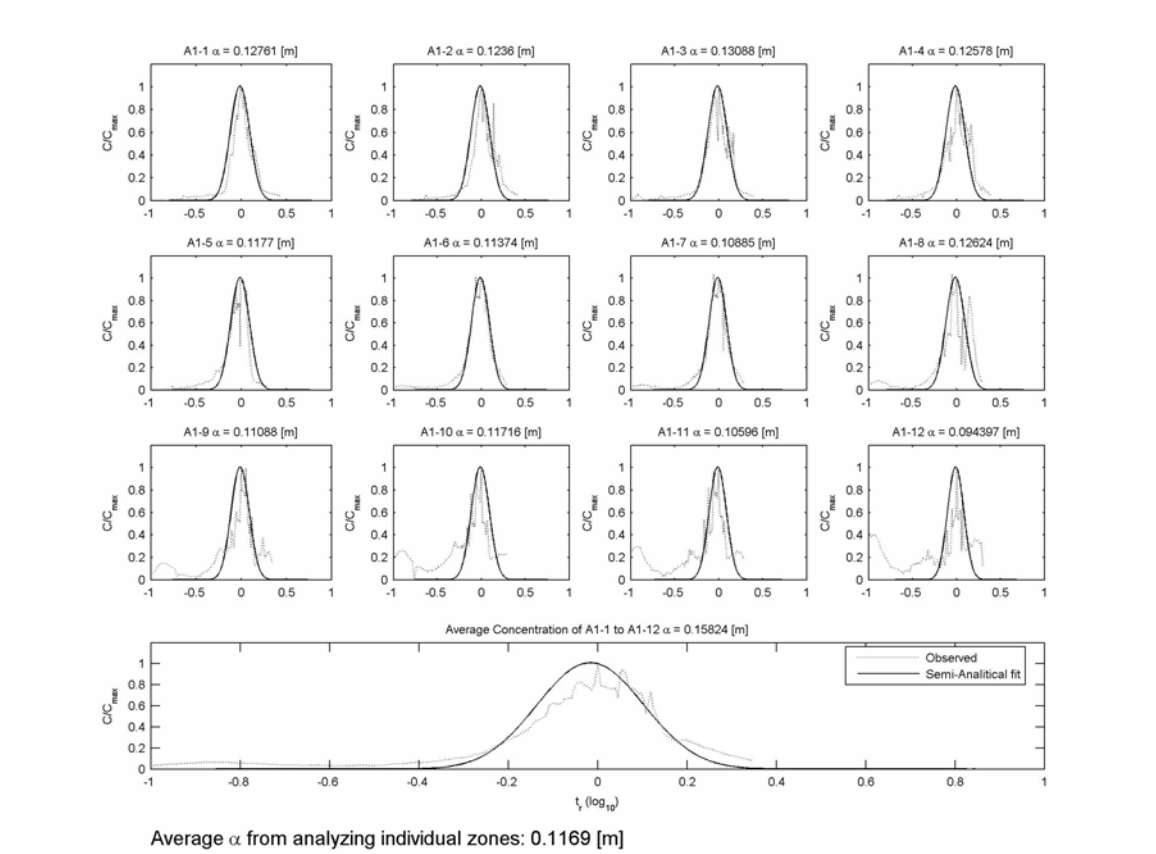

Figure 22: Type curve fits to the observed breakthrough curves measured in the bottom 12 sampling zones of well A1 (A1-1 through A1-12). Estimated longitudinal dispersivities are listed. The bottom-most plot shows the type curve fit to a breakthrough curve of the average of the 12 zones.

and the estimated longitudinal dispersivities from each breakthrough curve. Figure 22 also shows the type curve fit to a breakthrough curve generated from the average of all the breakthrough curves measured in the sampling zones of well A1.

The hydraulic gradient between wells B3 and A1 is estimated to have been 1.0 X 10^{-3} to 2.0 X 10^{-2} m/m during the TTLT based on head measurements at the BHRS under static conditions (Figure 7) and on a local gradient estimated from modeling the 5 gpm pumping rate at B6, respectively. Using these two hydraulic gradient estimates as the average gradients (1.0 X 10^{-3} and 2.0 X 10^{-2}) between well B3 and well A1 during the TTLT, the effective flow velocity determined from breakthrough curve fitting, and

porosity from porosity logs, hydraulic conductivity was estimated using equations 20 and 21. Figure 23 shows two hydraulic conductivity profiles at well A1 determined using the two hydraulic gradients mentioned above. Because hydraulic conductivity could only be estimated if there was a measurable breakthrough curve, hydraulic conductivity above the 12th sampling zone (839.575 m) and below the first sampling zone (836.575 m) at well A1 were taken as averages of the three estimated hydraulic conductivities below or above the uppermost and lowermost zones, respectively.

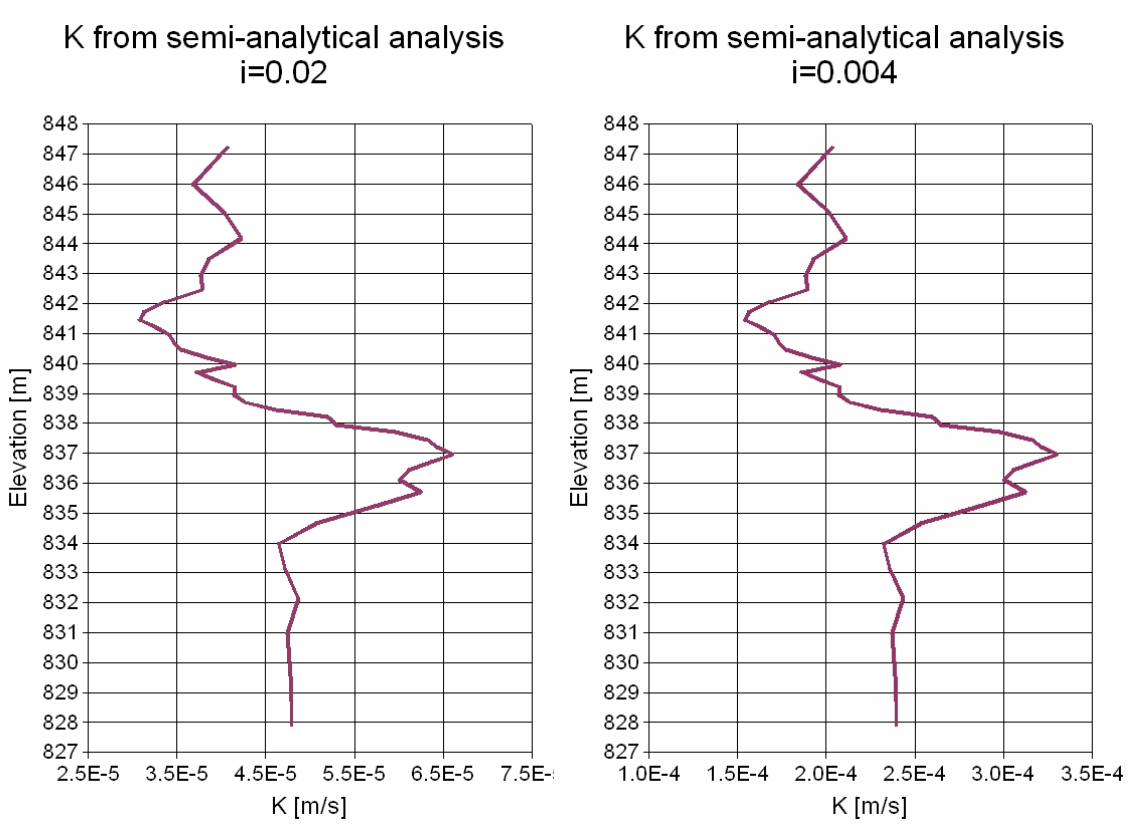

Figure 23: Two hydraulic conductivity profiles at well A1 determined using effective flow velocity, porosity from porosity logs, and two estimated hydraulic gradients (i).

This semi-analytical fitting of the breakthrough curves is an approach to estimating hydraulic conductivity and longitudinal dispersivity. As seen in Figure 23, depending upon the estimates of hydraulic gradient during the test, hydraulic conductivity estimates can vary by as much as an order of magnitude. Based upon simulations, an average hydraulic gradient near 4×10^{-3} is reasonable. Hydraulic conductivities based upon this estimate (4×10^{-3} plot of Figure 23) fall within the same range reported by Hughes (2005) and Fox (2006).

Several simulations were run using hydraulic conductivities derived from this analysis of the breakthrough curves (Table 8):

- Units 2a, 2b, and 3
- Many Horizontal Units
- ThLO
- ThL

Units 2a, 2b, and 3 and the Many Horizontal Units simulations were run using the uniform hydraulic gradient flow approach shown in Figures 15 and 16. The ThLO and ThL simulations were run with the complex boundaries flow approach shown in Figure 21. All four simulations included layering. The Units 2a, 2b, and 3 simulation and the ThLO simulation each had the same layering as shown in the cross section of Figure 24: three hydrogeologic units where the contact between hydrogeologic Units 3 and 2b is the kriged contact between porosity Units: 2 and 3 (Clemo, unpublished data); the contact between hydrogeologic Units 2b and 2a has the same topography as the contact between hydrogeologic Units 3 and 2b but with a vertical offset downward of 2.5 m. The Many

Horizontal Units simulation was layered according to the SEAWAT 2000 vertical discretization – every model layer was a separate hydrogeologic unit as seen in the cross section of Figure 25. The ThL simulation had layering according to the cross section shown in Figure 26; three hydrogeologic units where the contact between Units 2b and 3 is the kriged contact between porosity Units 2 and 3, and the contact between Units 2a and 2b is a horizontal plane at the same elevation as the middle of the packer between sampling zones A1-4 and A1-5 (see Figures 4 and 5). The hydrogeologic properties of these simulations are listed in Table 8.

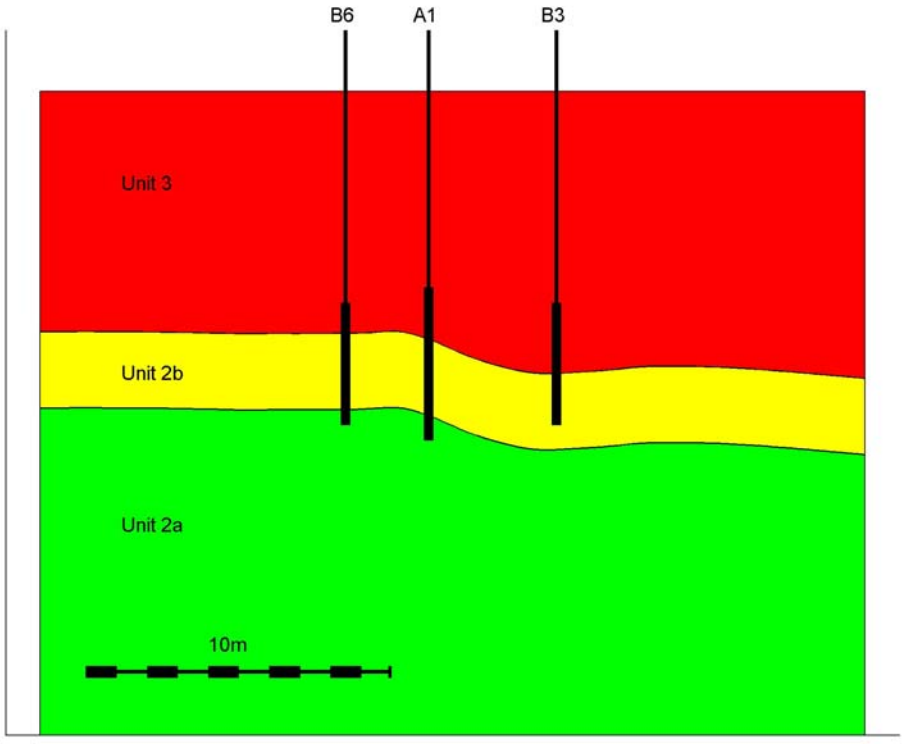

Figure 24: Cross section of the hydrostratigraphy of the Units 2a, 2b, and 3 simulation and the ThLO simulation. (No vertical exaggeration)

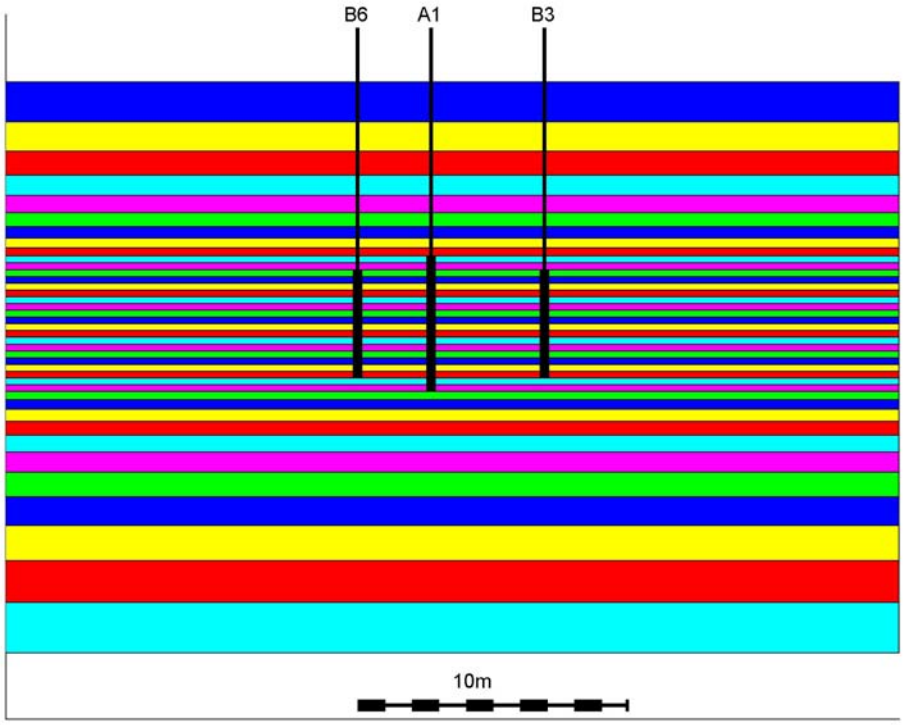

Figure 25: Cross section of the hydrostratigraphy of the Many Horizontal Units simulation. (No vertical exaggeration)

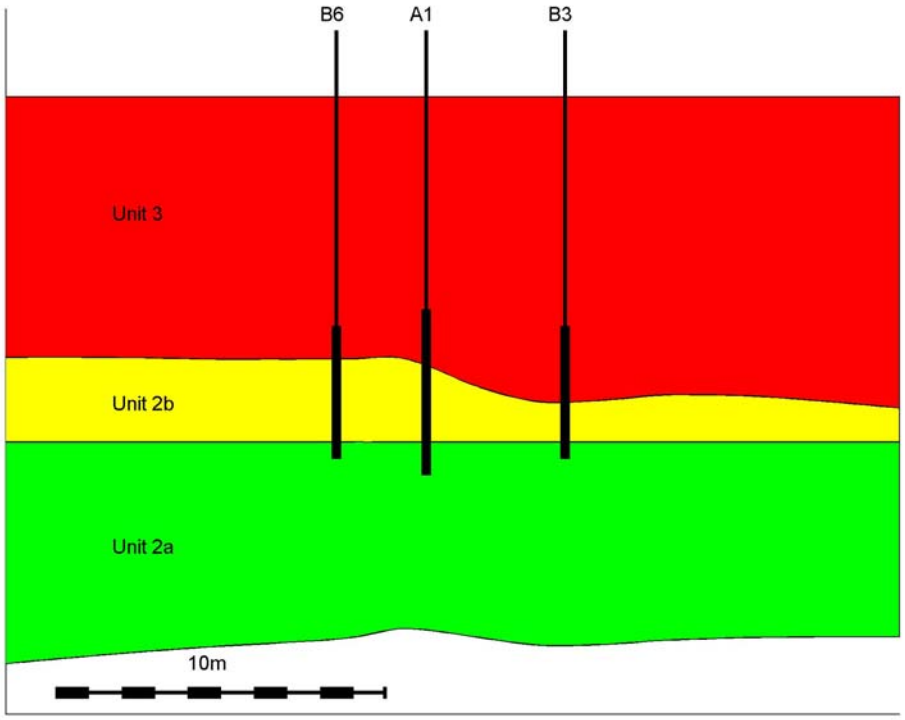

Figure 26: Cross section of the hydrostratigraphy of the ThL simulation. (No vertical exaggeration)

The ThLO, Units 2a, 2b, and 3, and the Many Horizontal Units simulations used hydraulic conductivities estimated with a higher hydraulic gradient (2×10^{-2}) whereas ThL used a lower hydraulic gradient (4×10^{-3}). Because Units 2a, 2b, and 3, Many Horizontal Units, and ThLO simulations all have hydraulic conductivities significantly lower than most all other simulations there is greater drawdown in the C wells compared to other simulations. Figure 27 is a plot of observed head changes in well C3 and simulated head changes for the Units 2a, 2b, and 3, Many Horizontal Units, ThLO, and ThL simulations. All simulations show greater drawdown then the ThL simulation. The

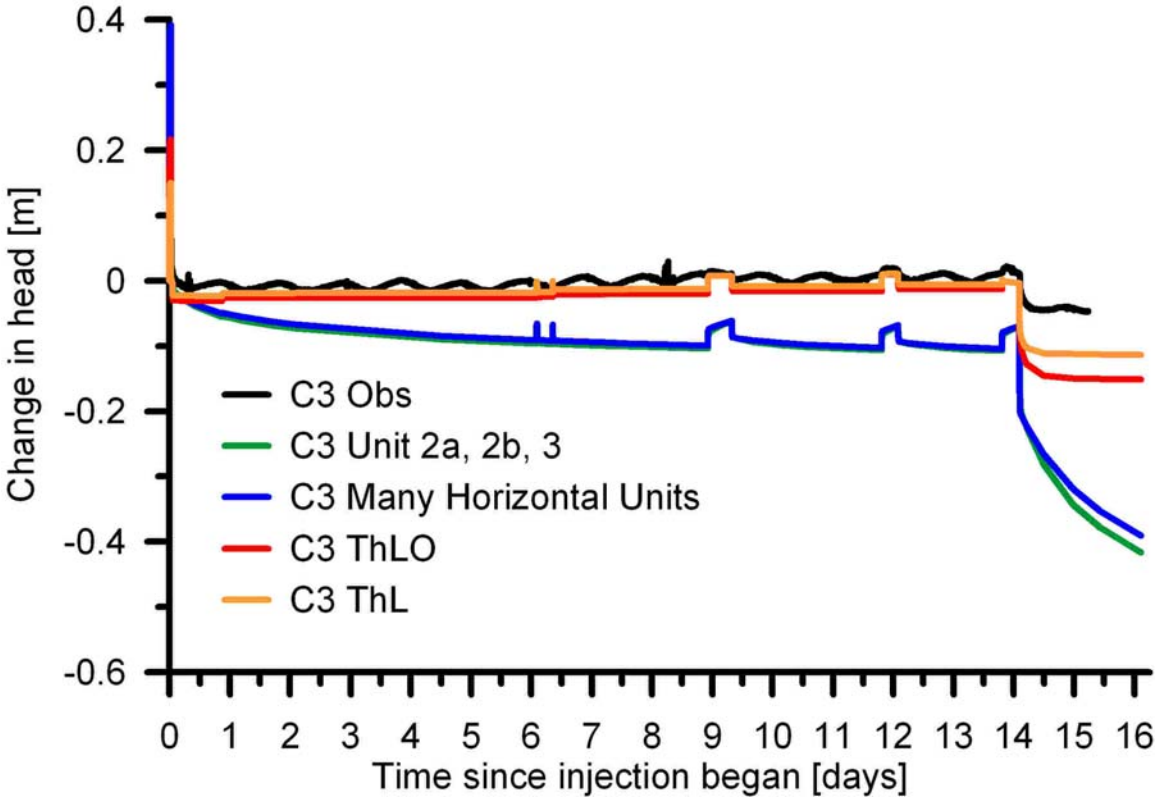

Figure 27: Observed and simulated head changes in well C3 for the Unit 2a, 2b, and 3, Many Horizontal Units, ThLO, and ThL simulations.

lower hydraulic conductivities of these simulations result in greater head changes and a higher average hydraulic gradient between wells B3 and A1.

At least some sampling zones in A1 in all of these simulations show early breakthrough (~3 days after injection began). Figure 28 shows the simulated breakthrough curves of sampling zone A1-10 for all four simulations. Simulations with a low hydraulic conductivity (Unit 2a, 2b, and 3, Many Horizontal Units, and ThLO have hydraulic conductivity close to an order of magnitude lower than TwL and ThL) show early breakthrough at roughly the same time as that of the simulation with a higher hydraulic conductivity. The combination of the pumping well (B6) and the simulation's hydrostratigraphy yields roughly the same water fluxes towards the pumping well

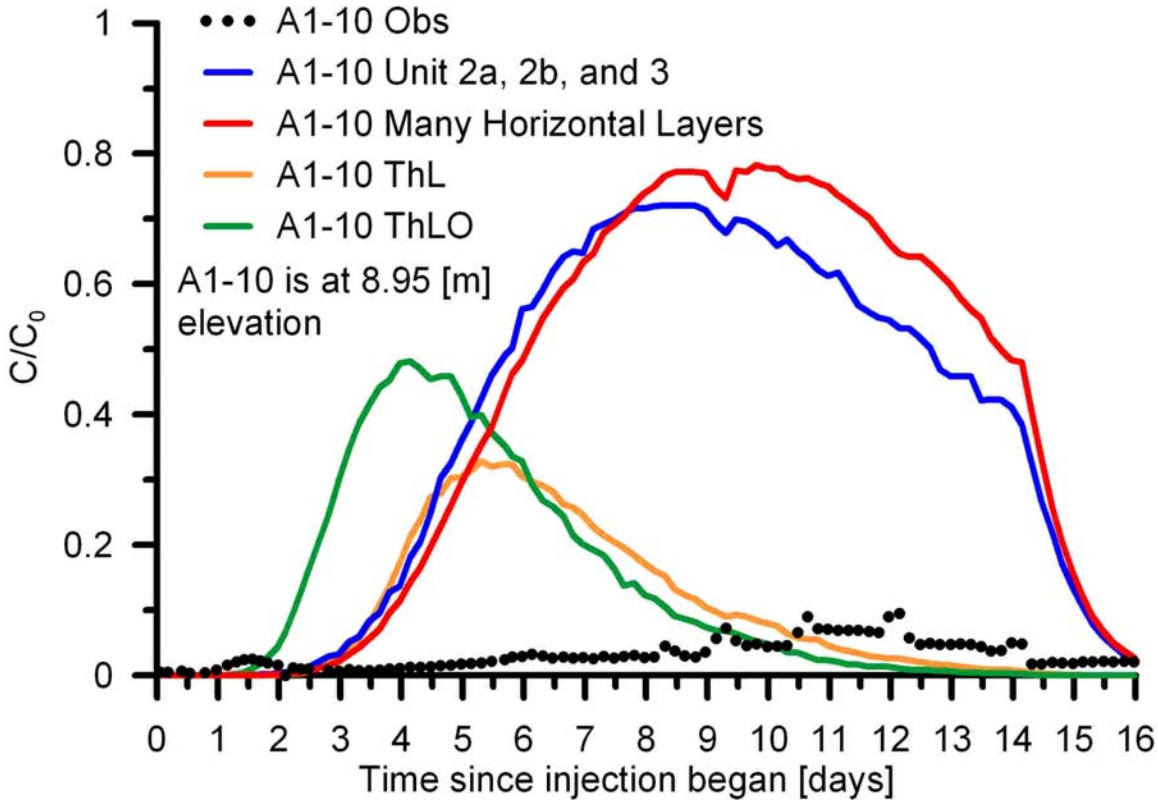

Figure 28: Observed and simulated breakthrough in sampling zone A1-10 for the Unit 2a, 2b, and 3, Many Horizontal Units, ThLO, and ThL simulations.

regardless of the simulation. The result is that by uniformly decreasing the hydraulic conductivity, the drawdown is increased and the simulated plume will not be slowed and simulated breakthrough timing will be similar for all simulations.

4.2 Variable Density Flow

Two simulations were run, one with variable density flow and one without, to examine the significance of variable density flow during the TTLT. Both simulations have the hydrogeologic properties of the Unit 2-3 simulation as listed in Table 8. There are two hydrogeologic units: Unit 2 and Unit 3. The contact between the two units is the

kriged contact between porosity Units 2 and 3. The layering within the system is shown in the cross section of Figure 29.

Figure 30 shows breakthrough curves from the sampling zones of well A1 in these two simulations. The simulation with variable density flow shows significant downward tracer movement similar to that observed in well A1 whereas the simulation without variable density flow does not. In particular, the variable density flow simulation shows a high magnitude of breakthrough in the lower sampling zones A1-1 through A1-4.

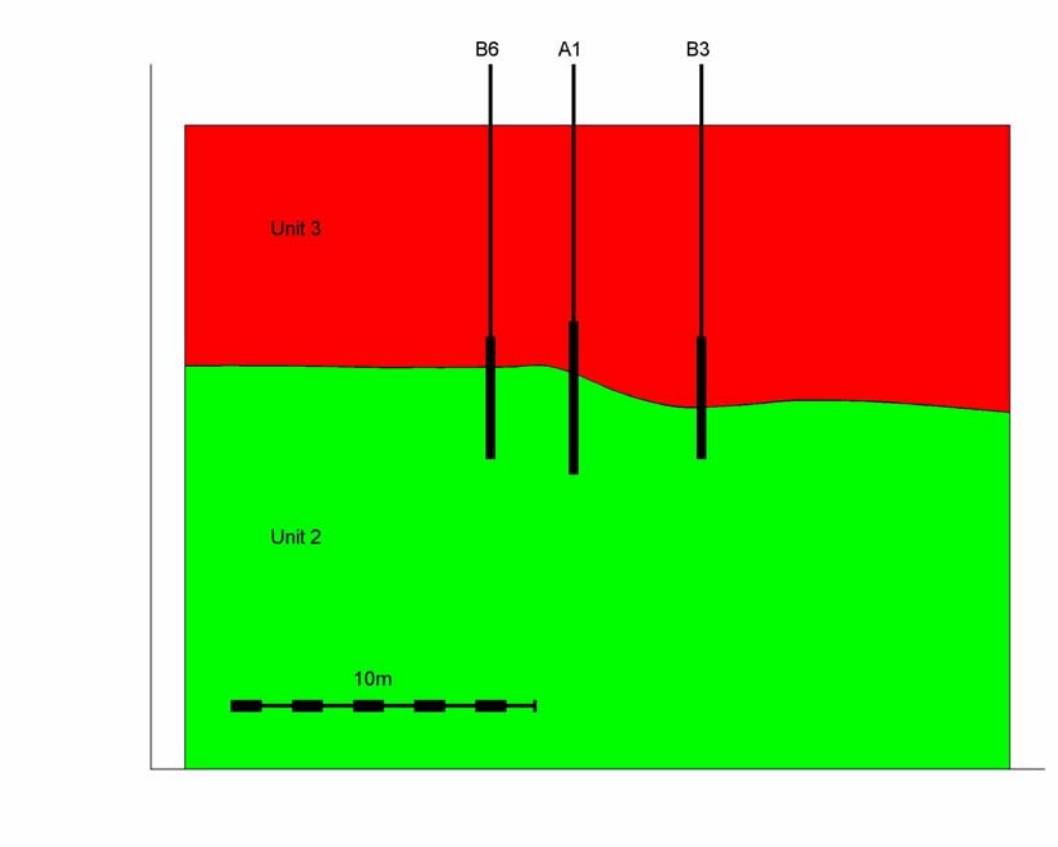

Figure 29: Cross section of the hydrostratigraphy of the Unit 2-3 and TwL simulations. This geometry was also used in the simulations run to investigate variable density flow. (No vertical exaggeration)

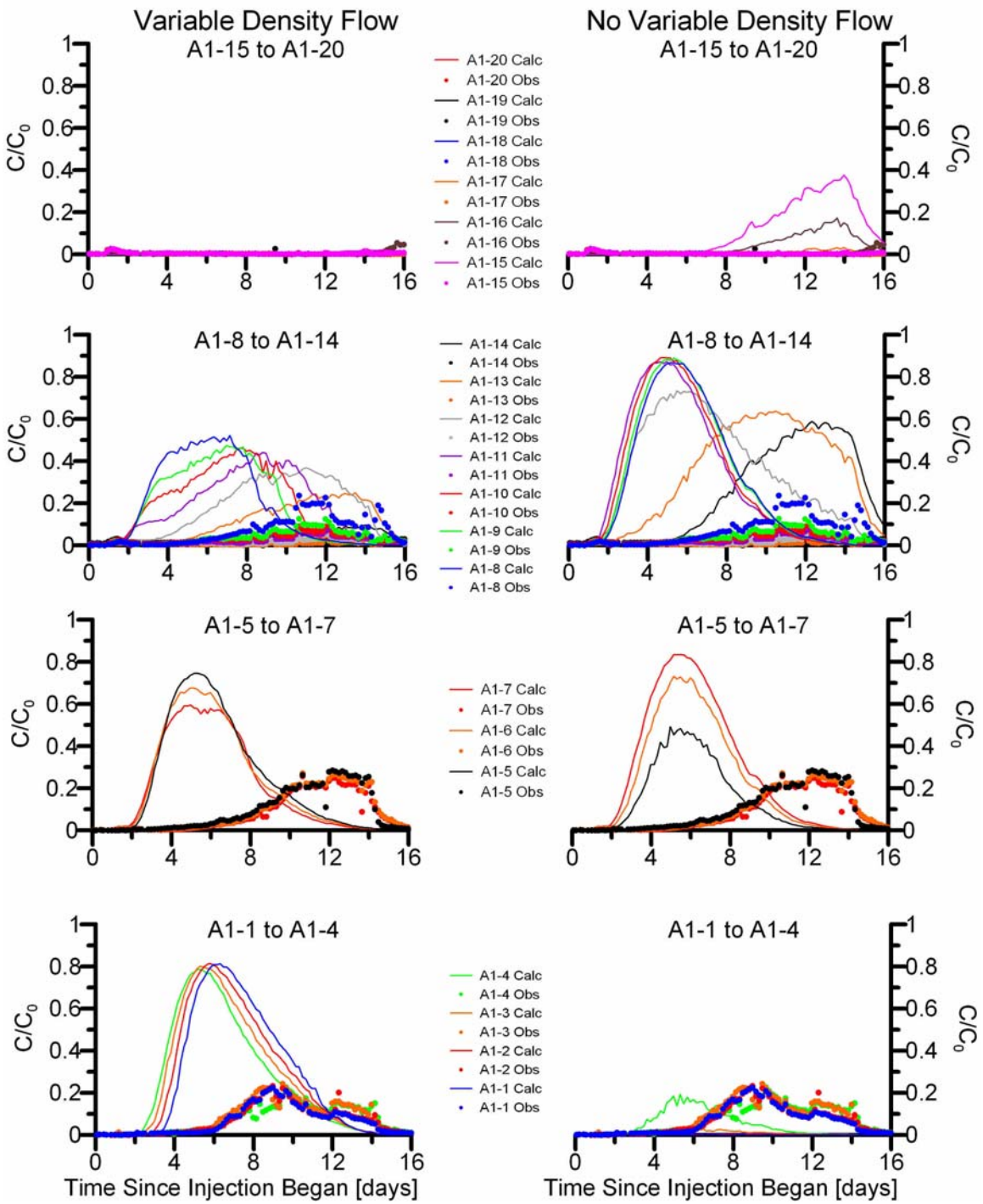

Figure 30: Observed and simulated breakthrough curves from the sampling zones of well A1 for two simulations, one with variable density flow and the other without. The left side corresponds to a simulation that allows variable density flow; the right side corresponds to a simulation that does not allow variable density flow. Other than the accounting for variable density flow, there is no difference between the two simulations.

4.2.1 Effects of a High Hydraulic Gradient

A high hydraulic gradient would dampen variable density flow effects (Barth et al., 2001). For example if two simulations had the same layering and hydrogeologic properties but had differing hydraulic gradients, the simulation with the higher hydraulic gradient would have breakthrough curves with higher magnitudes in higher sampling zones compared to the simulation with a lower hydraulic gradient. As estimates of the hydraulic gradient between the injection well (B3) and the sampling well (A1) increase, the α_2 values shown in Table 5 decrease showing a dampening of variable density effects. The bottom two rows of Table 5 show α_2 values calculated for hydraulic gradients of 4×10^{-2}, which is an unrealistically high hydraulic gradient for the TTLT between the injection well (B3) and the sampling well (A1); these α_2 values calculated with high hydraulic gradients indicate stability but are incorrect for the TTLT, as expected.

4.3 Evapotranspiration and its Effect on Transport

The BHRS has a marked diurnal water table fluctuation due to evapotranspiration during the seasonally warm period from mid-Spring to Fall. This is largely due to the phreatophytes (cottonwoods) that grow at the site. Invariably each Spring some of the wells need to be cleaned of cottonwood roots that grow as a mat across the water table over the Winter in these wells. Roots can be seen sporadically throughout the thickness of the aquifer (~15-20m) in video logs run in wells at the BHRS (W. Barrash, unpubl. data). Evapotranspiration causes the water table to fluctuate daily 0.5 to 2.5 cm (Figure 10 and Hausrath et al., 2002).

To investigate the effects of evapotranspiration on the transport of the bromide tracer during the TTLT at the BHRS, two identical simulations with the base model of Unit 2-3 Ave (Table 8) were run using SEAWAT 2000 with the only difference being that one simulation included evapotranspiration and the other did not. The model was stressed using the Evapotranspiration (ET) package in SEAWAT 2000. The ET package requires a maximum evapotranspiration rate, depth to maximum evapotranspiration, and depth to the point where evapotranspiration no longer occurs. The evapotransporation rate between these two depths varies linearly from the maximum at the higher elevation to zero at the lower elevation. These values can vary from cell to cell and from stress period to stress period within the ET package.

Changes to the base model associated with addition of the ET package include: (1) the stress periods and time steps had to be modified to only have evapotranspiration during the day, and (2) the higher constant head boundary along the northeast side was raised by 6 cm in the simulation containing evapotranspiration in order to maintain a hydraulic gradient across the central well field similar to that of the base case simulation.

Figure 31 shows the observed and simulated changes in head values in well C3 for both the base case simulation and the evapotranspiration simulation. Plots of the observed and simulated changes in head in all of the C wells are on the CD accompanying this thesis.

The hydraulic gradients across the central well field of the BHRS in the two simulations are similar but do not exactly match; the hydraulic gradient of the simulation with evapotranspiration included is higher. Figure 32 is a plot of the simulated

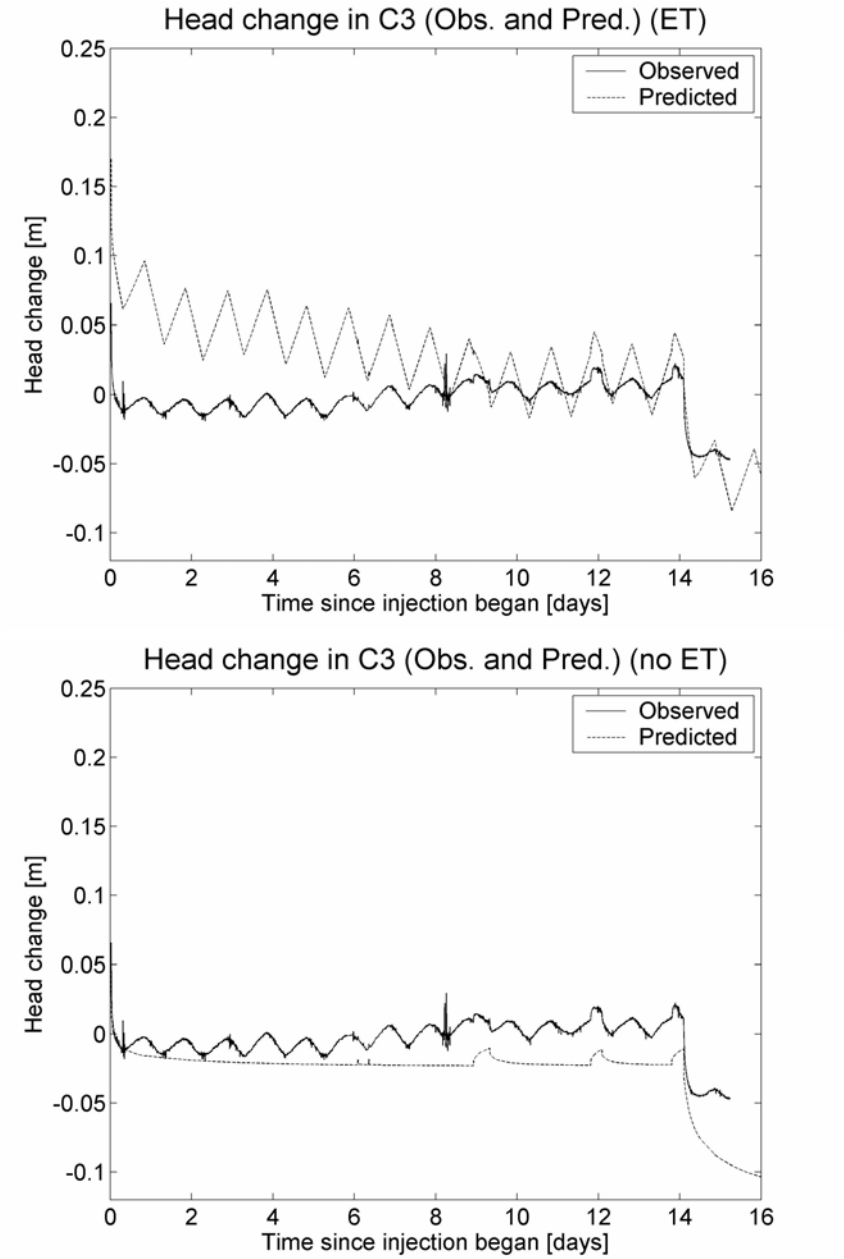

Figure 31: Observed and simulated head changes in well C3 for two simulations, one with evapotranspiration (above) and the other without (below).

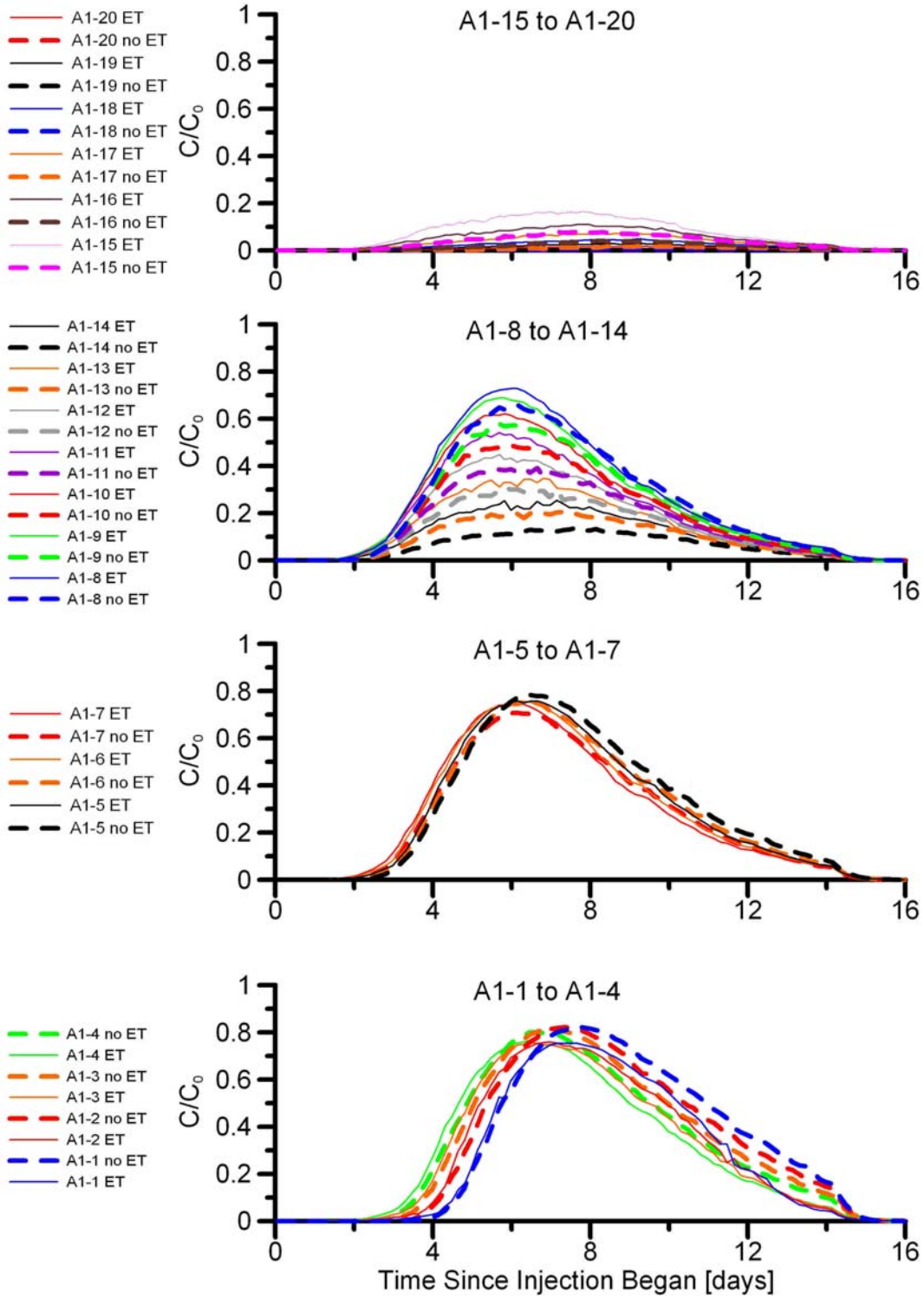

Figure 32: The simulated breakthrough curves in the sampling zones of well A1 for two simulations - one with evapotranspiration and one without.

breakthrough curves in the sampling zones of well A1 for both simulations and shows that there is relatively little difference in transport between the simulation with evapotranspiration and that without. Most of the differences can be attributed to the inability to mimic hydraulic gradients between the two simulations. The differences in the breakthrough curves occur because the variable density flow is dampened by the higher gradient and not as a result of evapotranspiration. Because evapotranspiration does not contribute substantially to transport, it is not necessary to include it in other simulations in this thesis.

4.4 Homogeneous Hydrogeologic Properties Throughout The Model

A number of simulations were run with homogeneous hydrogeologic properties throughout the entire modeling domain (Table 8):

- Unit 2-3 Ave
- Unit 2
- Unit 3
- U23A

The Unit 2-3 Ave, Unit 2, and Unit 3 simulations used the uniform gradient flow approach, while U23A was run with the complex boundaries flow approach. For each of the five hydrostratigraphic units described by Barrash and Clemo (2002) and Barrash and Reboulet (2004), a hydraulic conductivity was estimated by averaging the modified Kozeny-Carmen estimates of each unit in the wells (Hughes, 2005; Barrash et al., in prep.). The hydraulic conductivity estimates for Units 2 and 3 were used for the Unit 2

and Unit 3 simulations and are listed in Table 8. The hydraulic conductivities of the Unit 2-3 Ave simulation and U23A simulation are the same and were calculated using equation 22:

$$K_{2-3\text{Ave}} = \frac{\left(\left(L_{U2-A1s} + L_{U2-B3p}\right)K_2 + \left(L_{U3-A1s} + L_{U3-B3p}\right)K_3\right)}{\left(L_{A1s} + L_{B3p}\right)} \quad (22)$$

where $K_{2\text{-}3Ave}$ is the weighted hydraulic conductivity estimate between Units 2 and 3, $L_{U2\text{-}A1s}$ is the length of the sampling zones in well A1 that intersect Unit 2, $L_{U2\text{-}B3p}$ is the length of the injection zone in well B3 that intersects Unit 2, $L_{U3\text{-}A1s}$ is the length of the sampling zones in well A1 that intersect Unit 3, $L_{U3\text{-}B3p}$ is the length of the injection zone in well B3 that intersects Unit 3, L_{A1s} is the total length of the sampling zones in well A1, L_{B3p} is the total length of the injection zone of well B3, K_2 is the average hydraulic conductivity of Unit 2, and K_3 is the average hydraulic conductivity of Unit 3.

The Unit 2 and Unit 3 simulations use porosities reported by Barrash and Clemo (2002) for Units 2 and 3 respectively. The porosity for the Unit 2-3 Ave and U23A simulations were calculated in the same way as for hydraulic conductivity:

$$Por_{2-3\text{ave}} = \frac{\left(\left(L_{U2-A1s} + L_{U2-B3p}\right)Por_2 + \left(L_{U3-A1s} + L_{U3-B3p}\right)Por_3\right)}{\left(L_{A1s} + L_{B3p}\right)} \quad (23)$$

where $Por_{2\text{-}3ave}$ is the weighted porosity estimate for this simulation, and Por_2 and Por_3 are the porosities for Units 2 and 3 respectively (Table 1).

The observed and simulated changes in head for well C3 of the four simulations with homogeneous hydrogeologic property models are shown in Figure 33. Unit 2-3 Ave, Unit 2, and U23A have very similar changes relative to each other because their hydraulic conductivities are similar (3.05×10^{-4} and 3.94×10^{-4} m/s), and they have

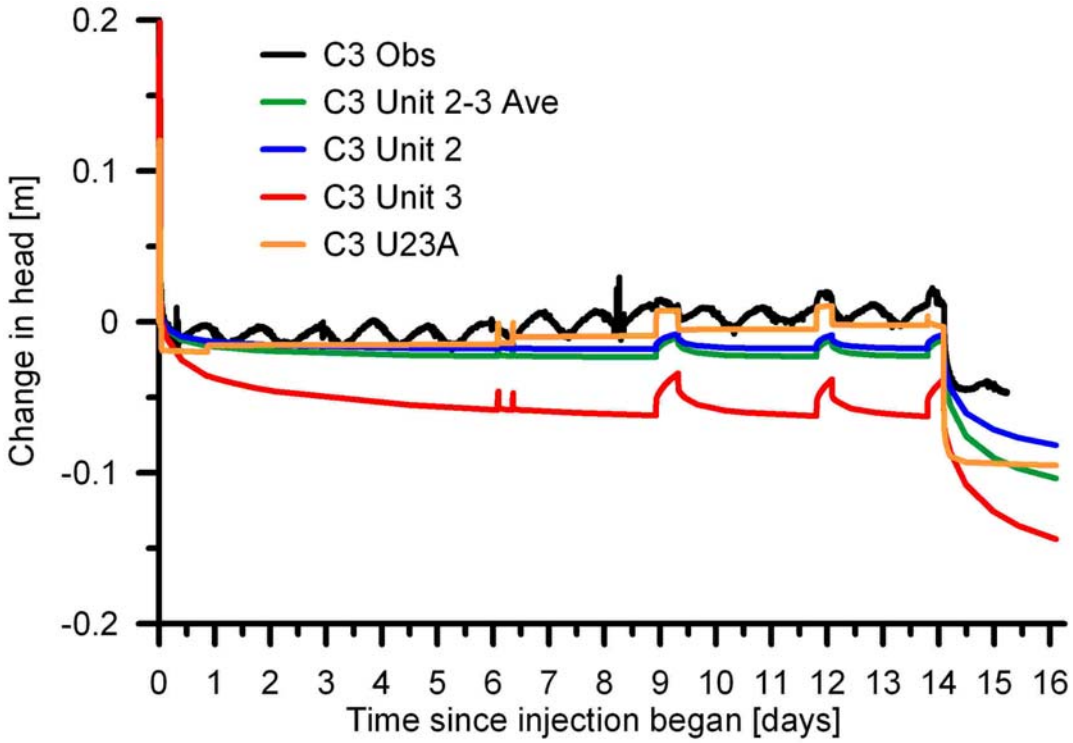

Figure 33: Observed and simulated head changes in well C3 for the Unit 2-3 Ave, Unit 2, Unit 3, and U23A simulations.

similar head changes with the observations made during the TTLT. Unit 3, however, has a marked increase in change in head (and corresponding poor fit with the head observations) because the hydraulic conductivity of Unit 3 (1.07×10^{-4} m/s) is about one third that of Unit 2-3 Ave, Unit 2, and U23A.

Figure 34 shows the Time to Peak and Time to Center of Mass transport statistics. The observed and simulated breakthrough curves for sampling zones A1-2, A1-6, and A1-10 for the Unit 2-3 Ave, Unit 2, Unit 3, and U23A simulations are shown in Figure 35. Unit 3 has dampened variable density flow because the hydraulic gradient is higher in this model. The simulated breakthrough for Unit 3 in Figure 35 shows a dampened variable density flow effect in that breakthrough magnitudes are higher in higher

sampling zones (A1-6 and A1-10) than in those of other simulations, and the breakthrough magnitude in the lower sampling zones of Unit 3 are lower (see sampling zone A1-2 of Figure 35). The Time to Peak and Time to Center of Mass transport statistics for these simulations are relatively similar but are early compared to the observed data; this shows that using average and homogeneous hydrogeologic properties throughout the modeling domain does not adequately characterize the bromide transport during the TTLT.

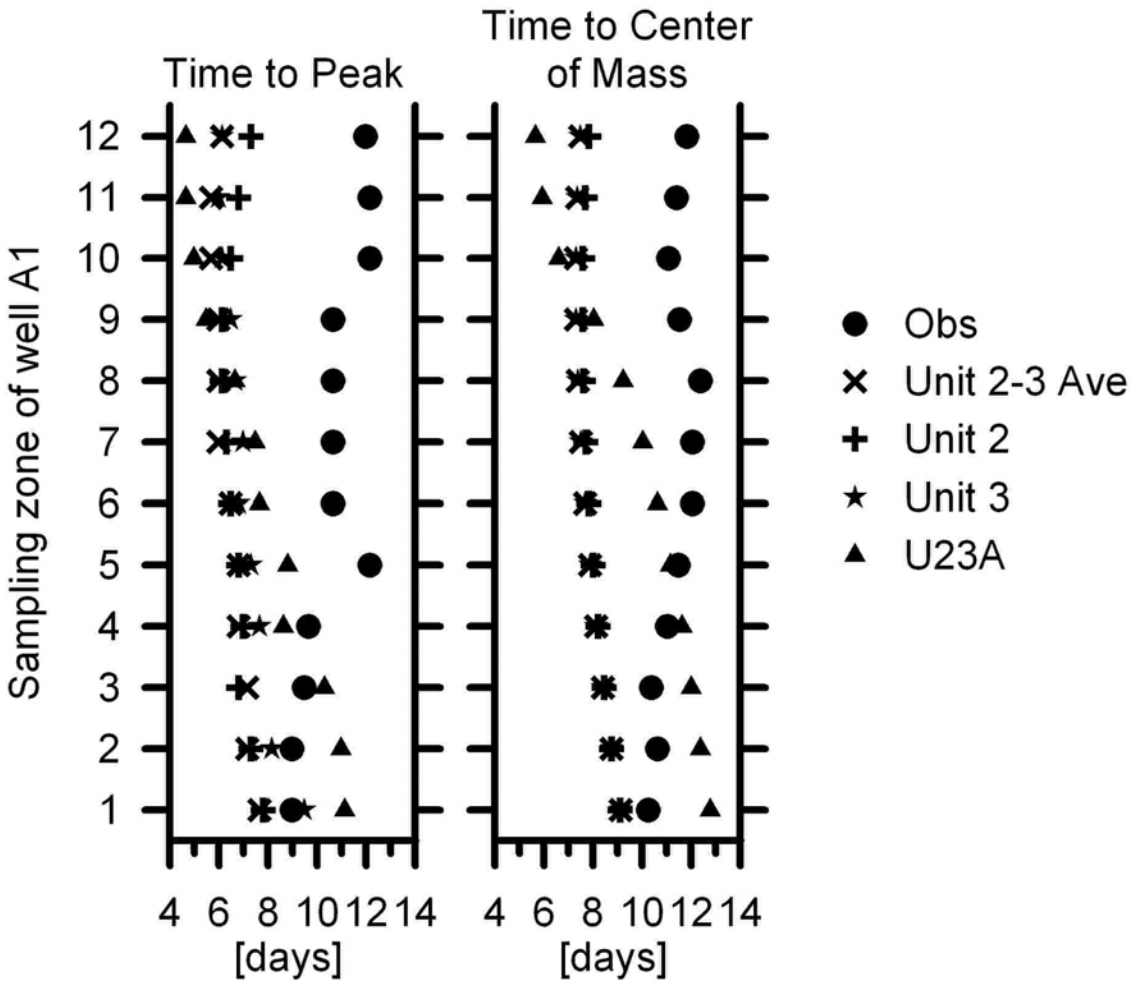

Figure 34: Time to Peak and Time to Center of Mass transport statistics calculated for the Unit 2-3 Ave, Unit 2, Unit 3, and U23A simulations.

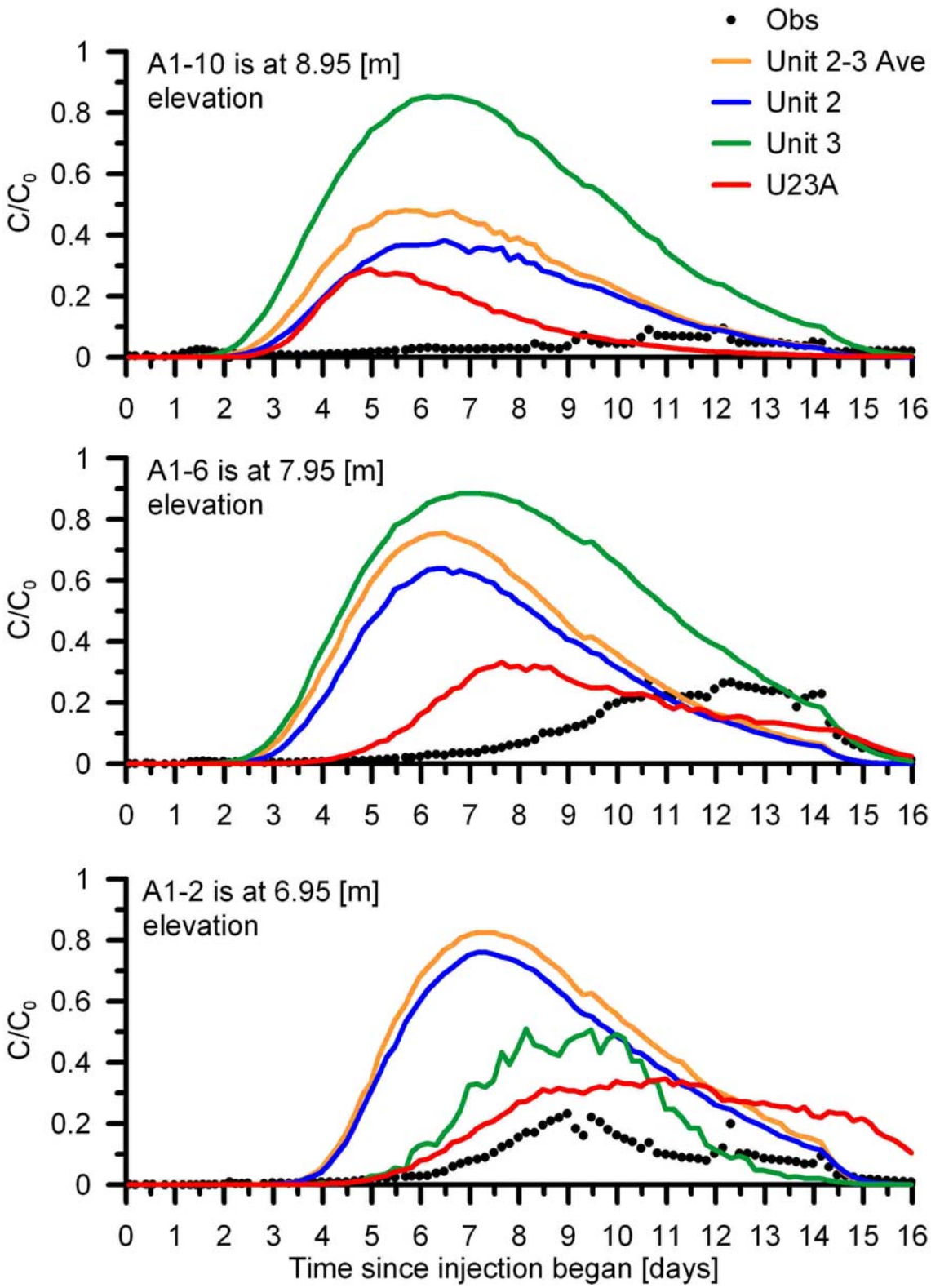

Figure 35: The simulated breakthrough curves in the sampling zones A1-2, A1-6, and A1-10 for the Unit 2-3 Ave, Unit 2, Unit 3, and U23A simulations.

4.5 Boundaries

Two different flow modeling approaches are used in this study: (1) the uniform gradient flow modeling approach where the boundaries are no flow and specified head as shown in Figures 15 and 16; and (2) a model framework with more complex boundaries – river as a groundwater divide, no flow, specified head, and general head boundaries as seen in Figure 21. Using the same hydrogeologic properties, a simulation was run using each flow modeling approach to evaluate the effects of boundary conditions (i.e., Unit 2-3 Ave and U23A, see Table 8 for property values).

Model drawdown behavior as seen at C wells (e.g., C3, Figure 33) is very similar for the two simulations but U23A has slightly less head change than Unit 2-3 Ave. This difference is most likely because of the different treatment of the boundaries. Another influence of the boundaries can be seen in the breakthrough magnitudes by comparing the Peak Concentration and Mass under the Breakthrough Curve transport statistics (Figure 36). The Peak Concentration and the Mass under the Breakthrough Curve transport statistics for the simulation with more complex boundaries (U23A) are closer to the observed values. This is primarily a consequence of including the river in the modeling, because the river boundary (i.e., losing river vs no flow in uniform gradient model Unit 2-3 Ave) induces a cross gradient which causes the Center of Mass of the tracer plume to travel by the northeast side of well A1 rather then go straight through well A1 (see - horizontal plume slices at ~7 days after injection for both simulations in Figures 37 and 38). Consequently in U23A, only the side of the plume is sampled in the sampling zones of well A1 which reduces the overall magnitude simulated in the sampling zones of well

A1. The plume centers appear to pass right through well A1 in Figure 37 (Unit 2-3 Ave), whereas the corresponding plume centers of Figure 38 (U23A) pass approximately 1 meter to the northeast side of well A1.

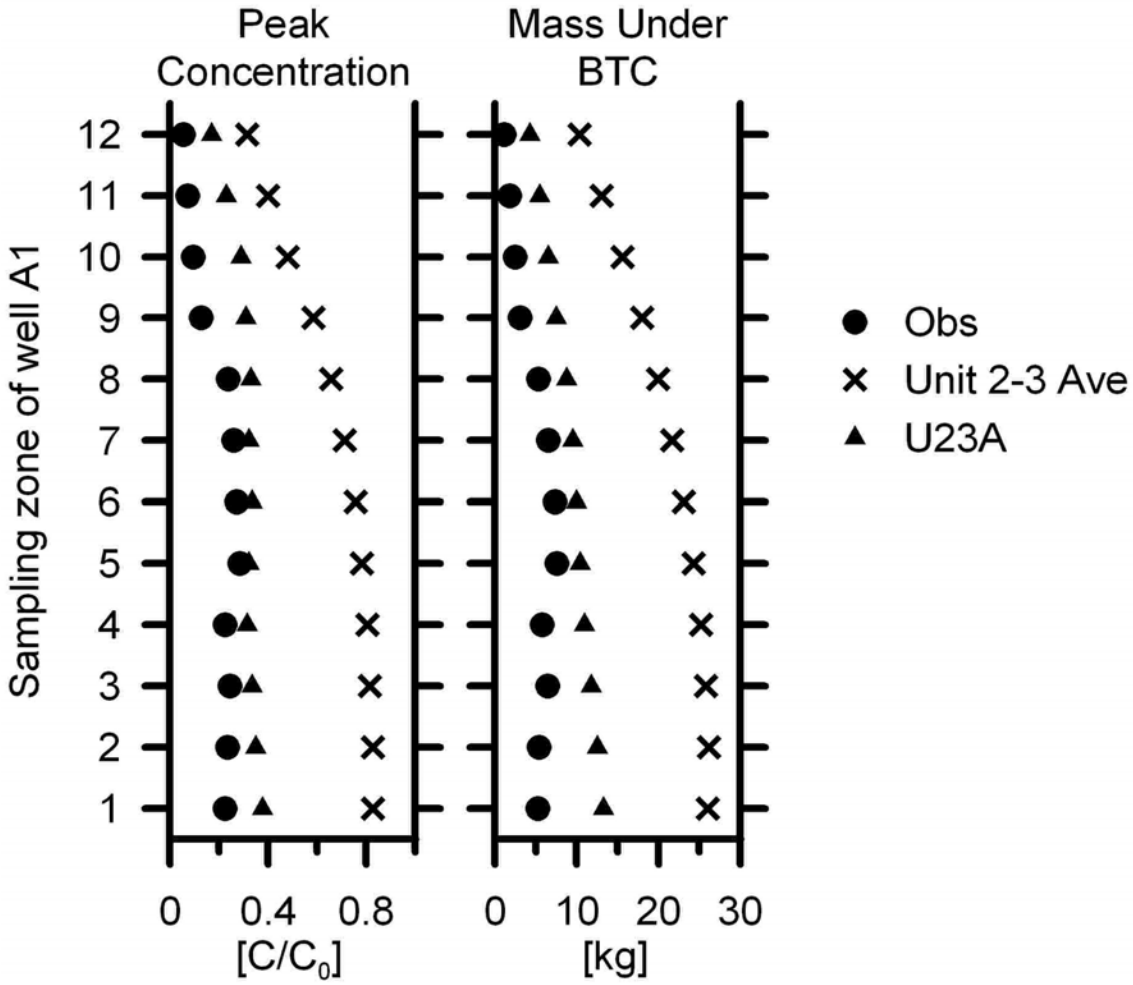

Figure 36: Peak Concentration and Mass Under the Breakthrough Curve transport statistics calculated for the Unit 2-3 Ave and U23A simulations.

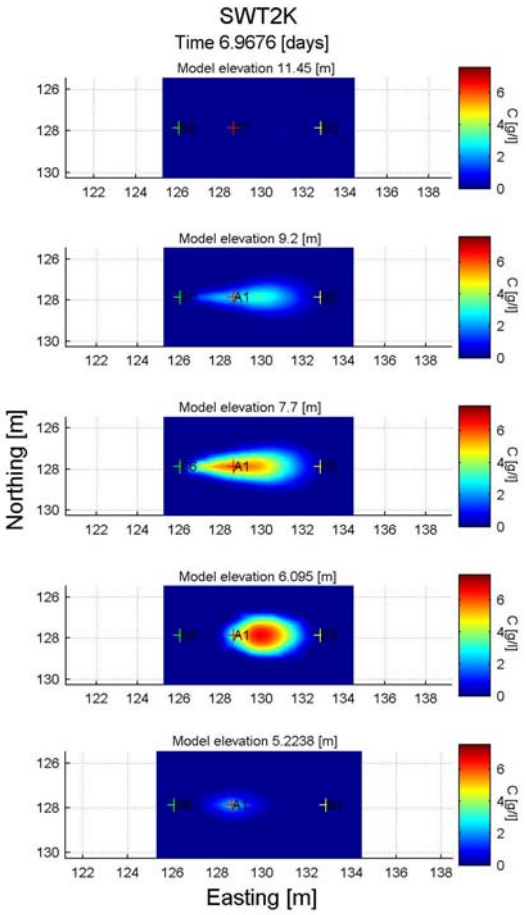

Figure 37: Horizontal plume slices from the Unit 2-3 Ave simulation ~7 days after injection at model elevations: 11.45, 9.2,7.7, 6.095, and 5.2238 m. For reference, the center of the 4 m injection zone in well B3 is at 9.075 m.

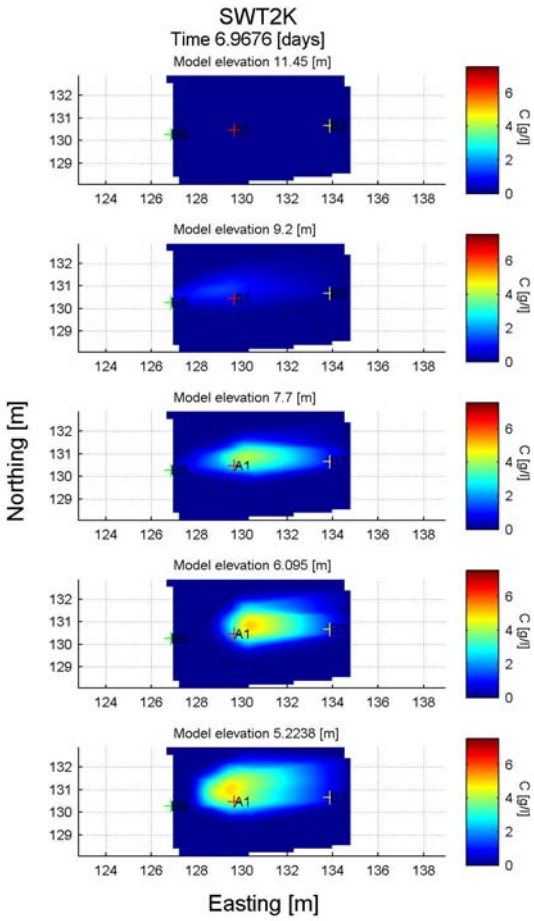

Figure 38: Horizontal plume slices from the U23A simulation ~7 days after injection at model elevations: 11.45, 9.2,7.7, 6.095, and 5.2238 m. For reference, the center of the 4 m injection zone in well B3 is at 9.075 m.

4.6 Layering

4.6.1 Homogeneous vs Two-Layer System Using The Uniform Hydraulic Gradient Flow Modeling Approach

Two simulations were run to examine the effect of layering using the uniform gradient flow approach: (1) Unit 2-3 Ave and (2) Unit 2-3. Unit 2-3 Ave has no layering (i.e., homogeneous distribution of aquifer properties), and Unit 2-3 has a two-layer system as shown in the cross section of Figure 29. The hydrogeologic properties of each simulation are shown in Table 8. Figure 39 shows the observed and simulated change in head for well C3 for both simulations; there is not much difference in change of head between the two simulations.

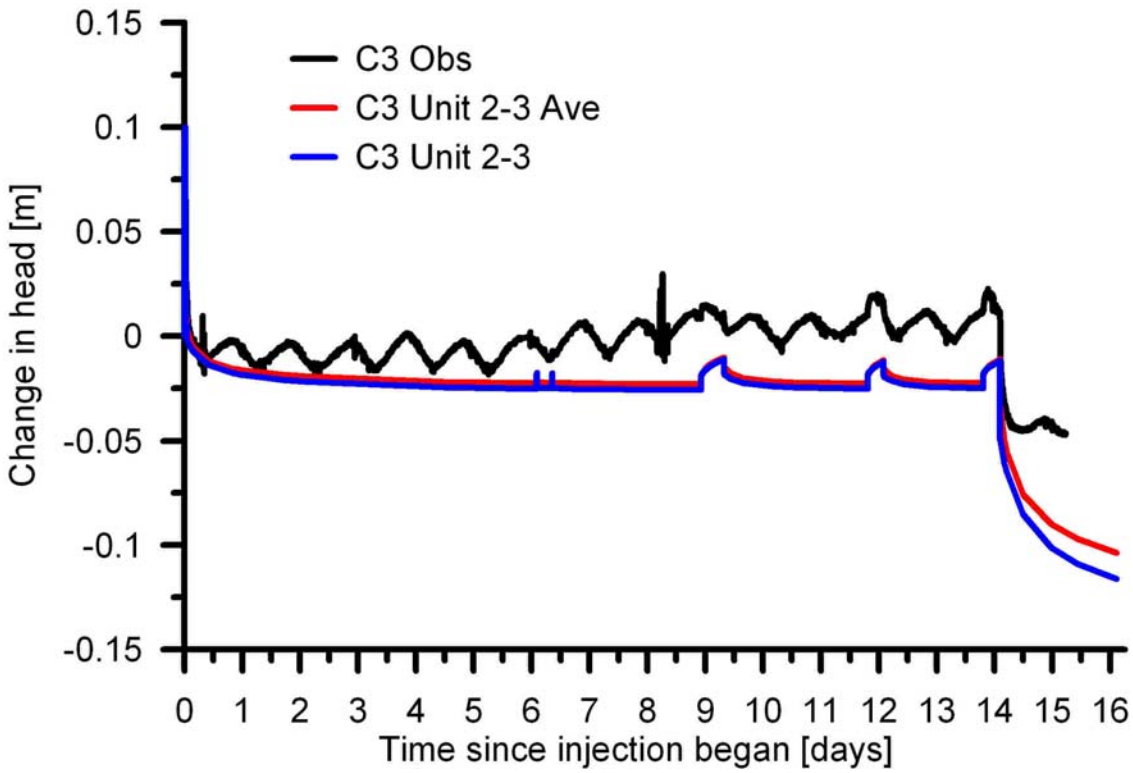

Figure 39: Observed and simulated head change in well C3 for the Unit 2-3 Ave and Unit 2-3 simulations.

There are however noticeable differences in simulated breakthrough in the sampling zones of A1. Figure 40 shows the observed and simulated breakthrough curves for sampling zones A1-10, A1-8, A1-6, and A1-2; the breakthrough curves from Unit 2-3 (with layering) are broader but begin earlier. Figure 41 shows the transport summary statistics for both of these simulations. The Time to the First Concentration over 7.5% injection concentration and the Time the Concentration Drops below 7.5% injection concentration are earlier in the simulation with layering. The Time to Center of Mass and Time to Peak statistics are generally later for the simulation without layering (Unit 2-3 Ave) in the lower zones (A1-1 through A1-6) and are earlier in the higher zones (A1-9 through A1-12). In the simulation with layering (Unit 2-3), the Peak Concentration statistic is lower over zones A1-6 through A1-9 because these zones are affected by the contact between the two layers of the simulation. This also yields a slightly higher estimate of longitudinal dispersivity in these zones. The layering is essentially splitting the tracer plume; the part of the plume in Unit 2 (which has a higher hydraulic conductivity) travels more quickly. As the plume moves faster in Unit 2, it leaks into Unit 3 above at the contact; this causes the additional spreading as seen in zones A1-8 and A1-10 of Unit 2-3 in Figure 40.

For both simulations, the Mass under the Breakthrough Curve statistics in all sampling locations are significantly high compared to observed; this is because the simple boundary approach was used in these simulations and the effects of the river boundary are not seen. Simulated horizontal plume slices at ~7 days after injection for the Unit 2-3 simulation show that plume centers of the Unit 2-3 model pass slightly off to

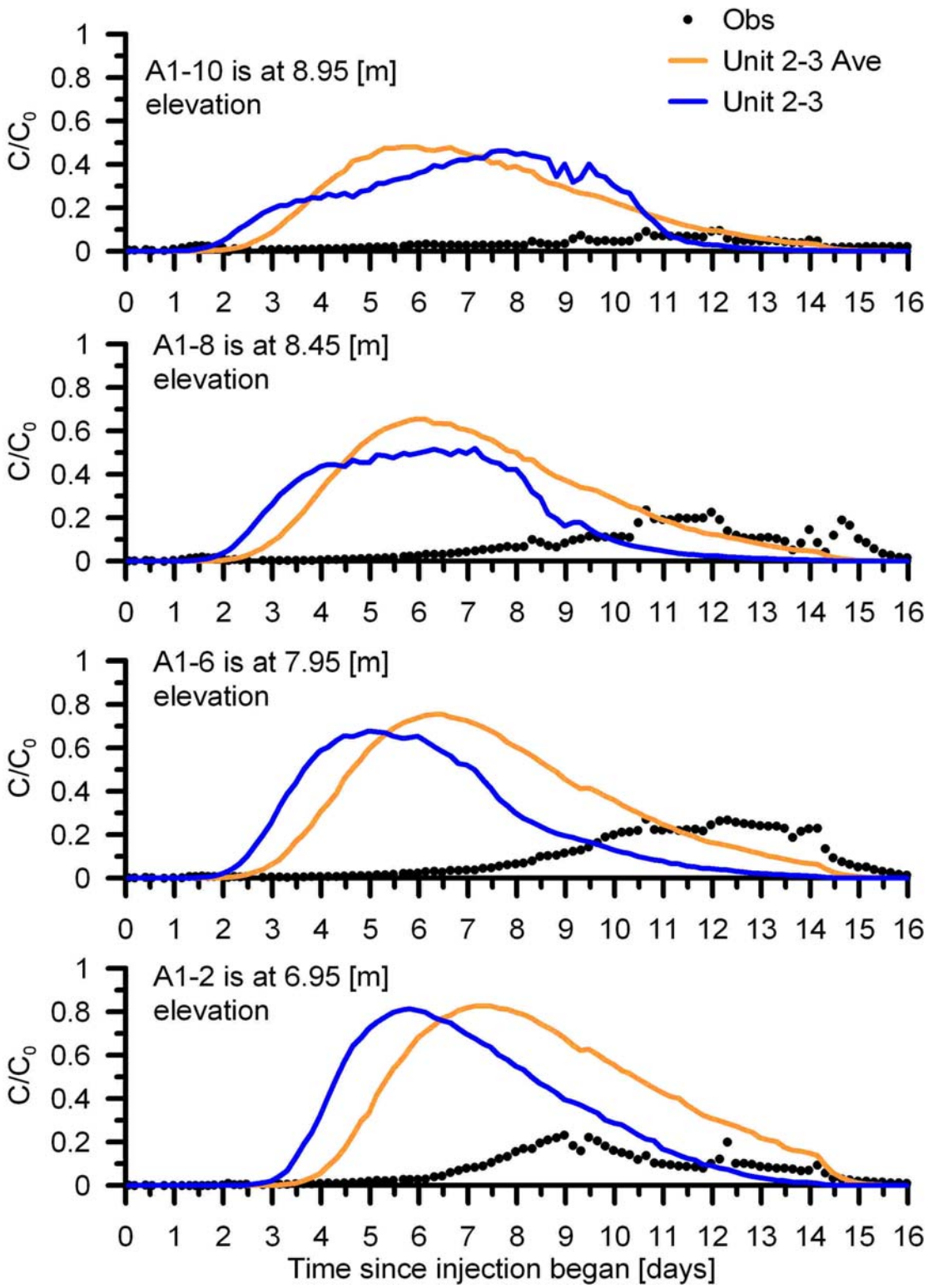

Figure 40: The simulated breakthrough curves in the sampling zones A1-2, A1-6, A1-8, and A1-10 for the Unit 2-3 Ave and Unit 2-3 simulations.

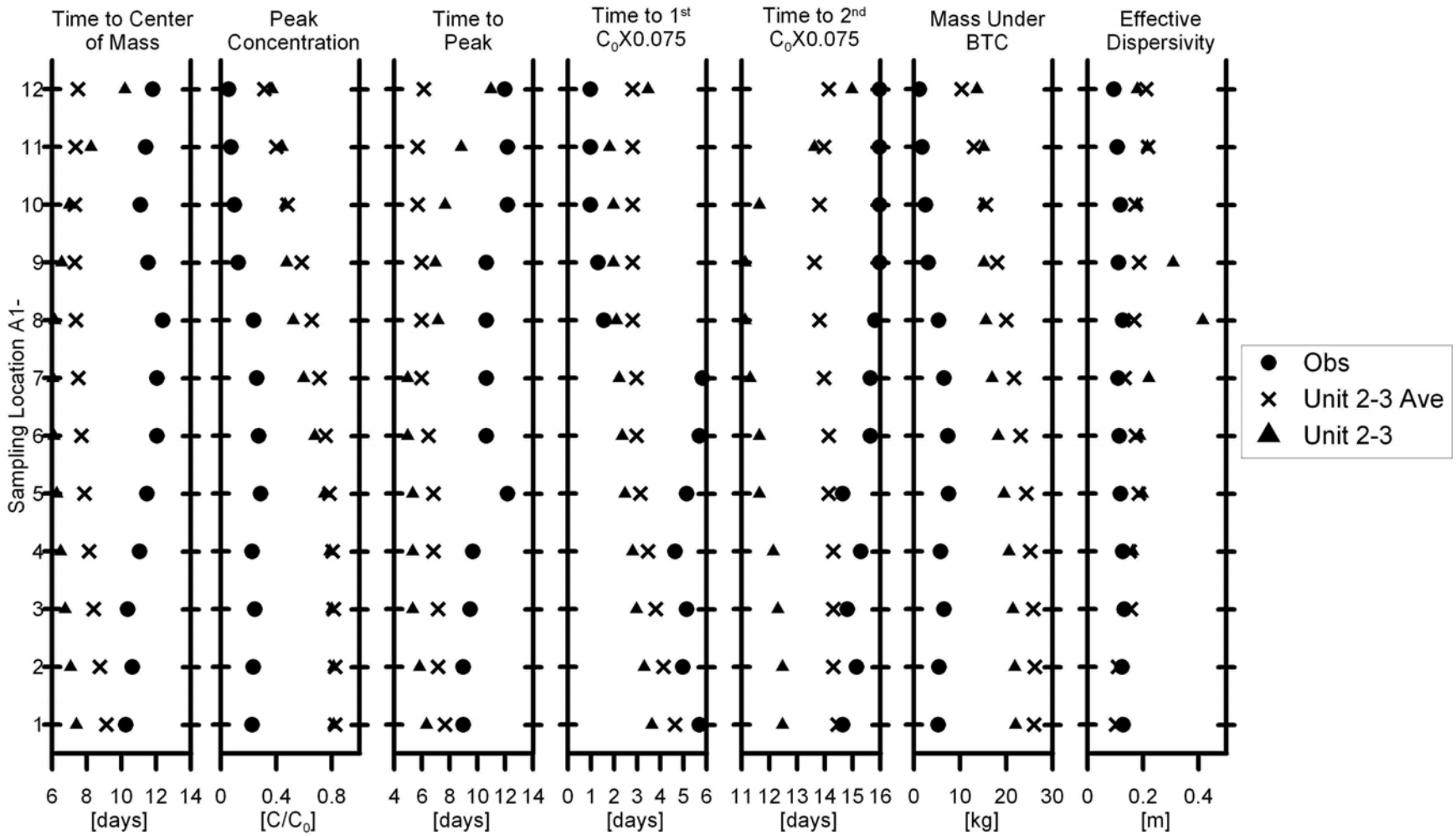

Figure 41: Transport summary statistics for the Unit 2-3 Ave and Unit 2-3 simulations.

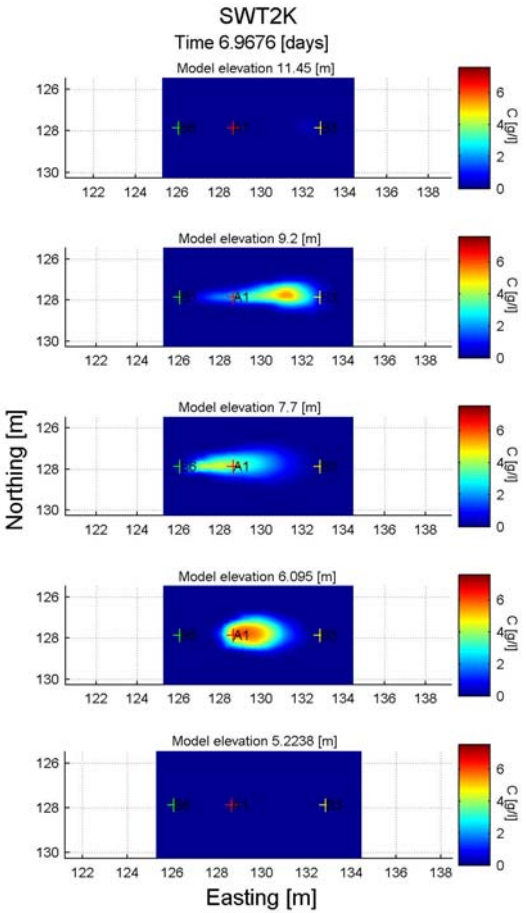

Figure 42: Horizontal plume slices from the Unit 2-3 simulation ~7 days after injection at model elevations: 11.45, 9.2,7.7, 6.095, and 5.2238 m. For reference, the center of the 4 m injection zone in well B3 is at 9.075 m.

the northeast side of A1 (Figure 42). This offset is not as great as that caused by including the river boundary (Figure 38), but is noticeable and is due to adding layering because of the topography on the contact between Units 2 and 3.

4.6.2 More Complex Boundaries Flow Modeling Approach

The effect of layering is further evaluated using the more-realistic complex boundaries flow modeling approach and a series of simulations with progressively more-subdivided hydrostratigraphy. In particular, simulations showing the effects of adding layering to the complex boundaries flow modeling approach were run with the following configurations (Table 8):

- U23A
- TwL
- FLw
- MLhp

The U23A simulation is the homogeneous case for comparison with those having layering, TwL has two layers (i.e., Units 2 and 3 extended up and down) as shown in Figure 29, FLw has five layers based on the five hydrostratigraphic units at the BHRS (Figure 43), and MLhp has the five layers based on the five hydrostratigraphic units at the BHRS but also with Unit 2 subdivided into many lenses as seen in Figure 44 and is consistent with hydrostratigraphic evidence from porosity data and core analysis (Barrash and Clemo, 2002; Barrash and Reboulet, 2004). Unit 2 of the MLhp simulation was subdivided by manually matching highs and lows of the modified Kozeny-Carman

hydraulic conductivity estimates in the wells as seen in Figure 44. The hydrogeologic properties of these simulations are listed in Table 8.

The observed and simulated changes in head for the C3 well in the U23A, TwL, FLw, and MLhp simulations (Figure 45) show that there is little difference between the simulated changes in head between these simulations.

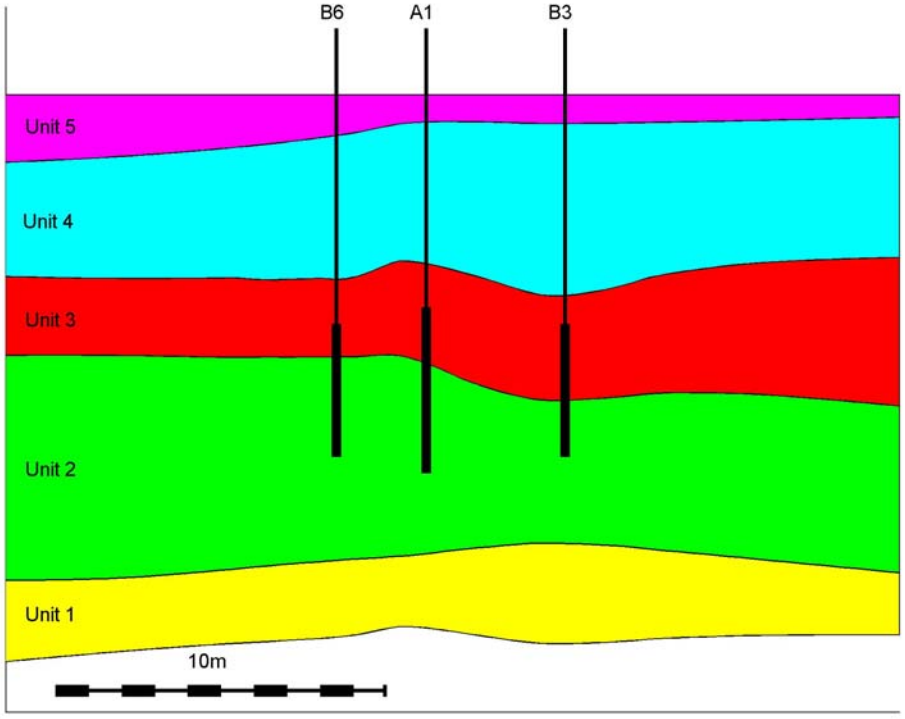

Figure 43: Cross section for all simulations with the Five Layer geometry. (No vertical exaggeration)

The observed and simulated breakthrough curves from sampling zones A1-2, A1-6, and A1-10 for the U23A, TwL, FLw, and MLhp simulations are shown in Figure 46. By adding layering, more heterogeneity is accounted for in the simulations. The breakthrough curves in Figure 46 show that as more layering is added, the simulated

breakthrough matches the observed breakthrough more closely. In the U23A, TwL, and FLw simulations, there is early breakthrough in sampling zones A1-5 and above, but in the MLhp simulations there is improved matching to the observed breakthrough in sampling zones above A1-5.

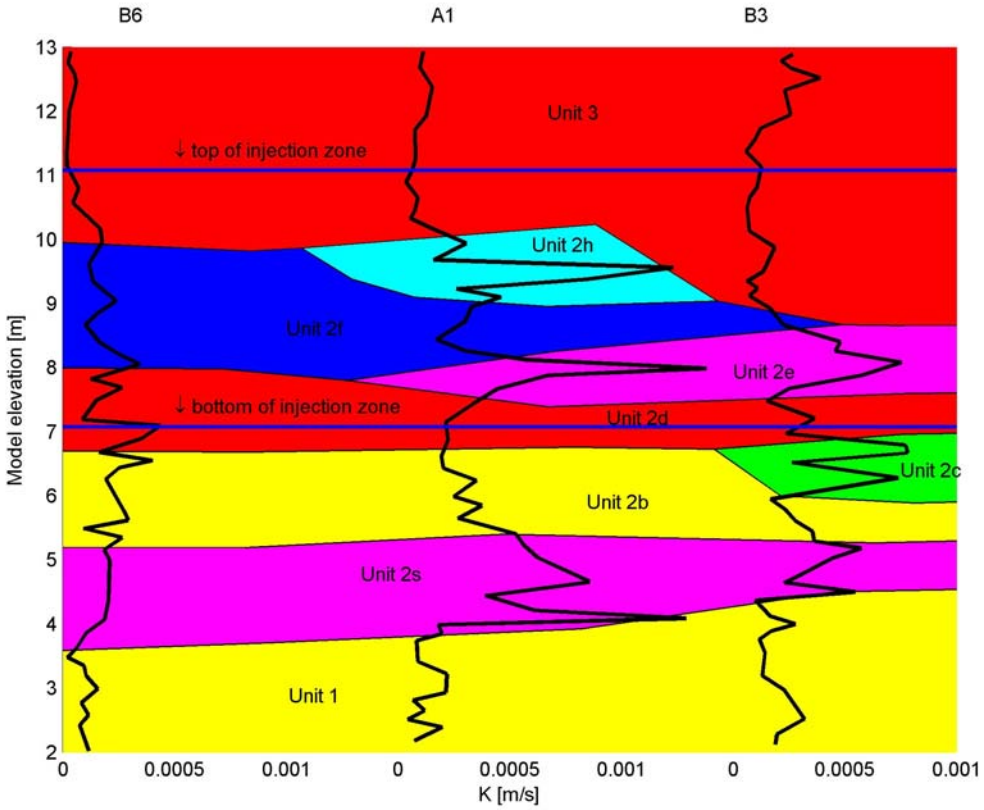

Figure 44: Cross section showing the lenses within Unit 2 for all simulations with the Five Layer geometry and Unit 2 subdivided into smaller lenses. (No vertical exaggeration)

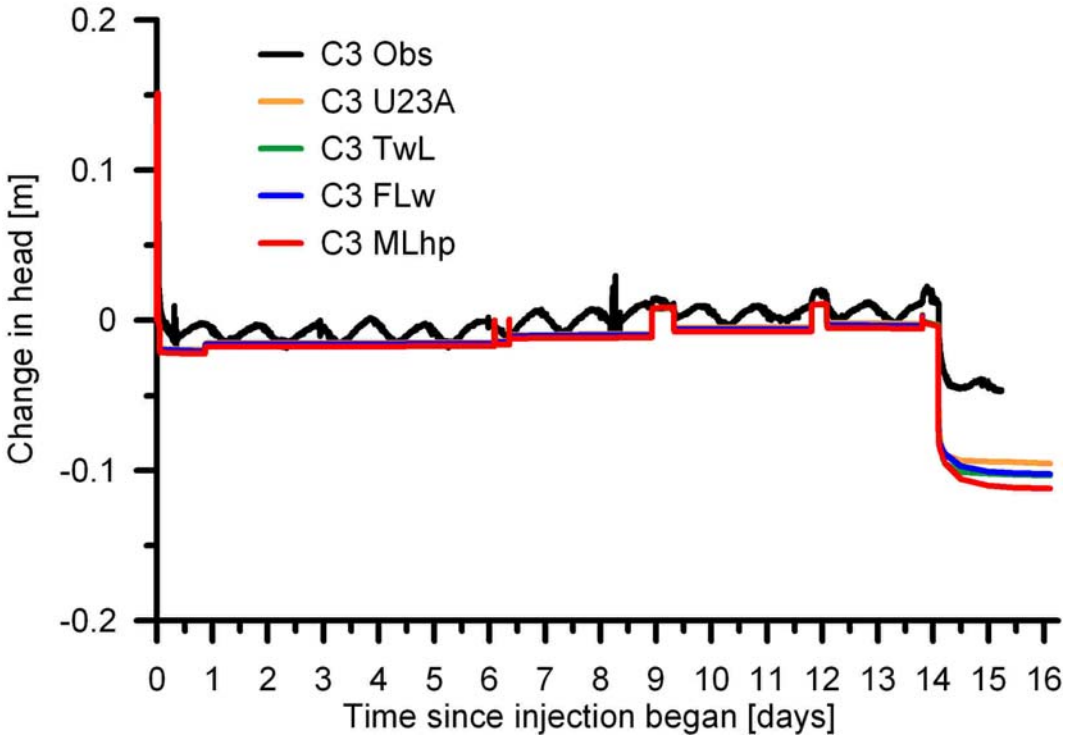

Figure 45: Observed and simulated head change in well C3 for the U23A, TwL, FLw, and MLhp simulations.

Figure 47 shows the transport summary statistics for the U23A, TwL, FLw, and MLhp simulations. The Peak Concentration and the Mass under the Breakthrough Curve statistics for the U23A simulation are higher than the other simulations, but overall Peak Concentration and Mass under the Breakthrough Curve statistics match the observed values reasonably well for all four simulations. The Time to Peak Concentration and the Time to Center of Mass statistics for the bottom four sampling zones (A1-1 through A1-4) for all four of these simulations agree reasonably with the observed. Above sampling zone A1-4, only the MLhp simulation's time to Peak Concentration and Time to Center of Mass statistics match observed breakthrough behavior. For the U23A, TwL, and FLw simulations, the Time to Peak Concentration and Time to Center of Mass statistics for the sampling zones above A1-4 are early. The estimated longitudinal

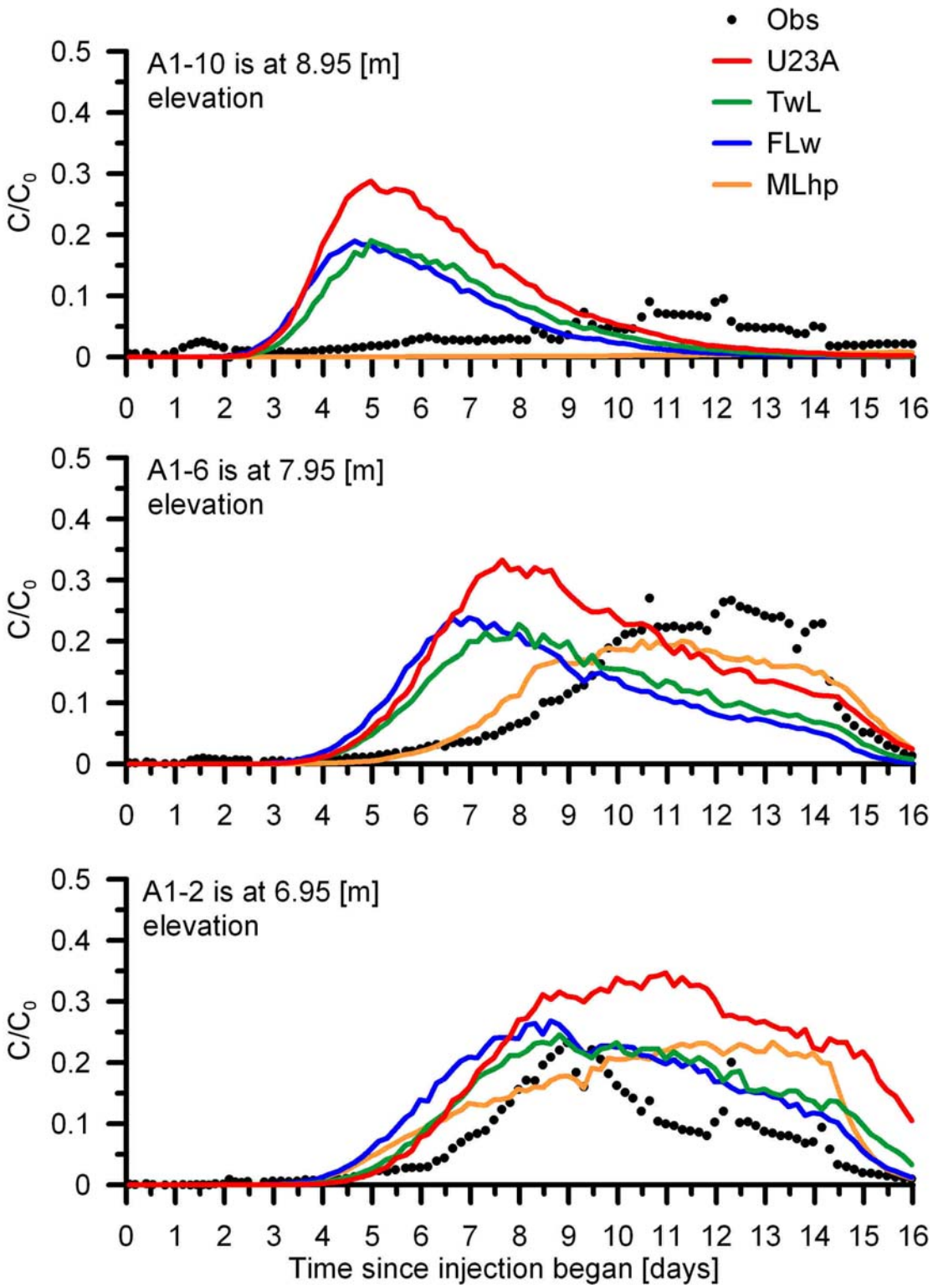

Figure 46: The simulated breakthrough curves in the sampling zones A1-2, A1-6, and A1-10 for the U23A, TwL, FLw, and MLhp simulations.

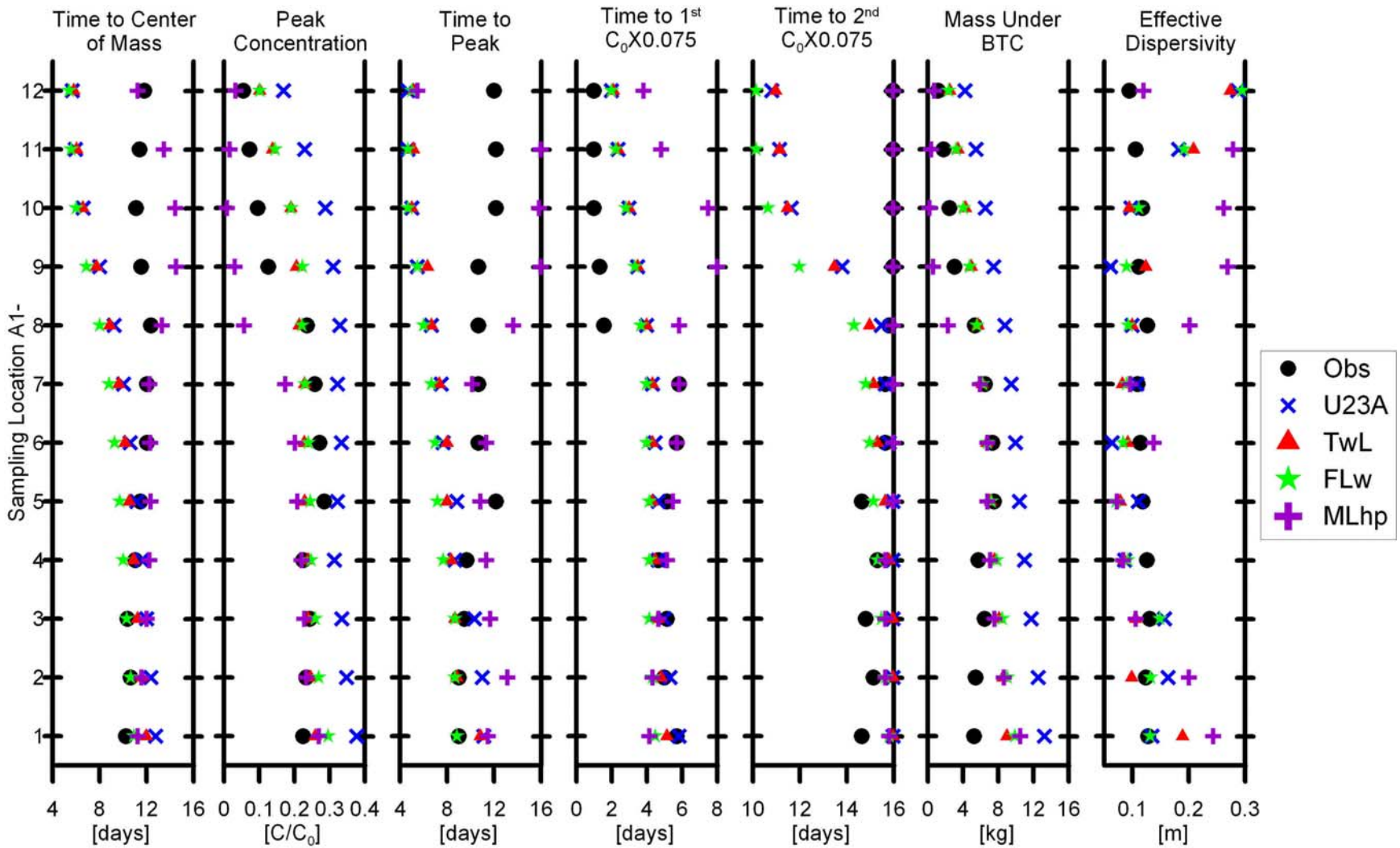

Figure 47: Transport summary statistics for the U23A, TwL, FLw, and MLhp simulations.

dispersivities for all of the simulations match observed dispersivities reasonably well with the exception of that calculated for sampling zone A1-11 in all simulations and for sampling zones A1-9 through A1-10 in the MLhp simulation. The time to first concentration above 7.5% of injection concentration and the time to where the concentration drops below 7.5% of injection concentration statistics are only matched well by the MLhp simulation.

Including layering in the simulations is a way of including more heterogeneity in the simulations. The increase in heterogeneity improves matches to observed breakthrough. Significant improvement in modeling is seen by further defining heterogeneity through zonation or lenses in the hydrogeologic Unit 2 of the Five layer system.

4.7 Well Bores

By specifically defining the presence of well bores in the simulations, improvements are made in fitting the observed breakthrough data. Simulations were run with increasing the presence of well bores to varying degrees (Table 8):

- FL
- FLw
- FLwsc
- MLhp
- MLsb

All five of these simulations used the complex boundaries flow approach. The FL, FLw, and FLwsc simulations all have the same five layer geometry with homogeneous hydrogeologic properties in each layer; MLhp and MLsb also have the same five layer geometry but with Unit 2 subdivided into patches and lenses. The FL simulation does not have well bores defined within it, FLw and MLhp have well bores defined only in the injection interval of B3 and in the pumping interval of well B6, and FLwsc and MLsb have well bores defined over the entire screened sections of wells B3, A1, and B6. Table 8 lists the hydrogeologic properties for simulations and the properties assigned to the well bores and packers.

Figure 48 shows the observed and simulated changes in head from well C3 for the FL, FLw, FLwsc, MLhp, and MLsb simulations and it can be seen that the differences in changes of head between the simulations are small.

It is important to note two tracer behavior tendencies as the presence of wells become more thoroughly defined in the simulations (Figures 49 and 50): 1) concentration magnitude decreases; and 2) the breakthrough in the lower sampling zones happens later. Figure 49 shows the observed and simulated breakthrough curves for sampling zones A1-2, A1-6, and A1-10 for all five simulations and Figure 50 shows the transport summary statistics for all five simulations. The Time to Peak and Time to Center of Mass statistics for the FL simulation are generally earlier than FLw, and FLw is generally earlier than FLwsc; MLhp Time to Peak and Time to Center of Mass statistics are generally earlier than MLsb. The Peak Concentration and the Mass under the

Breakthrough Curve statistics tend to decrease from FL to FLw to FLwsc, and from MLhp to MLsb.

By defining well bores in the simulations, high vertical flow conduits are created. This caused more vertical connectivity and increased the flux from the higher hydraulic conductivity sand channel (Unit 5) to the pumping zone (i.e., the 4 m interval spanning the Unit 2-3 contact). This resulted in a smaller flux from the direction of the plume and a later breakthrough in the sampling zones of well A1.

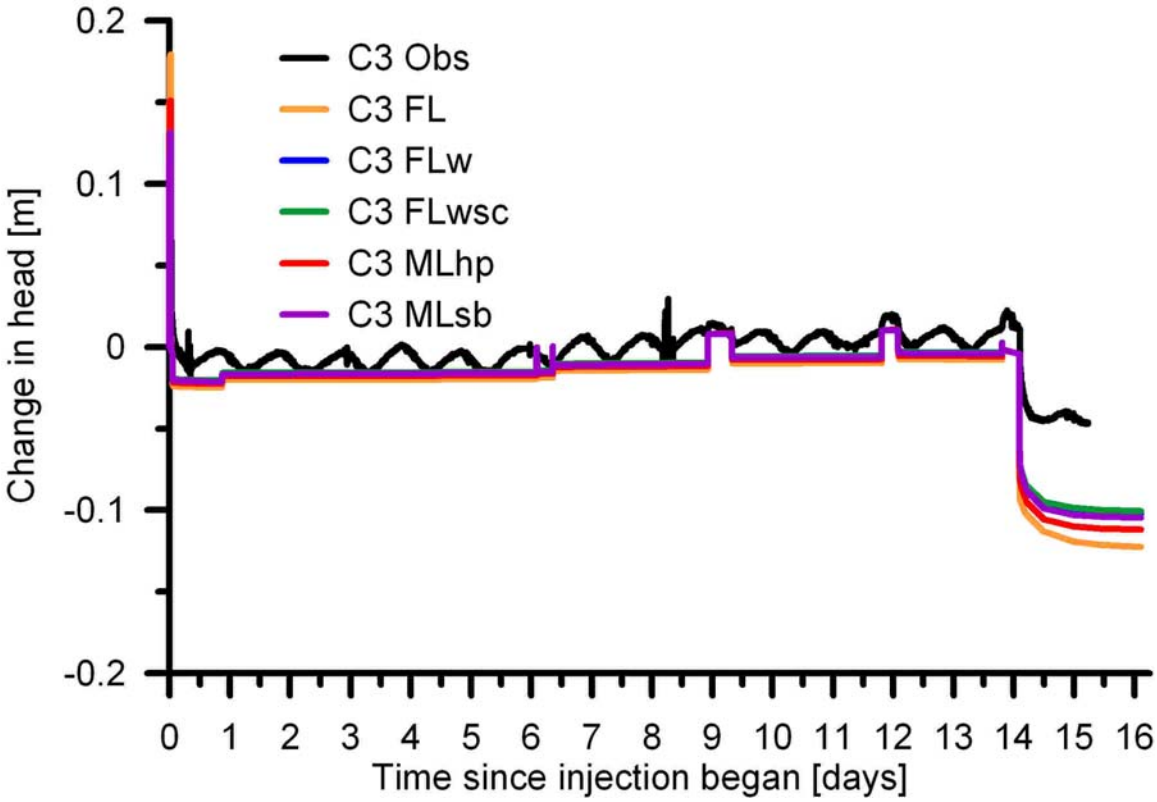

Figure 48: Observed and simulated head change in well C3 for the FL, FLw, FLwsc, MLhp, and MLsb simulations.

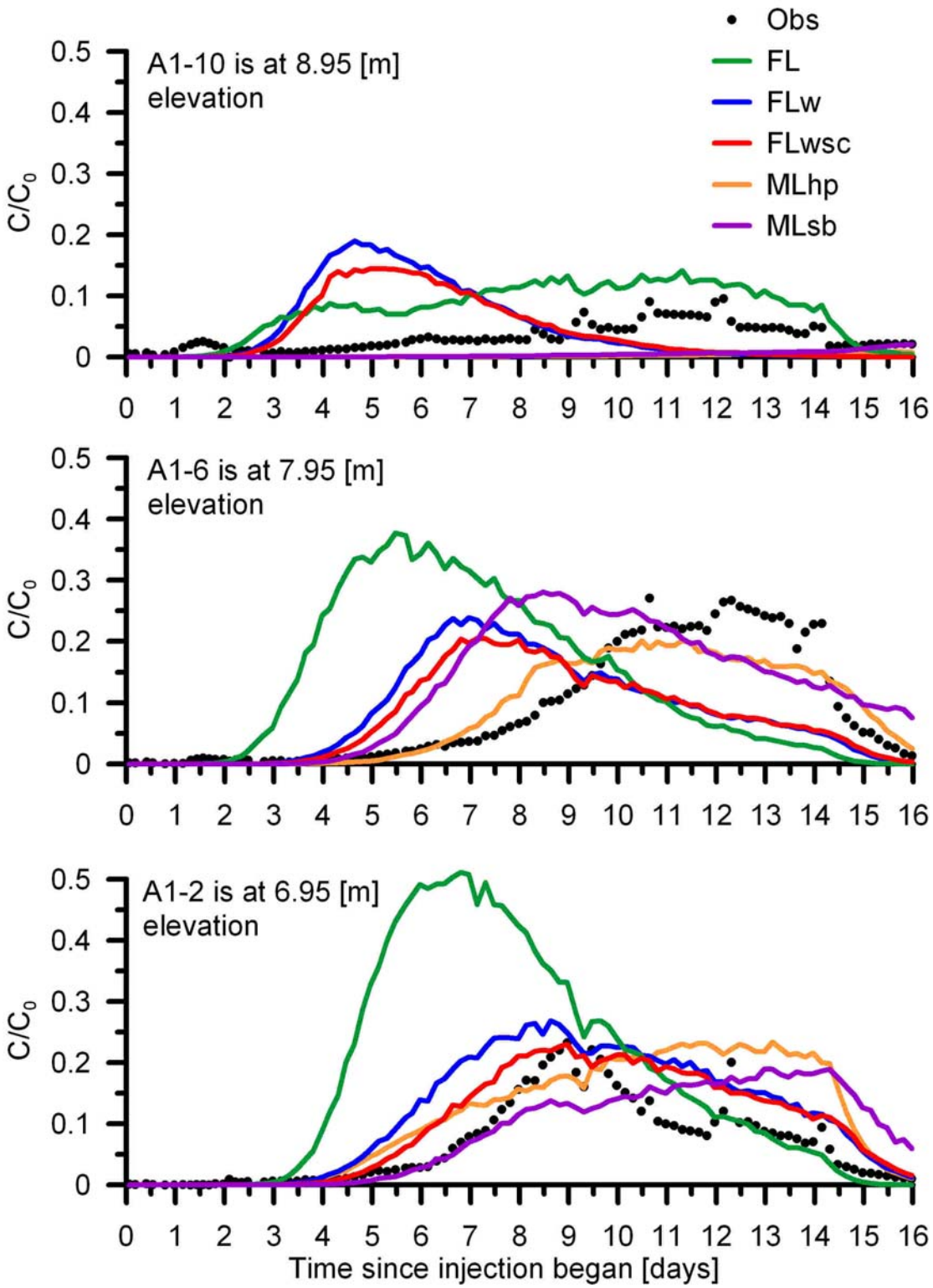

Figure 49: The simulated breakthrough curves in the sampling zones A1-2, A1-6, and A1-10 for the FL, FLw, FLwsc, MLhp, and MLsb simulations.

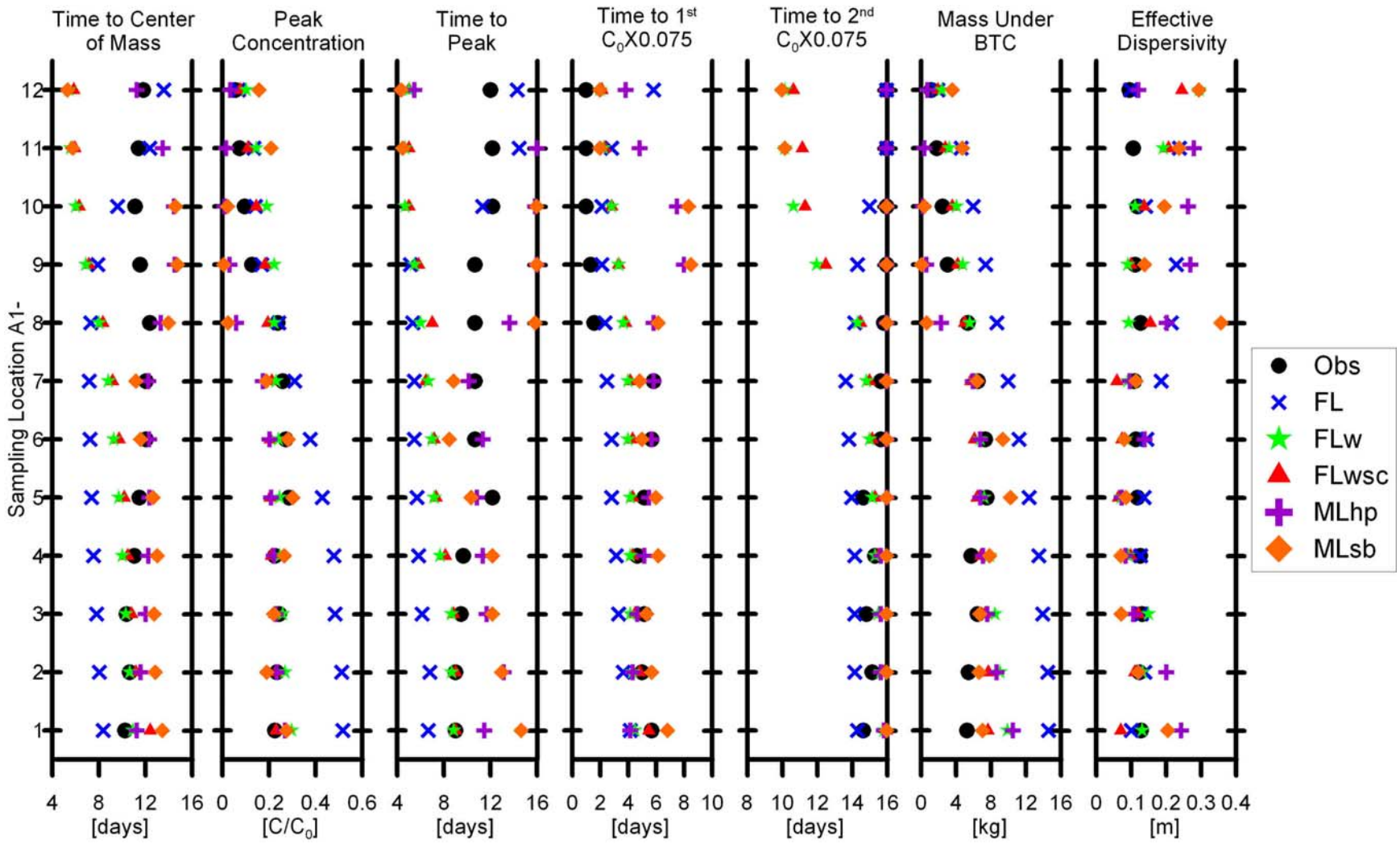

Figure 50: Transport summary statistics for the FL, FLw, FLwsc, MLhp, and MLsb simulations.

4.8 Dispersivity

The following four simulations were run with differing dispersivities (Table 8):

- FLw
- FLwa
- MLsbS
- MLsba2S

All of these four simulations were run using the complex boundaries flow approach with transverse dispersivity equal to 10% of the longitudinal dispersivity and with vertical dispersivity equal to 1% of the longitudinal dispersivity. FLw and MLsbS each had a longitudinal dispersivity of 0.1 m, and FLwa and MLsba2S each had a longitudinal dispersivity of 0.2 m. Other than their longitudinal dispersivities, FLw and FLwa have the same hydrogeologic properties; and likewise with MLsbS and MLsba2.

Figure 51 shows the observed and simulated changes in head from well C3 for the FLw, FLwa, MLsbS, and MLsba2S simulations. The differences in head changes between the simulations are minimal.

Figure 52 shows the observed and simulated breakthrough curves for the A1-2, A1-6, and A1-10 sampling zones from all four simulations. Figure 53 shows several of the transport summary statistics for these simulations. As is expected, the breakthrough curves from simulations with higher dispersivities have lower magnitudes, earlier first breakthrough, and longer tail, and the estimated longitudinal dispersivities for FLwa and MLsba2S calculated from model behavior are slightly higher than those calculated for FLw and MLsbS models. Likewise the time at which the concentration first exceeds

7.5% of the injection concentration is earlier for the FLwa and MLsba2S simulations, and the time that the concentration drops below 7.5 % of the injection concentration is later for the FLwa and MLsba2S simulations which have a higher dispersivity.

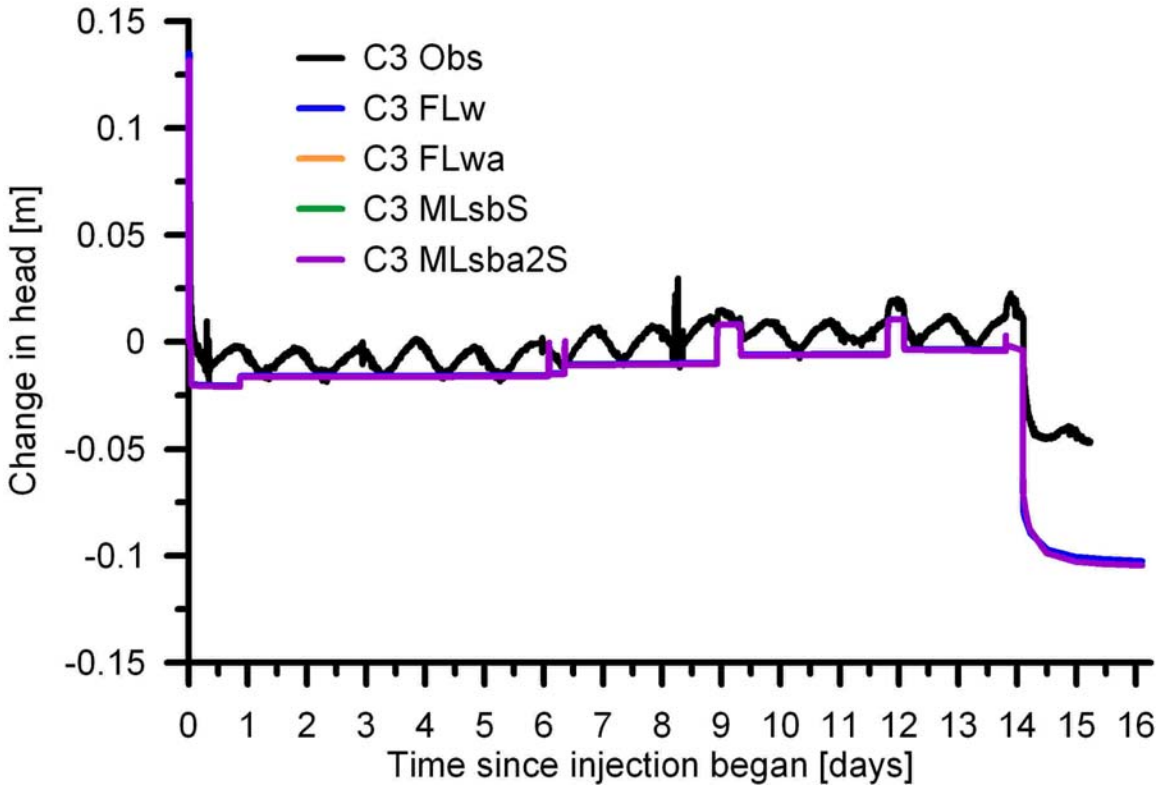

Figure 51: Observed and simulated head change in well C3 for the FLw, FLwa, MLsbS, and MLsba2S simulations.

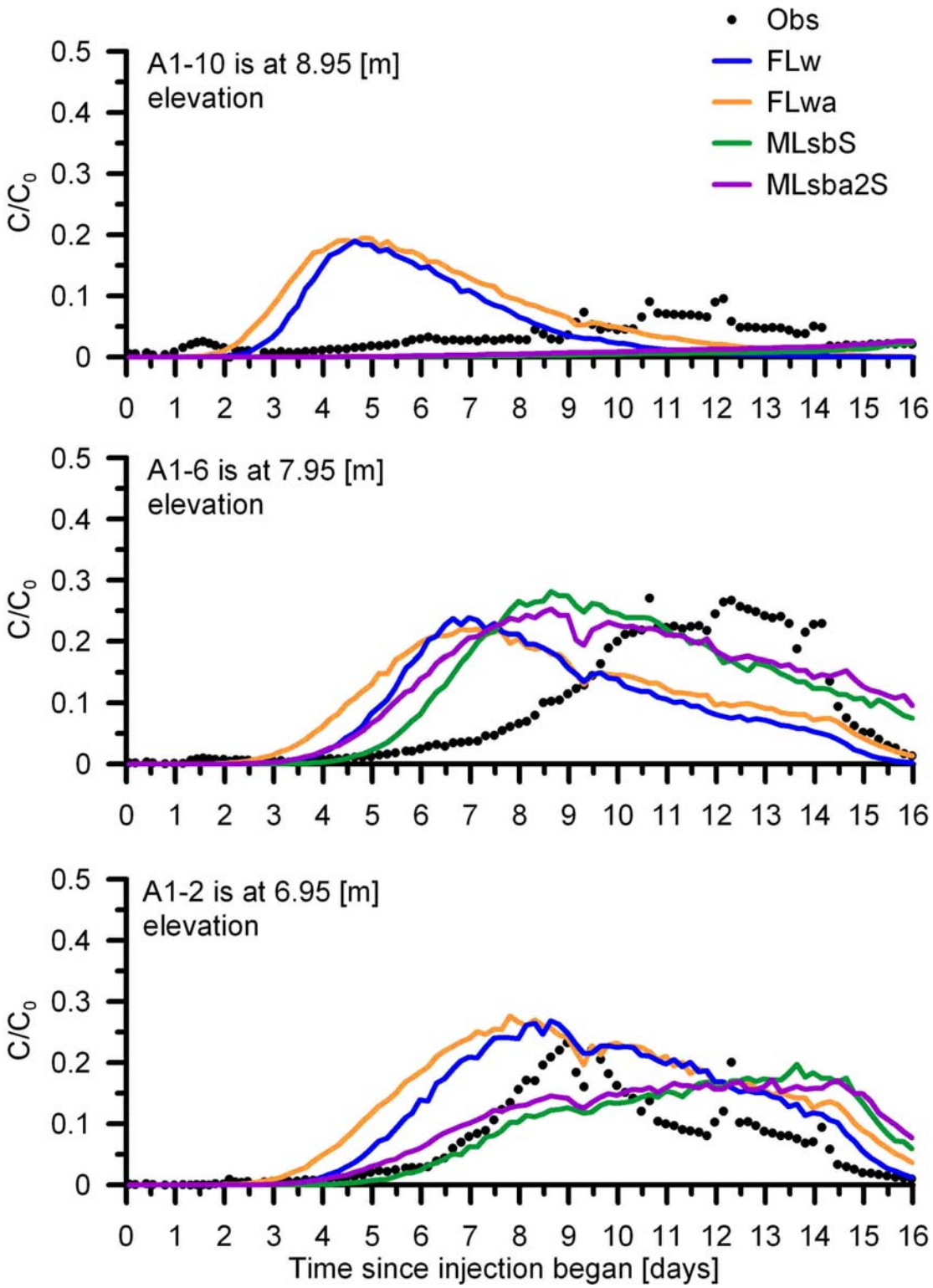

Figure 52: The simulated breakthrough curves in the sampling zones A1-2, A1-6, and A1-10 for the Flw, FLwa, MLsbS, and MLsba2S simulations.

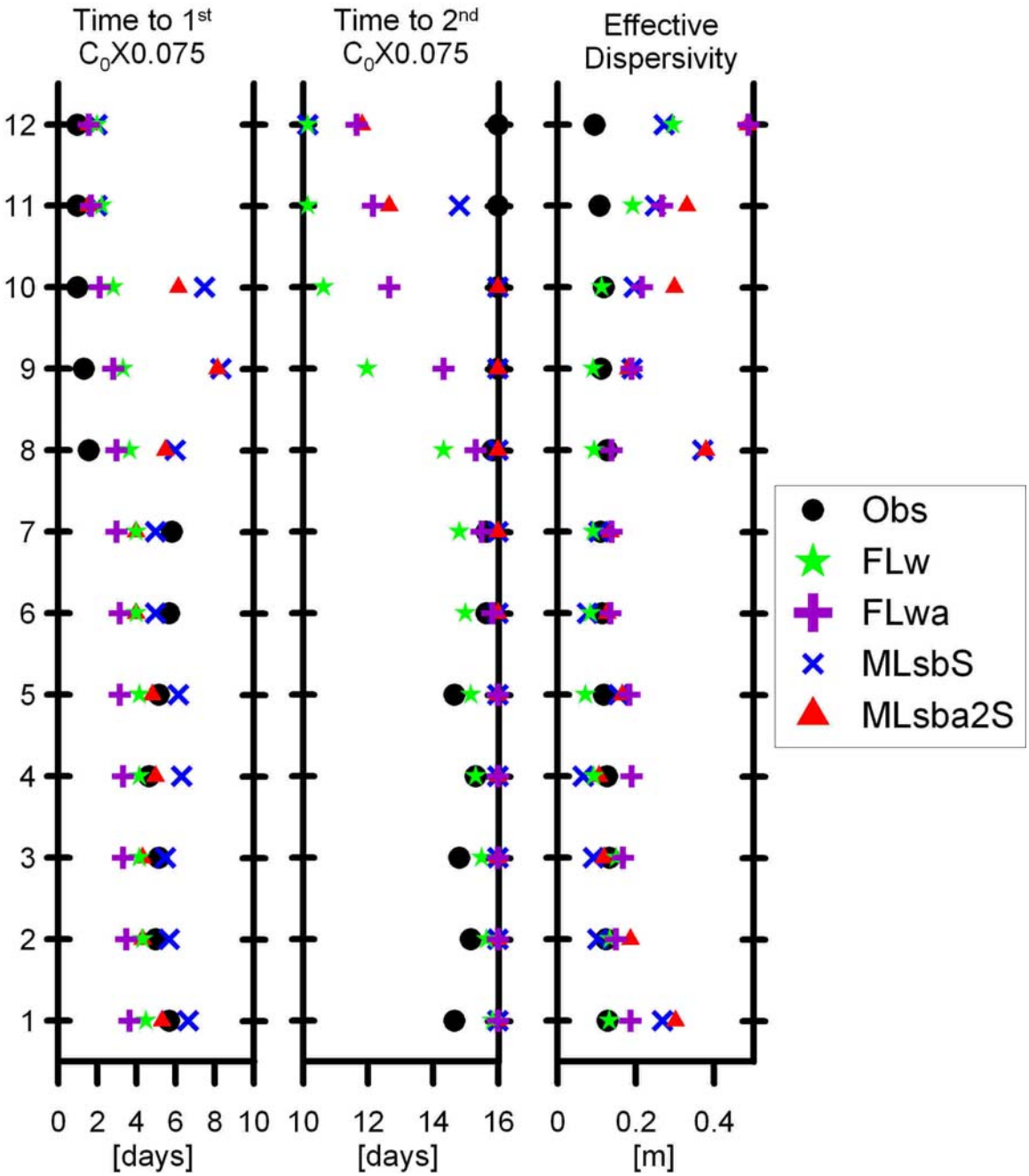

Figure 53: Transport summary statistics for the FLw, FLwa, MLsbS, and MLsba2S simulations.

4.9 Porosity

Equation 13 shows that advective transport is inversely proportional to effective porosity. Thus, if the effective porosity is increased, advective transport will be slowed. Because of early breakthrough in the upper sampling zones (see the simulated breakthrough behavior for sampling zones A1-10 and A1-6 from the U23A, TwL, and FLw simulations in Figure 46), simulations were run with increasing effective porosity. To show whether increasing the effective porosity would slow the plume in the upper sampling zones the following simulations were run using the complex boundaries flow modeling approach (Table 8):

- FLw
- FLpor1
- FLpor2
- FLpor3
- FLwa
- FLwab1
- FLwab2

All of the above seven simulations have the same five-unit hydrostratigraphy with uniform hydrogeologic properties per unit as listed in Table 8. FLw and FLwa have the porosities equal to those reported by Barrash and Clemo (2002). FLpor1, FLpor2, FLpor3 have porosities equal to 110%, 120%, and 130% of the porosities reported by Barrash and Clemo (2002). FLwab1 has porosities and the standard deviation calculated from the porosity variances reported by Barrash and Clemo (2002). FLwab2 has

porosities and two standard deviations calculated from the porosity variances reported by Barrash and Clemo (2002).

Figure 54 shows the observed and simulated breakthrough curves for sampling zones A1-2, A1-6, and A1-10 and, as expected, increasing the porosity causes later breakthrough. However the plume slowing is not sufficient in the upper sampling zones to match observed breakthrough, and the increases in porosity seem higher than is reasonable for the scenarios that better match breakthrough on the rising limbs. Figure 55 shows the Time to Center of Mass and the Time to Peak Concentration transport statistics which also show slowing of the plume, but not enough slowing to match observed breakthrough. That is, porosity is a contributing factor to tracer breakthrough behavior, but it is not the most significant factor.

4.10 Vertical Hydraulic Conductivity Anisotropy

Five simulations were run to test the effects of vertical hydraulic conductivity anisotropy on transport during the TTLT (Table 8):

- MLsba2S
- MLsbV15a2S
- MLsbV2a2S
- MLsbV3a2S
- MLsbV4a2S

The base model framework for these scenarios included five hydrostratigraphic units – with Unit 2 subdivided into many lenses, and longitudinal dispersivity of 2. Vertical

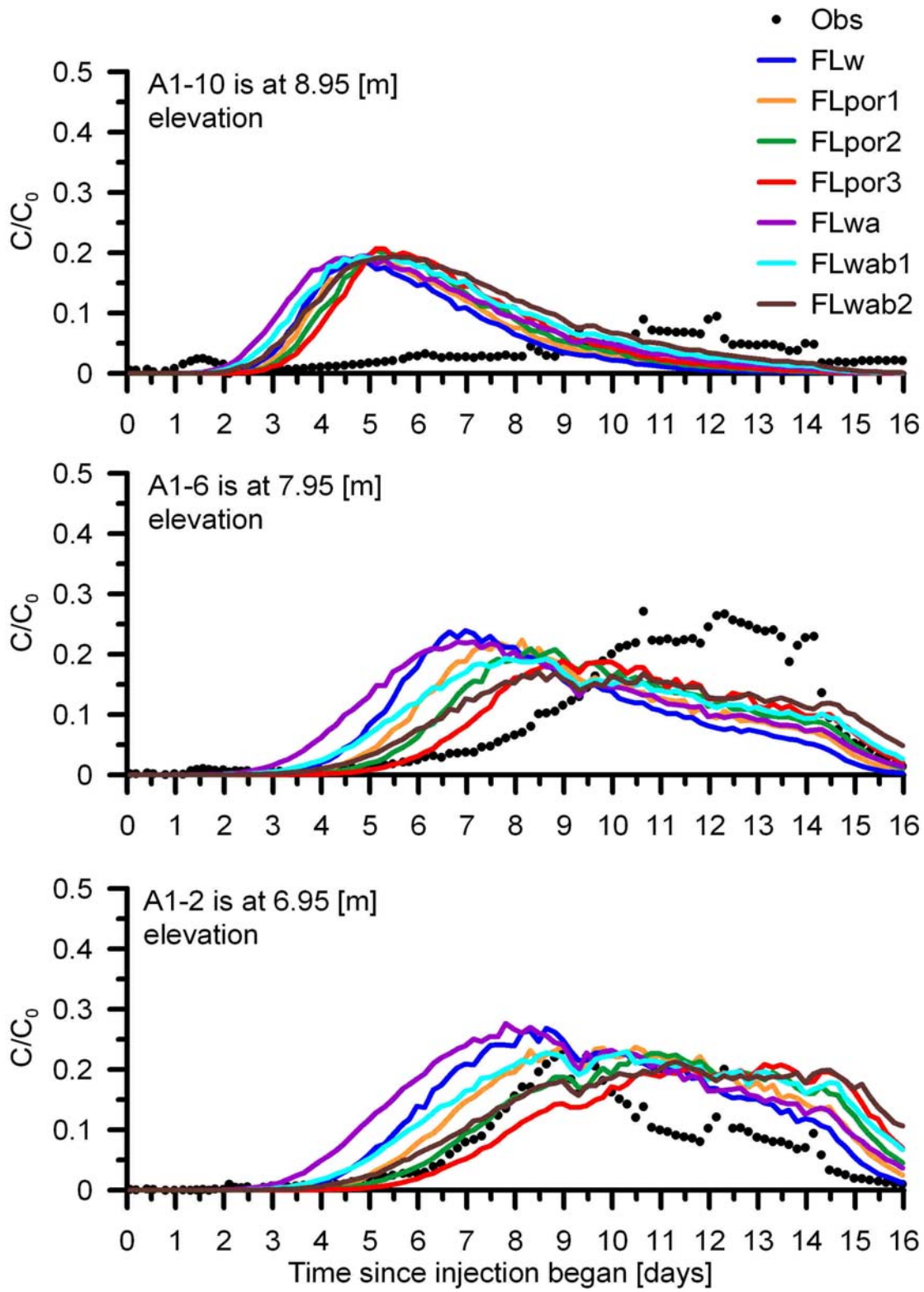

Figure 54: The simulated breakthrough curves in the sampling zones A1-2, A1-6, and A1-10 for the FLw, FLpor1, FLpor2, FLpor3, FLwa, FLwab1, and FLwab2 simulations.

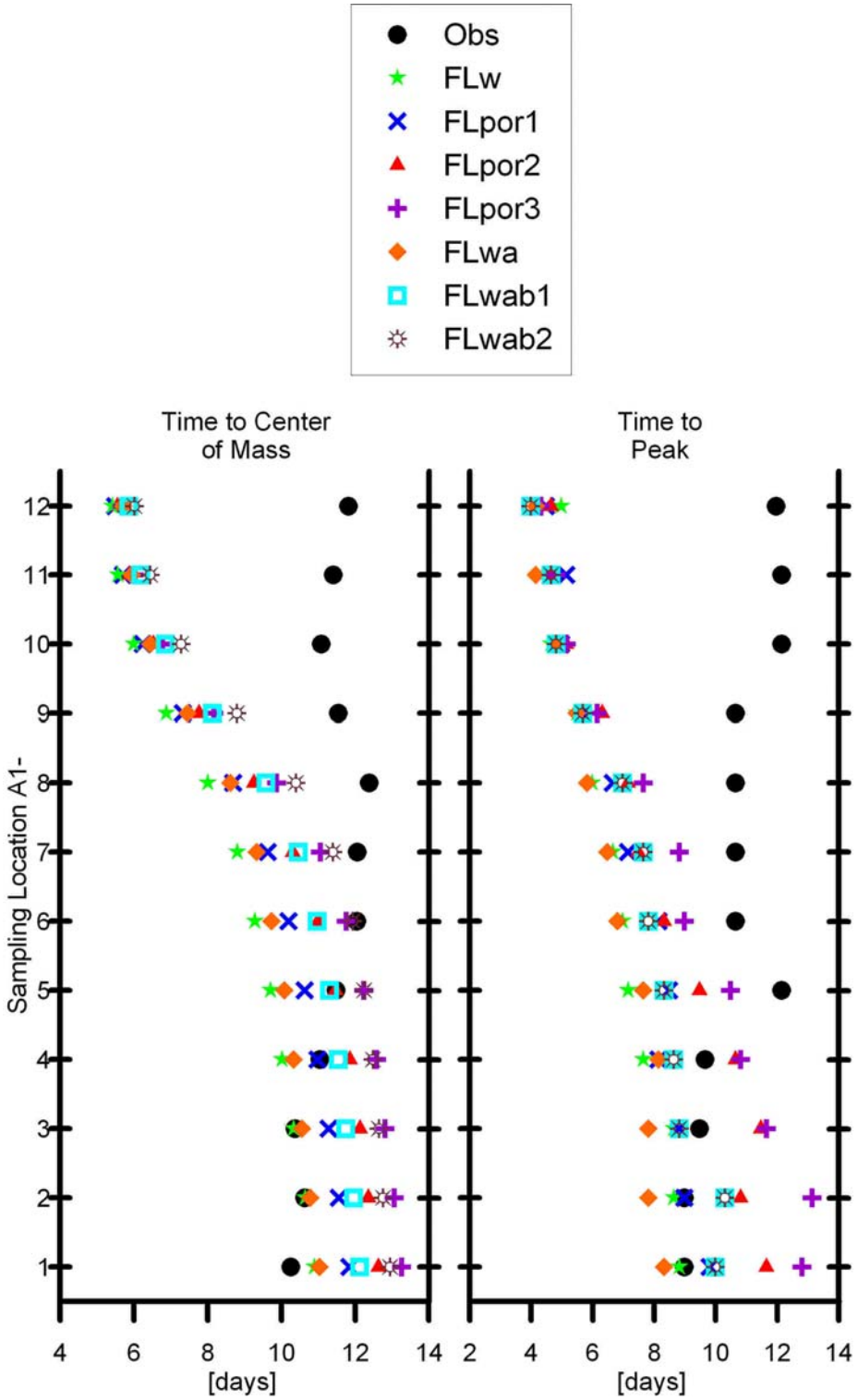

Figure 55: The Time to Center of Mass and the Time to Peak Concentration for the FLw, FLpor1, FLpor2, FLpor3, FLwa, FLwab1, and FLwab2 simulations.

hydraulic conductivity anisotropy (K_h/K_v) was varied from 1 (MLsba2S) to 4 (MLsbV15a2S of 1.5, MLsbV2a2S of 2, MLsbV3a2S of 3, and MLsbV4a2S of 4). The observed and simulated breakthrough curves from the sampling zones A1-2, A1-6, and A1-10 of these simulations are similar in zones A1-2 and A1-10 but show progressively greater breakthrough peaks and mass with increasing anisotropy in zone A1-6 (Figure 56). Figure 57 shows the Peak Concentration transport statistic for these simulations. The Peak Concentration tends to increase with higher vertical hydraulic conductivity anisotropy which would most likely be due to less spreading of the plume in the vertical direction.

4.11 Hydraulic Conductivity and Porosity Distributed Throughout the Well Field

By increasing complexity in the simulations, some improvements are seen in matching the observed breakthrough curves in sampling zones of well A1 such as seen by adding more complex boundary conditions and by adding layering. Another level of complexity is to fully distribute hydraulic conductivity and/or porosity in the central well field of the BHRS instead of treating the units as having uniform (homogeneous) distributions of hydrologic properties. To consider the effects of distributions on transport on a reconnaissance basis one stochastic realization of a porosity distribution, one stochastic realization of a hydraulic conductivity distribution, and one model that combined the porosity and hydraulic conductivity realizations were created using the geostatistics listed in Table 9. That is, conducting a rigorous stochastic analysis with many realizations is beyond the scope of this thesis. Each distribution was generated by

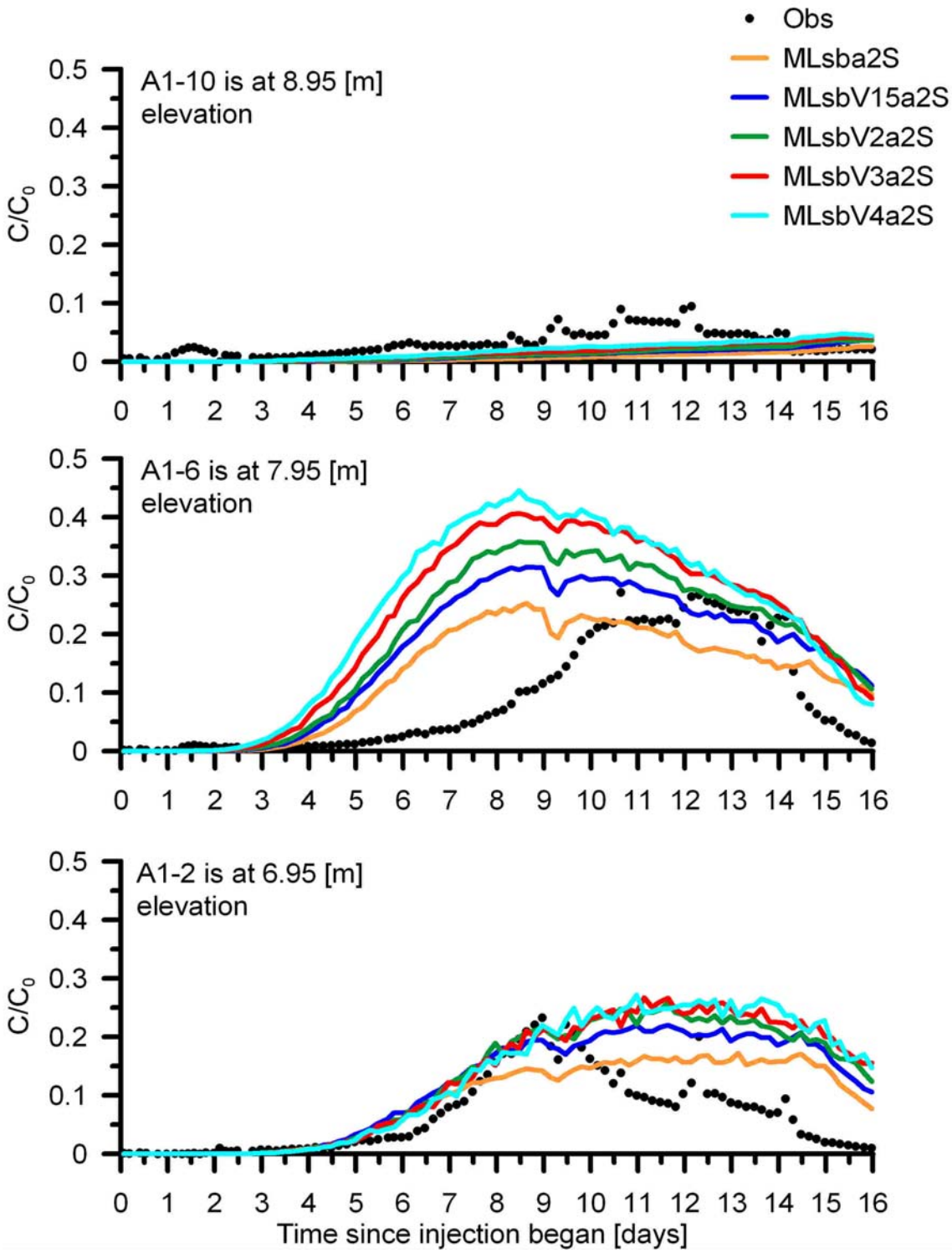

Figure 56: The simulated breakthrough curves in the sampling zones A1-2, A1-6, and A1-10 for the MLsba2S, MLsbV15a2S, MLsbV2a2S, MLsbV3a2S, and MLsbV4a2S simulations.

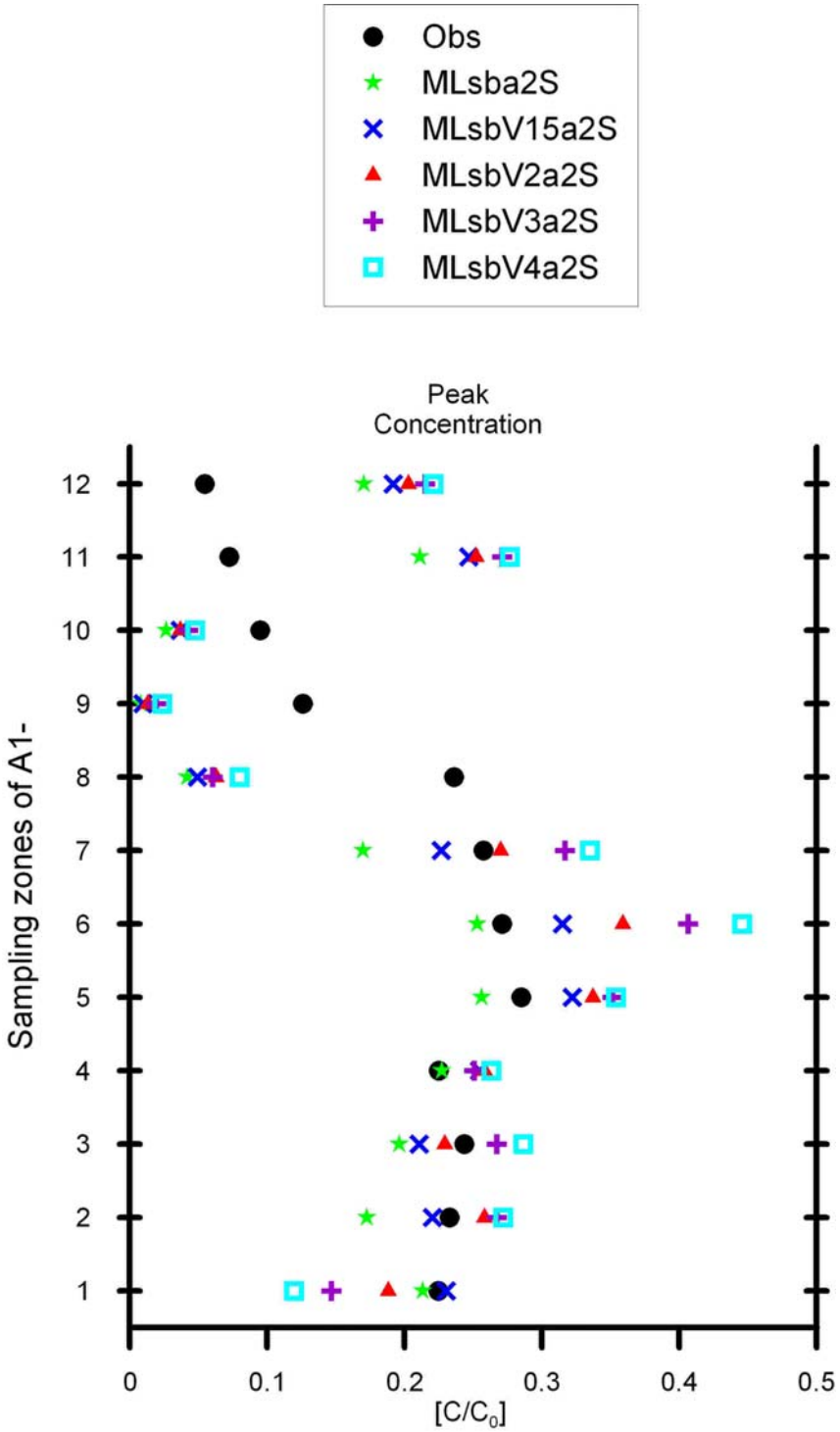

Figure 57: The Peak Concentration transport statistic for the MLsba2S, MLsbV15a2S, MLsbV2a2S, MLsbV3a2S, and MLsbV4a2S simulations.

Table 9: Statistics used in the generation of a hydraulic conductivity and a porosity distribution.

	Hydraulic Conductivity				
Unit	***Variogram Model***	***Horizontal Range [m]***	***Vertical Range [m]***	***Nugget***	***Sill***
Unit 5	Exponential	7	1	0	0
Unit 4	Exponential	7	1.8	0	0
Unit 3	Exponential	7	0.9	0	0
Unit 2	Exponential	7	1.3	0	0
Unit 1	Exponential	7	1.4	0	0
	Porosity				
Unit 5	Exponential	7	1.9	0.2	0.53
Unit 4	Exponential	7	1	0.2	0.79
Unit 3	Exponential	7	1.9	0.1	0.36
Unit 2	Exponential	7	3	0.2	0.48
Unit 1	Exponential	7	1.9	0.1	0.43

creating distributions within each of the five hydrostratigraphic units according to the parameter pdf and the geostatistical structure of each unit, and then by splicing the five units together. The resulting hydraulic conductivity and porosity distributions were used in three simulations (Table 8):

- DK
- DP
- DKP

DK has only the hydraulic conductivity distributed throughout the central well field; DP has only the porosity distributed throughout the central well field; and DKP has both the hydraulic conductivity and the porosity distributed throughout the central well field. There is little difference in the simulated changes in head values of these three

simulations as seen in a plot of the observed and simulated changes in head in well C3 shown in Figure 58. Figure 59 shows the observed and simulated breakthrough curves from sampling zones A1-2, A1-6, and A1-10 from the DK, DP, and DKP simulations. Figure 60 shows the transport summary statistics for these three simulations. The DK Time to Center of Mass statistics agree well with the observed. All but the lower four sampling zones of the DP Peak Concentration statistics agree well with the observed statistics. Both of these two observations translate somewhat to the DKP simulation. These realizations lead me to believe that stochastic simulations will more fully capture the bromide transport behavior, especially if used in combination with the inclusion of lenses in Unit 2.

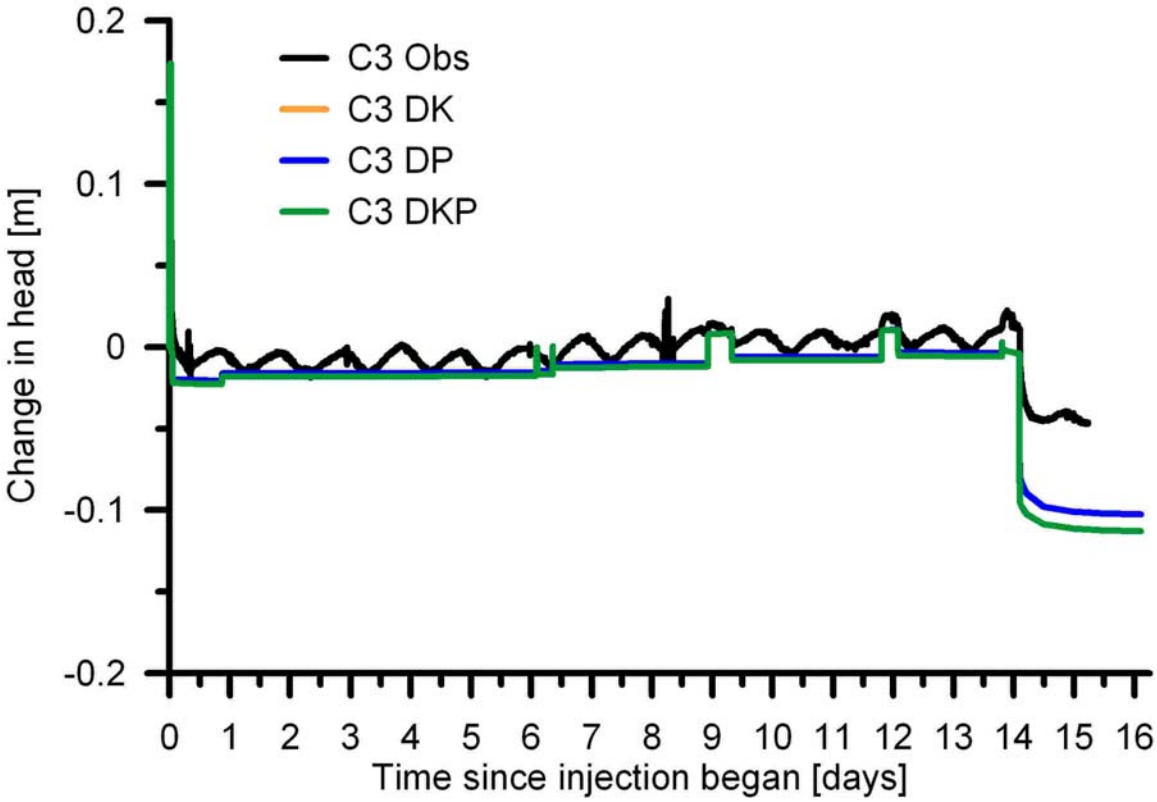

Figure 58: Observed and simulated head change in well C3 for the DK, DP, and DKP simulations.

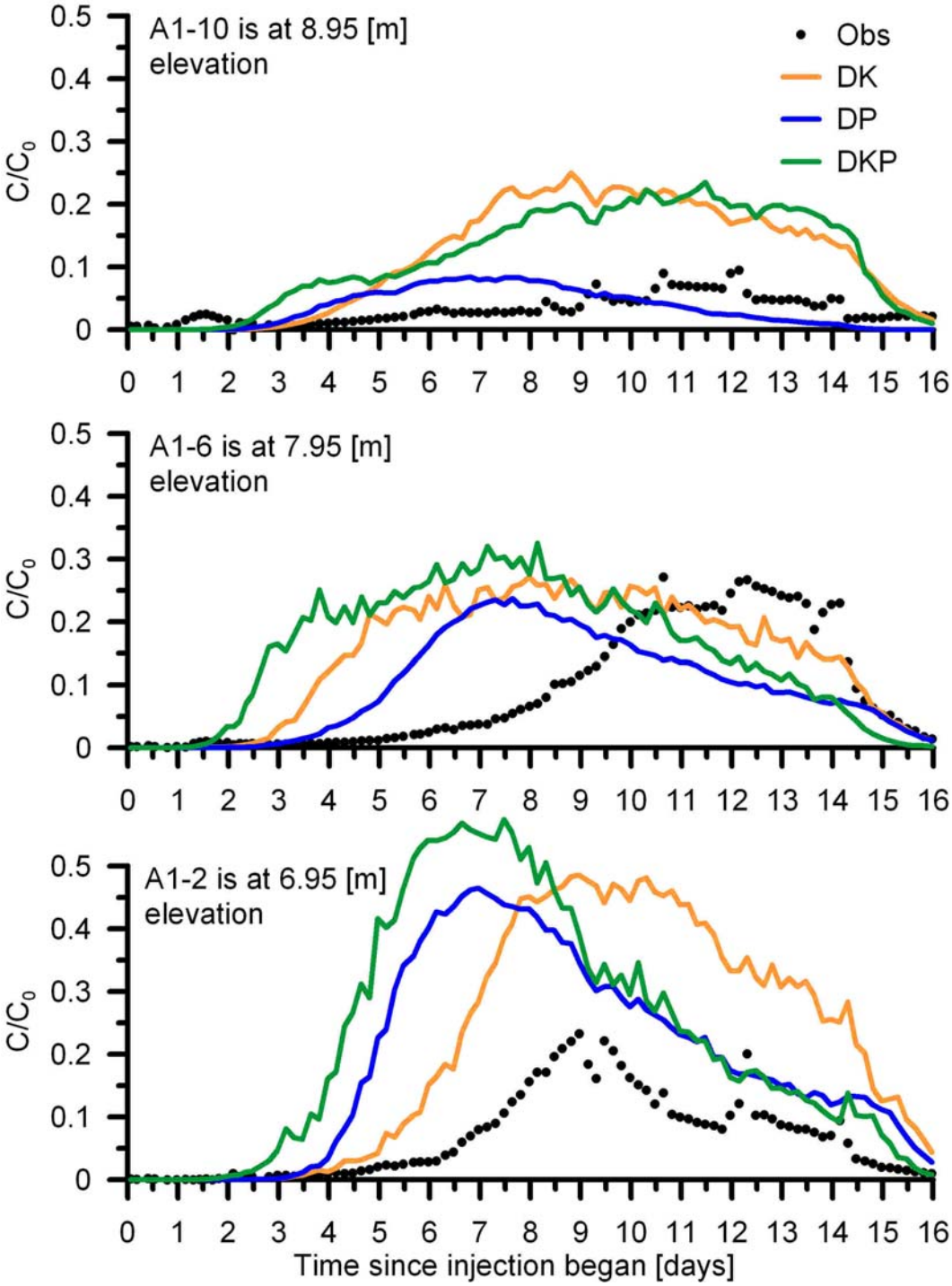

Figure 59: The simulated breakthrough curves in the sampling zones A1-2, A1-6, and A1-10 for the DK, DP, and DKP simulations.

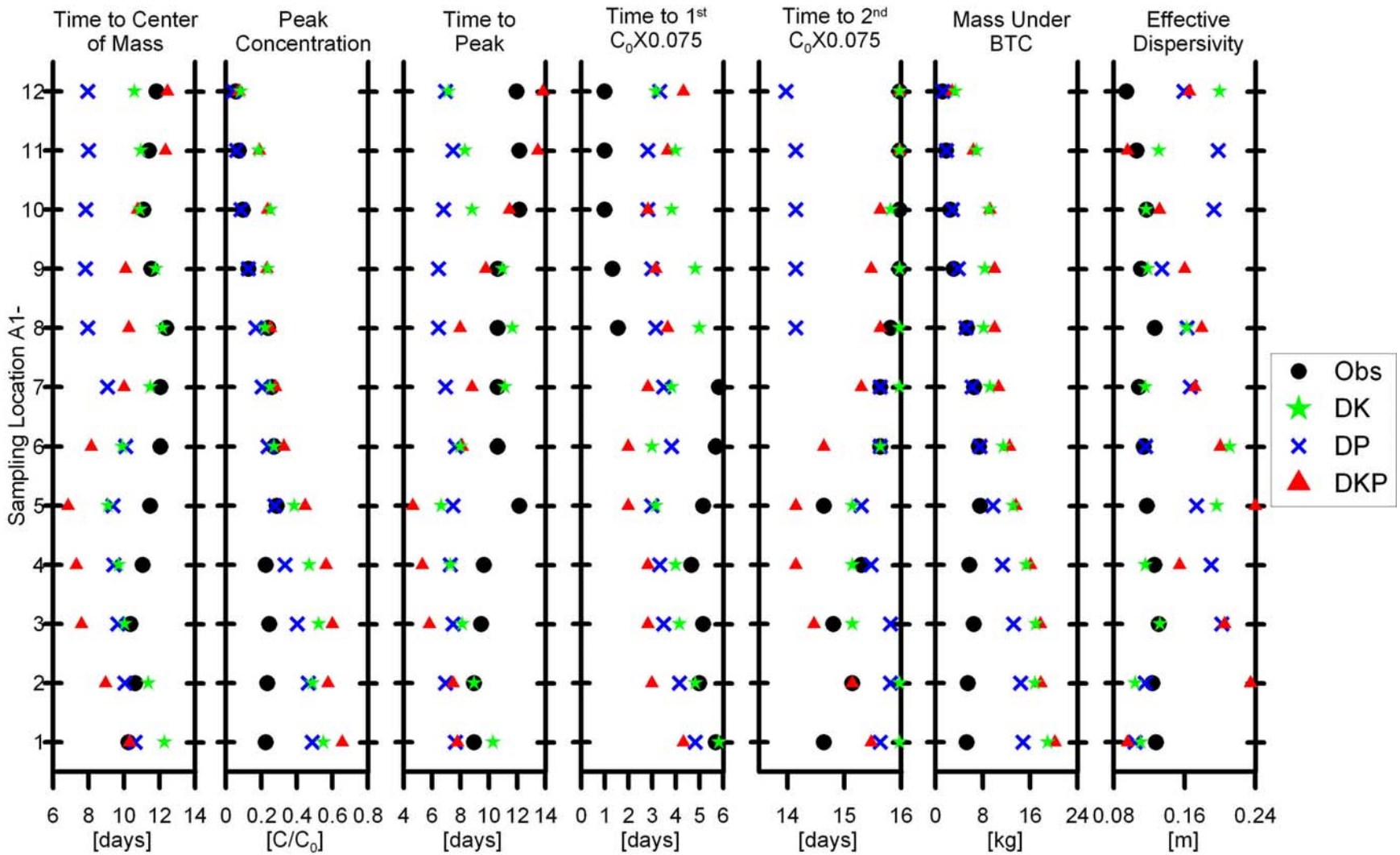

Figure 60: Transport summary statistics for the DK, DP, and DKP simulations.

5 SUMMARY AND CONCLUSIONS

5.1 Summary

This thesis has been an exercise in deterministic modeling. There is a large amount of data available at the BHRS that can be used to constrain the modeling. By adding complexity to the model – both hydrogeologic complexity and boundary condition complexity – better fits between the modeled and observed tracer test data are seen. Results of modeling with these added complexities are summarized below.

- Analysis of the breakthrough curves measured during the TTLT gives estimates of longitudinal dispersivity and hydraulic conductivity.
    - Accurate estimates of hydraulic gradients yield better estimates of hydraulic conductivities.
- Variable density flow is significant in the TTLT.
- Evapotranspiration does not need to be simulated for the TTLT.
- The use of homogeneous hydrogeologic properties throughout the BHRS in simulations yields early breakthrough.
- The river boundary essentially creates a relative hydraulic gradient away from the river and shifts the tracer plume northeastward from well A1 which lowers the magnitudes of the simulated breakthrough curves to levels comparable to observed breakthrough curves.

- Layering better characterizes the 3D distribution of hydrogeologic properties and improves timing and magnitude matches of the observed breakthrough curves.
- Well bores need to be included in simulations.
- Dispersivity needs to be accurately estimated.
- Better characterization of hydraulic conductivity and porosity in the simulations improves the match between simulated and observed breakthrough.

Given the bromide concentration of the injectate, relatively low hydraulic gradient at the site, and correlation lengths of the hydraulic conductivity heterogeneity at the BHRS there is a tendency for variable density flow in the aquifer flow system at the BHRS. This is based on an evaluation using the criteria of Barth et al. (2001) for variable density flow in heterogeneous material. Furthermore the effects of variable density flow are easily seen by comparing simulations run with and without accounting for variable density flow (i.e. SEAWAT 2000 simulations verses MODFLOW 2000 – MT3DMS simulations).

ET is very noticeable at the BHRS. During the TTLT it appears that the ET influence on hydraulic head is on the order of 0.5-2.5 cm change per day. However through comparison of two simulations – one with ET and one without ET – it was determined that ET does not significantly affect the transport of the bromide tracer during the TTLT.

The simplest conceptual model evaluated had homogeneous hydrogeologic properties in the modeling domain with two constant head boundaries and two no-flow

boundaries to induce a regional hydraulic gradient matching the measured gradient at the BHRS. Three simulations were run in this manner but none of them fit the observed tracer breakthrough data very well; all show high magnitude and early arrival times.

By more realistically accounting for the various boundary conditions at the BHRS (i.e. by adding complexity), improvements can be seen in fitting the observed data. The effect of including the river boundary is to increase the relative hydraulic gradient away from the river which causes a shift in the plume trajectory away from the river. When the bromide plume does not pass directly through well A1, the magnitudes are lower and more closely match the observed magnitudes.

Further improvement was seen in matching the observed breakthrough curves by subdividing Unit 2 into many different lenses. The best matches to the observed data come from models that include: the river as a boundary; lower hydraulic gradients from B3 to A1; layering – specifically Unit 2 subdivided into lenses; and the presence of well bores. Based on these findings and the remaining differences between modeled and observed breakthrough behavior, further study should involve determining the full heterogeneity of hydraulic conductivity and porosity of the system (i.e., distributions within layers and lenses) and should incorporate more data from the site and test such as information from the geophysics taken during the TTLT (e.g., Goldstein et al., 2003; Johnson et al., 2007) and from site characterization.

5.2 Conclusions

It is clear from this study that as more aspects of the real hydrogeologic system are added to simulations of the TTLT, a better fit between observed and simulated breakthrough curves can be achieved. For example, the addition of well bores and modeling using variable density flow better matched observed breakthrough. Also boundary conditions are important to any groundwater modeling and by using more realistic boundaries for the BHRS, the simulated transport more closely resembles the observed transport during the TTLT. And heterogeneity in porosity and hydraulic conductivity also have large influences on transport. By better characterizing this heterogeneity and including it in modeling, better transport matches and predictions can be made. For example, by subdividing Unit 2 into many smaller lenses and by including spatially correlated distributions of hydraulic conductivity and/or porosity (rather than homogeneous hydraulic conductivity and/or porosity distributions) simulated breakthrough more closely match observed breakthrough for the TTLT at the BHRS in 2001.

REFERENCES CITED

Adams, E. E. and L. W. Gelhar, 1992, Field Study of Dispersion in a Heterogeneous Aquifer 2, Spatial Moments Analysis, *Water Resources Research*, 28:12 P 3293-3307.

Barlebo, H. C., M. C. Hill, and D. Rosbjerg, 2004, Investigating the Macrodispersion Experiment (MADE) site in Columbus, Mississippi, using a three-dimensional inverse flow and transport model, *Water Resources Research*, 40:4 P 18.

Barrash, W., Unpublished hydraulic conductivity estimates using the Kozeny-Carman empirical relationship from porosity logs and grain size distribution, Center for the Geophysical Investigation of the Shallow Subsurface, Boise State University.

Barrash, W., and T. Clemo, 2000, Hierarchical geostatistics of porosity derived from neutron logs at the Boise Hydrogeophysical Research Site, Boise, Idaho: Proceedings of TraM'2000, Liege, Belgium, May 23-26, 2000, IAHS Publ. No, 262 P 333-338.

Barrash, W., and T. Clemo, 2002, Hierarchical geostatistics and multifacies systems: Boise Hydrogeophysical Research Site, Bose, Idaho, *Water Resources Research,* 38:10.

Barrash, W., T. Clemo, J. Fox, C. Hughes, and E. Reboulet, in prep., Hydraulic conductivity estimates at two scales in a coarse fluvial aquifer, Boise Hydrogeophysical Research Site.

Barrash, W., T. Clemo, J. J. Fox, and T. C. Johnson, 2006, Field, laboratory, and modeling investigation of the skin effect at wells with slotted casing, Boise Hydrogeophysical Research Site, *Journal of Hydrology,* 326:1-4 P 181-198.

Barrash, W., T. Clemo, D. W. Hyndman, E. C. Reboulet, and E. M. Hausrath, 2002, Tracer/Time-Lapse Radar Imaging Test; Design, Operation, and Preliminary Results: Report to EPA for Grant X-970085-01-0 and to the Army Research Office for Grant DAAH04-96-1-0318, Center for Geophysical Investigation of the Shallow Subsurface Technical Report BSU CGISS 02-03, Boise State University, Boise, ID, 120 p.

Barrash, W., T. Clemo, and M.D. Knoll, 1999, Boise Hydrogeophysical Research Site (BHRS): Objectives, design, initial geostatistical results: Proceedings of SAGEEP99, The Symposium on the Application of Geophysics to Engineering and Environmental Problems, March 14-18, 1999, Oakland, CA, P 389-398.

Barrash, W. and Reboulet, E.C., 2004, Significance of porosity for stratigraphy and textural composition in subsurface coarse fluvial deposits, Boise Hydrogeophysical Research Site: *Geological Society of America Bulletin*, 116:9/10 P 1059-1073, doi:10.1130/B25370.1.

Barth, G. R., T. H. Illangasekare, M. C. Hill, and H. Rajaram, 2001, A new tracer-density criterion for heterogeneous porous media, *Water Resources Research*, 37:1 P 21-31.

Boggs, J. M., S. C. Young, L. M. Beard, L. W. Gelhar, K. R. Rehfeldt, and E. E. Adams, 1992, Field Study of Dispersion in a Heterogeneous Aquifer 1. overview and Site Description, *Water Resources Research*, 28:12 P 3281-3291.

Boggs, J. M. and E. E. Adams, 1992, Field Study of Dispersion in a Heterogeneous Aquifer 4. Investigation of Adsorption and Sampling Bias, *Water Resources Research*, 28:12 P 3325-3336.

Bohling, G.C., J. J. Butler, X. Zhan, and M. D. Knoll, 2007, A field assessment of the value of steady-shape hydraulic tomography for characterization of aquifer heterogeneitie, *Water Resources Research.*

Brusseau, M. L., and R. Srivastava, 1997, Nonideal Transport of Reactive Solute in Heterogeneous Porous Media 2. Quantitative Analysis of the Borden Natural Gradient Field Experiment, *Journal of Contaminant Hydrology*, 28:1-2 P 115-155.

Carman, P. C., 1937, Fluid flow through granular beds, *Trans. Inst. Chem. Eng.*, 15, P 150-166.

Clement, W.P., Barrash, W., and Knoll, M.D., 2006, Reflectivity modeling of ground-penetrating radar: *Geophysics,* 71:3 P K59-K66, 10.1190/1.2194528.

Clement, P. C., M. D. Knoll, L. M. Liberty, P. R. Donaldson, P. M. Michaels, W. Barrash, and J. R. Pelton, 1999, Geophysical surveys across the Boise Hydrogeophysical Research Site to determine geophysical parameters of a shallow, alluvial aquifer: Proceedings of the Symposium on the Application of Geophysics to Engineering and Environmental Problems, March 14-18, 1999, Oakland, CA, P 399-408.

Clemo, T., Unpublished estimates of the contacts between hydrostratigraphic units at the Boise Hydrogeophysical Research Site, Center for the Geophysical Investigation of the Shallow Subsurface, Boise State University.

Curtis, G. P., P. V. Roberts, and M. Reinhard, 1986, A Natural Gradient Experiment on Solute Transport in a Sand Aquifer 4. Sorption of Organic Solutes and its Influence on Mobility, *Water Resources Research*, 22:13 P 2059-2067.

Dagan, G., 1984, Solute transport in heterogeneous porous formations, *J. Fluid Mech.*, 145 P 151-177.

Domenico, P. A. and F. W. Schwartz, 1998, Physical and Chemical Hydrogeology, Second Edition, John Wiley and Sons, Inc, New York, NY, P 220-223.

Fox, J., 2006, Analytical modeling of fully penetrating pumping tests at the Boise Hydrogeophysical Research Site for aquifer parameters and wellbore skin, M.S. Thesis, Boise State University, Boise, Idaho.

Freyberg, D. L., 1986, A Natural Gradient Experiment on Solute Transport in a Sand Aquifer 2. Spatial Moments and the Advection and Dispersion of Nonreactive Tracers, *Water Resources Research*, 22:13 P 2031-2046.

Garabedian, S. P., D. R. LeBlanc, L. W. Gelhar, and M. A. Celia, 1991, Large-Scale Natural Gradient Tracer Test in Sand and Gravel, Cape Cod, Massachusetts 2. Analysis of Spatial Moments for a Nonreactive Tracer, *Water Resources Research*, 27:5 P 911-924.

Gelhar, L. W., and C. L. Axness, 1983, Three-dimensional stochastic analysis of macrodispersion in a stratified aquifer, *Water Resources Research*, 19:1 P 161–180.

Gelhar, L. W, C. Welty, and K. R. Rehfeldt, 1992, A Critical Review of Data on Field-Scale Dispersion in Aquifers, *Water Resources Research*, 28:7 P 1955-1974.

Goldstein, S.E., 2004, Cross-well radar attenuation-difference tomography to monitor a bromide tracer test, MS Thesis, Boise State University, 132 p.

Goldstein, S.E., T. C. Johnson, M. D. Knoll, W. Barrash, and W. P. Clement, 2003, Borehole radar attenuation tomography during the Tracer/Time-Lapse Test at the Boise Hydrogeophysical Research Site: Proceedings of SAGEEP03, The Symposium on the Application of Geophysics to Engineering and Environmental Problems, April 6-10, 2003, San Antonio, TX, P 147-162.

Güven, O., F. J. Molz, J. G. Melville, S. El Didy, and G. K. Boman, 1992, Three-Dimensional Modeling of a Two-Well Tracer Test, *Ground Water*, 30:6 P 945-957.

Guo, W., C. D. Langevin, 2002, User's Guide to SEAWAT: A Computer Program for Simulation of Three-Dimensional Variable-Density Ground-Water Flow: Techniques of Water Resources Investigations Book 6, Chapter A7, U.S. Geological Survey, 77p.

Harbaugh, A. W., E. R. Banta, M. C. Hill, and M. G. McDonald, 2000, MODFLOW-2000, The U.S. Geological Survey Modular Ground-water Model – User Guide to Modularization Concepts and the Ground-water Flow Process. U.S. Geological Survey, Open File Report 00-92, 130 p.

Hausrath, E. M., W. Barrash, E. C. Reboulet, 2002, Water sampling and analysis for the Tracer/Time-Lapse Radar Imaging Test at the Boise Hydrogeophysical Research Site: Report to EPA for Grant X-970085-01-0 and to the U.S. Army Research Office for Grant DAAH04-96-1-0318, Center for Geophysical Investigation of the Shallow Subsurface Technical Report BSU CGISS 02-03, Boise State University, Boise, ID, 86 p.

Heinz, J., Kleineidam, S., Teutsch, G., and Aigner, T., 2003, Heterogeneity patterns of Quaternary glaciofluvial gravel bodies (SW-Germany): Application to hydrogeology: Sedimentary Geology, 158 P 1-23, doi: 10.1016/S0037-0738(02)00239-7.

Hess, K. M., S. H. Wolf, and M. A. Celia,1992, Large-Scale Natural Gradient Tracer Test in Sand and Gravel, Cape Cod, Massachusetts 3. Hydraulic Conductivity Variability and Calculated Macrodispersivites, *Water Resources Research*, 28:8 P 2011-2027.

Hughes, C., 2005, Comparison of empirical relationships for hydraulic conductivity using Grain size distribution, packing, and porosity information from the Boise Hydrogeophysical Research Site, Boise, Idaho, M. S. Thesis, Boise State University, 123 p.

Huyakorn, P. S., P. F. Andersen, F. J. Molz, O. Güven, and J. G. Melville, 1986, Simulations of two-well tracer tests in stratified aquifers at the Chalk River and the Mobile sites, *Water Resources Research*, 22:7 P 1016-1030.

Johnson, T. C., P. S. Routh, and M. D. Knoll, 2005, Fresnel volume georadar attenuation-difference tomography, *Geophys. J. Int.*, 162: P 9-24.

Johnson, T., P. S. Routh, W. Barrash, and M. D. Knoll, 2007, A comparison of Fresnel zone and ray-based GPR attenuation-difference tomography for time-lapse imaging of electrically anomalous plumes, *Geophysics*, 72:2.

Kapoor, V. and L. W. Gelhar, 1994, Transport in three-dimensionally heterogeneous aquifers 2. Predictions and observations of concentration fluctuations, *Water Resources Research*, 30:6 P 1789-1801.

Käss, W., 1998, Tracing technique in geohydrology: Rotterdam, A.A. Balkema, 581 p.

Knoll, M. D., and W. P. Clement, 1999, Vertical radar profiling to determine dielectric constant, water content and porosity values at well locations: Proceedings of the Symposium on the Application of Geophysics to Engineering and Environmental Problems, March 14-18, 1999, Oakland, CA P 821-830.

Kozeny, J., 1927, Ueber Kapillare Leitung des Wassers im Boden: *Sitzungsberichte der Akademie der Wissenschaften in Wien*, 136 P 271-306.

Langevin, C. D., W. B. Shoemaker, and W. Guo, 2003, MODFLOW-2000, the U.S. Geological Survey Modular Ground-Water Model–Documentation of the SEAWAT-2000 Version with the Variable-Density Flow Process (VDF) and the Integrated MT3DMS Transport Process (IMT): U.S. Geological Survey Open-File Report 03-426, 43 p.

LeBlanc, D. R., S. P. Garabedian, K. M. Hess, L. W. Gelhar, R. D. Quadri, K. G. Stollenwerk, and W. W. Wood, 1991, Large-Scale Natural Gradient Tracer Test in Sand and Gravel, Cape Cod, Massachusetts 1. Experimental Design and Observed Tracer Movement, *Water Resources Research*, 27:5 P 895-910.

Leven, C., W. Barrash, D. W. Hyndman, and T. C. Johnson, 2002, Modeling a combined tracer and time-lapse radar imaging test in the heterogeneous fluvial aquifer at the Boise Hydrogeophysical Research Site (abs.): Fall AGU Meeting, December 6-10, 2002, San Francisco, CA, EOS, 83:47 P F487.

List, E. J., 1965, The stability and mixing of a density-stratified horizontal flow in a saturated porous medium, *Rep. KH-R-11*, California Institute of Technology, Pasadena.

Mackay, D. M., D. L. Freyberg, P. V. Roberts, and J. A. Cherry, 1986, A Natural Gradient Experiment on Solute Transport in a Sand Aquifer 1. Approach and Overview of Plume Movement, *Water Resources Research*, 22:13 P 2017-2029.

Mas-Pla, J., T.-C. Jim Yeh, J. F. McCarthy, and T. M. Williams, 1992, A Forced Gradient Tracer Experiment in a Coastal Sandy Aquifer, Georgetown Site, South Carolina. *Ground Water*, 30:6 P 958-964.

Moltz, F. J., O. Güven, J. G. Melville, R. D. Crocker, and K. T. Matteson, 1986, Performance, analysis, and simulation of a two-well tracer test at the Mobile site, *Water Resources Research*, 22:7 P 1031-1037.

Oostrom, M., J. S. Hayworth, J. H. Dane, and O. Güven, 1992a, Behavior of Dense Aqueous Phase Leachate Plumes in Homogeneous Porous Media, *Water Resources Research*, 28:8 P 2123-2134.

Oostrom, M., J. H. Dane, O. Güven, and J. S. Hayworth, 1992b, Experimental Investigation of Dense Solute Plumes in an Unconfined Aquifer Model, *Water Resources Research*, 28:9 P 2315-2326.

Othberg, K. L., 1994, Geology and geomorphology of the Boise Valley and Adjoining Areas, Western Snake River Plain, Idaho, Idaho Geological Survey, University of Idaho, Moscow, Idaho.

Paschke, N. W. and J. A. Hoopes, 1984, Buoyant Contaminant Plumes in Groundwater, *Water Resoureces Research*, 20:9 1183-1192.

Peng, W.-S., D. R. Hampton, L. F. Konikow, K. Kambham, and J. J. Benegar, 2000, Can contaminant transport models predict breakthrough? *Ground Water Monitoring & Remediation*, 20:4 P 104-113.

Peretti, W.R., M. D. Knoll, W. P. Clement, and W. Barrash, 1999, 3-D GPR imaging of complex fluvial stratigraphy at the Boise Hydrogeophysical Research Site: Proceedings of SAGEEP99, March 14-18, 1999, Oakland, CA, P 555-564.

Peterson, J. E., Jr., E. L. Majer, and M. D. Knoll, 1999, Hydrogeological property estimation using tomographic data at the Boise Hydrogeophysical Research Site: Proceedings of the Symposium on the Application of Geophysics to Engineering and Environmental Problems, March 14-18, 1999, Oakland, CA, P 629-638.

Ptak, T., T. Piepenbrink, and E. Martac, 2004, Tracer tests for the investigation of heterogeneous porous media and stochastic modelling of flow and transport – a review of some recent developments, *Journal of Hydrology* 294 P 122-163.

Reboulet, E. C., and W. Barrash, 1999, Identification of hydrostratigraphic facies in course, unconsolidated, braided-stream deposits at the Boise Hydrogeophysical Research Site (abstract), Geol. Soc. Am. Annu. Meet., Oct. 25-29, 1999, Denver, Colo., *Abstr. Programs Geol.Soc. Am.,* 31:7 P A350.

Reboulet, E. C., and W. Barrash, 2000, Statistical analysis of grain-size distribution and porosity data from coarse braided-stream deposits at the Boise Hydrogeophysical Research Site (abstract), Geol. Soc. Am. Annu. Meet., Reno, Nev., Nov 13-16, 2000, *Abstr. Programs Geol. Soc. Am., 32:*7 P A410.

Reboulet, E. C., 2003, Statistical and geostatistical analysis of grain-size distribution and porosity data from coarse braided-stream deposits at the Boise Hydrogeophysical Research Site (M.S. Thesis): Boise, Idaho, Boise State University, 154 p.

Reboulet, E.C. and Barrash, W., 2003, Core, grain-size, and porosity data from the Boise Hydrogeophysical Research Site: Center for Geophysical Investigation of the Shallow Subsurface Technical Report BSU CGISS 03-02, Boise State University, Boise, ID, 87 p.

Rehfeldt, K. R. J. M. Boggs, and L. W. Gelhar, 1992, Field Study of Dispersion in a Heterogeneous Aquifer 3. Geostatistical Analysis of Hydraulic Conductivity, *Water Resources Research*, 28:12 P 3309-3324.

Roberts, P. V., M. N. Goltz, and D. M. Mackay, 1986, A Natural Gradient Experiment on Solute Transport in a Sand Aquifer 3. Retardtion Estimtes and Mass Balances for Organic Solutes, *Water Resources Research*, 22:13 P 2047-2058.

Sauty J. P., 1977, Contribution à l'identification des paramètres de dispersion dans les aquifères par interprétation des expériences de tracage. – Bur. de Recherches Géol. et Minières; Dépt Hydrogéol 77SGN515HYD, P 157 , Orléans

Scheibe, T. D., and Y. Chien, 2003, An Evaluation of Conditioning Data for Solute Transport Prediction, *Groundwater,* 41:2 P 128-141.

Schincariol, R. A. and F. W. Schwartz, 1990, An Experimental Investigation of Variable Density Flow and Mixing in Homogeneous and Heterogeneous Media, *Water Resources Research*, 26:10 P 2319-2329.

Schincariol, R. A., F. W. Schwartz, and C. A. Mendoza, 1994, On the generation of instabilities in variable density flow, *Water Resources Research*, 30:4 P 913-927.

Schincariol, R. A., F. W. Schwartz, and C. A. Mendoza, 1997, Instabilities in variable density flows: Stability and sensitivity analyses for homogeneous and heterogeneous media, *Water Resources Research*, 33:1 P 31-41.

Simmons, C. T., T. R. Fenstemaker, and J. M. Sharp, Jr., 2001, Variable-density groundwater flow and solute transport in heterogeneous porous media: approaches, resolutions and future challenges, *Journal of Contaminant Hydrology*, 52:1-4 P 245-275.

Sudicky, E. A., 1986, A Natural Gradient Experiment on Solute Transport in a Sand Aquifer: Spatial Variability of Hydraulic Conductivity and Its Role in the Dispersion Process, *Water Resources Research*, 22:13 P 2069-2082.

Sudicky, E. A., and P. S. Huyakorn. 1991. Contaminant migration in imperfectly known heterogeneous groundwater systems. Contributions in hydrology: U.S. national report 1987-1990. P 240-253 in Proceedings of the Twentieth General Assembly of the International Union of Geodesy and Geophysics, Vienna, Austria, August, 1991.

Thoma, M., G. Nelson, W. Barrash, and T. Clemo, 2007, Development of a Transient MODFLOW Simulation for the Boise Hydrogeophysical Research Site Tracer Test, Center for Geophysical Investigation of the Shallow Subsurface Technical Report, Boise State University, Boise, ID, 77 p.

Zhang, H., F. W. Schwarz, W. W. Wood, S. P. Garabedian, and D. R. LeBlanc, 1998, Simulation of Variable-Density Flow and Transport of Reactive and Nonreactive Solutes during a tracer test at Cape Cod, Massachusetts, *Water Resources Research*, 34:1 P 67-82.

Zheng, C, 2005, MT3DMS v5 Supplemental User's Guide, Technical Report to the U.S. Army Engineer Research and Development Center, Department of Geological Sciences, University of Alabama, 24 p.

Zheng, C., and P. P. Wang, 1999, MT3DMS: A Modular Three-Dimensional Multispecies Transport Model for Simulation of Advection, Dispersion, and Chemical Reactions of Contaminants in Groundwater Systems; Documentation and User's Guide, US Army Corps of Engineers, Engineer Research and Development Center, Contract Report SERDP – 99 – 1, 220 p.

Zheng, C. and G. D. Bennett, 1995, Applied Contaminant Transport Modeling: Theory and Practice, Van Nostrand Reinhold, New York, NY.

APPENDIX A

Chemical Sampling

(after Hausrath et al., 2002)

Event	Date	Time	samples	QC
Bkgrd	31-Jul-01	15:00	38	2
Bkgrd	1-Aug-01	7:00	50	5
Inject	1-Aug-01	11:40	13	0
1	1-Aug-01	13:00	32	3
2	1-Aug-01	16:00	34	6
3	1-Aug-01	20:00	50	4
4	2-Aug-01	0:14	50	5
5	2-Aug-01	6:30	52	5
6	2-Aug-01	11:00	51	5
7	2-Aug-01	15:00	51	5
8	2-Aug-01	19:00	51	5
9	2-Aug-01	22:00	51	5
10	3-Aug-01	1:00	51	5
11	3-Aug-01	4:00	51	5
12	3-Aug-01	7:00	50	5
13	3-Aug-01	10:00	50	5
14	3-Aug-01	14:00	51	5
15	3-Aug-01	17:00	50	5
16	3-Aug-01	20:00	50	4
17	3-Aug-01	23:00	50	6
18	4-Aug-01	7:00	50	6
19	4-Aug-01	11:00	50	6
20	4-Aug-01	15:00	50	5
21	4-Aug-01	19:00	50	5
22	4-Aug-01	23:00	50	5
23	5-Aug-01	3:00	50	5
24	5-Aug-01	7:00	49	6
25	5-Aug-01	11:00	50	7
26	5-Aug-01	15:00	50	6
27	5-Aug-01	19:00	50	5
28	5-Aug-01	23:00	50	5
29	6-Aug-01	3:00	50	6
30	6-Aug-01	7:00	50	5
31	6-Aug-01	11:00	50	5
32	6-Aug-01	15:00	51	5

Event	Date	Time	samples	QC
33	6-Aug-01	19:00	51	5
34	6-Aug-01	23:00	51	5
35	7-Aug-01	4:00	51	5
36	7-Aug-01	7:00	51	5
37	7-Aug-01	11:00	51	5
38	7-Aug-01	15:00	51	5
39	7-Aug-01	19:00	50	5
40	7-Aug-01	23:00	51	5
41	8-Aug-01	3:00	51	5
42	8-Aug-01	7:00	51	5
43	8-Aug-01	11:00	51	5
44	8-Aug-01	15:00	51	5
45	8-Aug-01	19:00	51	5
46	8-Aug-01	23:00	51	5
47	9-Aug-01	3:00	51	5
48	9-Aug-01	7:00	51	7
49	9-Aug-01	11:00	51	6
50	9-Aug-01	15:00	51	5
51	9-Aug-01	19:00	51	5
52	9-Aug-01	23:00	51	5
53	10-Aug-01	3:00	51	5
54	10-Aug-01	7:00	52	5
55	10-Aug-01	11:00	49	5
56	10-Aug-01	15:00	49	5
57	10-Aug-01	19:00	50	4
58	10-Aug-01	23:00	51	5
59	11-Aug-01	3:00	51	5
60	11-Aug-01	7:00	51	6
61	11-Aug-01	11:00	51	5
62	11-Aug-01	15:00	51	5
63	11-Aug-01	19:00	51	5
64	11-Aug-01	23:00	50	5
65	12-Aug-01	3:00	52	5
66	12-Aug-01	7:00	51	5
67	12-Aug-01	11:00	51	5

Event	Date	Time	samples	QC
68	12-Aug-01	15:00	51	5
69	12-Aug-01	19:00	52	4
70	12-Aug-01	23:00	51	5
71	13-Aug-01	3:00	51	5
72	13-Aug-01	7:00	50	5
73	13-Aug-01	11:00	50	5
74	13-Aug-01	15:00	51	5
75	13-Aug-01	19:00	52	4
76	13-Aug-01	23:00	51	5
77	14-Aug-01	3:00	51	5
78	14-Aug-01	7:00	52	4
79	14-Aug-01	11:00	51	5
80	14-Aug-01	15:00	51	5
81	14-Aug-01	19:00	51	5
82	14-Aug-01	23:00	51	5
83	15-Aug-01	3:00	52	4
84	15-Aug-01	7:00	51	4
85	15-Aug-01	11:00	50	5
86	15-Aug-01	15:00	51	5
87	15-Aug-01	19:00	51	5
88	15-Aug-01	23:00	51	5
89	16-Aug-01	3:00	51	5
90	16-Aug-01	7:00	52	4
91	16-Aug-01	11:00	52	4
92	16-Aug-01	15:00	51	5
93	16-Aug-01	19:00	51	5
94	16-Aug-01	23:00	51	5
95	17-Aug-01	3:00	51	4
96	17-Aug-01	7:00	51	5
97	17-Aug-01	11:00	51	5

APPENDIX B

MODFLOW 2000 Discretization File

MODFLOW 2000 Discretization File

```
# MF2K DISCRETIZATION FILE
#
#
# NLAY NROW NCOL NPER TIMEUNITS LENUNITS
40 120 110 15 1 2
0 0 0 0 0 0 0 0 0 0 0 0 0 0 0 0 0 0 0 0 0 0 0 0 0 0 0 0 0 0 0 0 0 0 0 0 0 0 0 0
INTERNAL 1.0 (free) 0
42.763236 29.904361 20.91214 14.623874 10.226486 7.151388 5.000971 3.497182
2.445582 1.710197 1.195942 0.8363232 0.5848414 0.40898 0.286 0.2 0.2 0.2 0.2 0.2 0.2
0.2 0.2 0.2 0.2 0.2 0.2 0.2 0.2 0.2 0.2 0.2 0.2 0.2 0.2 0.2 0.2 0.2 0.2 0.2 0.2 0.2 0.2 0.2 0.2
0.2 0.2 0.2 0.2 0.2 0.2 0.2 0.2 0.2 0.2 0.2 0.2 0.2 0.2 0.2 0.2 0.2 0.2 0.2 0.2 0.2 0.2 0.2 0.2
0.2 0.2 0.2 0.2 0.2 0.2 0.2 0.2 0.2 0.2 0.2 0.2 0.2 0.2 0.2 0.2 0.2 0.2 0.2 0.2 0.2 0.2 0.2 0.2
0.2 0.2 0.286 0.40898 0.5848414 0.8363232 1.195942 1.710197 2.445582 3.497182
5.000971 7.151388 10.226486 14.623874 20.91214 29.904361 42.763236
INTERNAL 1.0 (free) 0
42.763236 29.904361 20.91214 14.623874 10.226486 7.151388 5.000971 3.497182
2.445582 1.710197 1.195942 0.8363232 0.5848414 0.40898 0.286 0.2 0.2 0.2 0.2 0.2 0.2
0.2 0.2 0.2 0.2 0.2 0.2 0.2 0.2 0.2 0.2 0.2 0.2 0.2 0.2 0.2 0.2 0.2 0.2 0.2 0.2 0.2 0.2 0.2 0.2
0.2 0.2 0.2 0.2 0.2 0.2 0.2 0.2 0.2 0.2 0.2 0.2 0.2 0.2 0.2 0.2 0.2 0.2 0.2 0.2 0.2 0.2 0.2 0.2
0.2 0.2 0.2 0.2 0.2 0.2 0.2 0.2 0.2 0.2 0.2 0.2 0.2 0.2 0.2 0.2 0.2 0.2 0.2 0.2 0.2 0.2 0.2 0.2
0.2 0.2 0.2 0.2 0.2 0.2 0.2 0.2 0.2 0.2 0.2 0.2 0.286 0.40898 0.5848414 0.8363232
1.195942 1.710197 2.445582 3.497182 5.000971 7.151388 10.226486 14.623874
20.91214 29.904361 42.763236
CONSTANT 18.0
CONSTANT 16.52472544
CONSTANT 15.4497712
CONSTANT 14.553976
CONSTANT 13.80748
CONSTANT 13.1854
CONSTANT 12.667
CONSTANT 12.235
CONSTANT 11.875
CONSTANT 11.575
CONSTANT 11.325
CONSTANT 11.075
CONSTANT 10.825
CONSTANT 10.575
CONSTANT 10.325
CONSTANT 10.075
CONSTANT 9.825
```

CONSTANT 9.575
CONSTANT 9.325
CONSTANT 9.075
CONSTANT 8.825
CONSTANT 8.575
CONSTANT 8.325
CONSTANT 8.075
CONSTANT 7.825
CONSTANT 7.575
CONSTANT 7.325
CONSTANT 7.075
CONSTANT 6.825
CONSTANT 6.575
CONSTANT 6.275
CONSTANT 5.915
CONSTANT 5.483
CONSTANT 4.9646
CONSTANT 4.34252
CONSTANT 3.596024
CONSTANT 2.7002288
CONSTANT 1.62527456
CONSTANT 0.335329472
CONSTANT -1.212604633
CONSTANT -3.07012556
500000.0 1 1.0 SS
2000.0 15 1.5 TR
2100.0 45 1.5 TR
70900.0 35 1.5 TR
450780.0 44 1.2 TR
1020.0 12 1.2 TR
22200.0 28 1.2 TR
420.0 10 1.2 TR
222180.0 41 1.2 TR
34200.0 30 1.2 TR
214800.0 40 1.2 TR
23700.0 28 1.2 TR
148500.0 50 1.5 TR
25200.0 60 1.5 TR
172800.0 80 1.5 TR

APPENDIX C

Descriptions of Simulations

For all of the simulations described below, the simulated and observed breakthrough curves for all of the sampling zones in well A1, and the observed and simulated change in head plots for well B3 and for the C wells are included on the CD accompanying this thesis.

Unit 2-3 Ave

The Unit 2-3 Ave simulation has homogeneous hydrogeologic properties throughout the modeling domain. The hydrogeologic properties of this model are listed in Table 8. This simulation used the uniform, regional hydraulic gradient framework. Flow was implemented through the Layer Property Flow package of SEAWAT 2000. Pumping and injection were defined in the pumping zone of well B6, injection zone of well A1, and in all of the sampling zones of well A1 and in the B wells through the Well package of SEAWAT 2000.

Unit 2

The Unit 2 simulation has homogeneous hydrogeologic properties throughout the modeling domain. The hydrogeologic properties of this model are listed in Table 8. This simulation used the uniform, regional hydraulic gradient framework. Flow was implemented through the Layer Property Flow package of SEAWAT 2000. Pumping and injection were defined in the pumping zone of well B6, injection zone of well A1, and in all of the sampling zones of well A1 and in the B wells through the Well package of SEAWAT 2000.

Unit 3

The Unit 3 simulation has homogeneous hydrogeologic properties throughout the modeling domain. The hydrogeologic properties of this model are listed in Table 8. This simulation used the uniform, regional hydraulic gradient framework. Flow was implemented through the Layer Property Flow package of SEAWAT 2000. Pumping and injection were defined in the pumping zone of well B6, injection zone of well A1, and in all of the sampling zones of well A1 and in the B wells through the Well package of SEAWAT 2000.

Unit 2-3

The Unit 2-3 simulation has two layers defined within it. A cross section of this model is seen in Figure 29. The hydrogeologic properties of this model are listed in Table 8. This simulation used the uniform, regional hydraulic gradient framework. Flow was implemented through the Hydrogeologic Unit Flow package of SEAWAT 2000. Pumping and injection were defined in the pumping zone of well B6, injection zone of well A1, and in all of the sampling zones of well A1 and in the B wells through the Well package of SEAWAT 2000.

Unit 2a, 2b, and 3

The Unit 2a, 2b, and 3 simulation has three layers defined within it. A cross section of this model is seen in Figure 24. The hydrogeologic properties of this model are listed in Table 8. This simulation used the uniform, regional hydraulic gradient

framework. Flow was implemented through the Hydrogeologic Unit Flow package of SEAWAT 2000. Pumping and injection were defined in the pumping zone of well B6, injection zone of well A1, and in all of the sampling zones of well A1 and in the B wells through the Well package of SEAWAT 2000.

Many Horizontal Units

The Many Horizontal Units simulation has layering according to the layers of the modeling framework (40 layers). The hydrogeologic properties of this model are listed in Table 8 and a cross section is shown in Figure 25. This simulation used the uniform, regional hydraulic gradient framework. Flow was implemented through the Layer Property Flow package of SEAWAT 2000. Pumping and injection were defined in the pumping zone of well B6, injection zone of well A1, and in all of the sampling zones of well A1 and in the B wells through the Well package of SEAWAT 2000.

U23A

The U23A simulation has homogeneous hydrogeologic properties throughout the modeling domain. The hydrogeologic properties of this model are listed in Table 8. This simulation used the complex boundaries framework. Flow was implemented through the Layer Property Flow package of SEAWAT 2000. Pumping and injection were defined in the pumping zone of well B6, injection zone of well A1, and in all of the sampling zones of well A1 and in the B wells through the Well package of SEAWAT 2000. Well bores

and packers were defined in the injection zone of well B3 and in the pumping zone of well B6.

TwL

The TwL simulation has two layers defined within it. A cross section of this model is seen in Figure 29. The hydrogeologic properties of this model are listed in Table 8. This simulation used the complex boundaries framework. Flow was implemented through the Hydrogeologic Unit Flow package of SEAWAT 2000. Pumping and injection were defined in the pumping zone of well B6, injection zone of well A1, and in all of the sampling zones of well A1 and in the B wells through the Well package of SEAWAT 2000. Well bores and packers were defined in the injection zone of well B3 and in the pumping zone of well B6.

ThL

The ThL simulation has three layers defined within it. A cross section of this model is seen in Figure 26. The hydrogeologic properties of this model are listed in Table 8. This simulation used the complex boundaries framework. Flow was implemented through the Hydrogeologic Unit Flow package of SEAWAT 2000. Pumping and injection were defined in the pumping zone of well B6, injection zone of well A1, and in all of the sampling zones of well A1 and in the B wells through the Well package of SEAWAT 2000. Well bores and packers were defined in the injection zone of well B3 and in the pumping zone of well B6.

ThLO

The ThLO simulation has three layers defined within it. A cross section of this model is seen in Figure 24. The hydrogeologic properties of this model are listed in Table 8. This simulation used the complex boundaries framework. Flow was implemented through the Hydrogeologic Unit Flow package of SEAWAT 2000. Pumping and injection were defined in the pumping zone of well B6, injection zone of well A1, and in all of the sampling zones of well A1 and in the B wells through the Well package of SEAWAT 2000. Well bores and packers were defined in the injection zone of well B3 and in the pumping zone of well B6.

FL

The FL simulation has five layers defined within it where each layer corresponds to one of the hydrostratigraphic units identified by Barrash and Clemo (2002). A cross section of this model is seen in Figure 43. The hydrogeologic properties of this model are listed in Table 8. This simulation used the complex boundaries framework. Flow was implemented through the Hydrogeologic Unit Flow package of SEAWAT 2000. Pumping and injection were defined in the pumping zone of well B6, injection zone of well A1, and in all of the sampling zones of well A1 and in the B wells through the Well package of SEAWAT 2000.

FLw

The FLw simulation has five layers defined within it where each layer corresponds to one of the hydrostratigraphic units identified by Barrash and Clemo (2002). A cross section of this model is seen in Figure 43. The hydrogeologic properties of this model are listed in Table 8. This simulation used the complex boundaries framework. Flow was implemented through the Hydrogeologic Unit Flow package of SEAWAT 2000. Pumping and injection were defined in the pumping zone of well B6, injection zone of well A1, and in all of the sampling zones of well A1 and in the B wells through the Well package of SEAWAT 2000. Well bores and packers were defined in the injection zone of well B3 and in the pumping zone of well B6.

FLwsc

The FLwsc simulation has five layers defined within it where each layer corresponds to one of the hydrostratigraphic units identified by Barrash and Clemo (2002). A cross section of this model is seen in Figure 43. The hydrogeologic properties of this model are listed in Table 8. This simulation used the complex boundaries framework. Flow was implemented through the Hydrogeologic Unit Flow package of SEAWAT 2000. Pumping and injection were defined in the pumping zone of well B6, injection zone of well A1, and in all of the sampling zones of well A1 and in the B wells through the Well package of SEAWAT 2000. Well bores were defined in all of the screened sections of wells B3, A1, and B6. Packers were also define in the injection zone of well B3 and in the pumping zone of well B6.

FLwa

The FLwa simulation has five layers defined within it where each layer corresponds to one of the hydrostratigraphic units identified by Barrash and Clemo (2002). A cross section of this model is seen in Figure 43. The hydrogeologic properties of this model are listed in Table 8. This simulation used the complex boundaries framework. Flow was implemented through the Hydrogeologic Unit Flow package of SEAWAT 2000. Pumping and injection were defined in the pumping zone of well B6, injection zone of well A1, and in all of the sampling zones of well A1 and in the B wells through the Well package of SEAWAT 2000. Well bores and packers were defined in the injection zone of well B3 and in the pumping zone of well B6. For this simulation the longitudinal dispersivity was raised to 0.2 meters in the Dispersion package of SEAWAT 2000.

FLwab1

The FLwab1 simulation has five layers defined within it where each layer corresponds to one of the hydrostratigraphic units identified by Barrash and Clemo (2002). A cross section of this model is seen in Figure 43. The hydrogeologic properties of this model are listed in Table 8. This simulation used the complex boundaries framework. Flow was implemented through the Hydrogeologic Unit Flow package of SEAWAT 2000. Pumping and injection were defined in the pumping zone of well B6, injection zone of well A1, and in all of the sampling zones of well A1 and in the B wells through the Well package of SEAWAT 2000. Well bores and packers were defined in

the injection zone of well B3 and in the pumping zone of well B6. For this simulation the longitudinal dispersivity was raised to 0.2 meters in the Dispersion package of SEAWAT 2000. The effective porosities of this simulation were increased by their calculated standard deviation (square root of the variance listed in Table 1, and reported by Barrash and Clemo – 2002). The effective porosities are input through the Basic Transport package of SEAWAT 2000.

FLwab2

The FLwab2 simulation has five layers defined within it where each layer corresponds to one of the hydrostratigraphic units identified by Barrash and Clemo (2002). A cross section of this model is seen in Figure 43. The hydrogeologic properties of this model are listed in Table 8. This simulation used the complex boundaries framework. Flow was implemented through the Hydrogeologic Unit Flow package of SEAWAT 2000. Pumping and injection were defined in the pumping zone of well B6, injection zone of well A1, and in all of the sampling zones of well A1 and in the B wells through the Well package of SEAWAT 2000. Well bores and packers were defined in the injection zone of well B3 and in the pumping zone of well B6. For this simulation the longitudinal dispersivity was raised to 0.2 meters in the Dispersion package of SEAWAT 2000. The effective porosities of this simulation were increased by two times their calculated standard deviation (square root of the variance listed in Table 1, and reported by Barrash and Clemo – 2002). The effective porosities are input through the Basic Transport package of SEAWAT 2000.

FLpor1

The FLpor1 simulation has five layers defined within it where each layer corresponds to one of the hydrostratigraphic units identified by Barrash and Clemo (2002). A cross section of this model is seen in Figure 43. The hydrogeologic properties of this model are listed in Table 8. This simulation used the complex boundaries framework. Flow was implemented through the Hydrogeologic Unit Flow package of SEAWAT 2000. Pumping and injection were defined in the pumping zone of well B6, injection zone of well A1, and in all of the sampling zones of well A1 and in the B wells through the Well package of SEAWAT 2000. Well bores and packers were defined in the injection zone of well B3 and in the pumping zone of well B6. The effective porosities of this simulation were increased by 10% of the porosities reported by Barrash and Clemo (2002), or 10% of those listed in Table 1. The effective porosities are input through the Basic Transport package of SEAWAT 2000.

FLpor2

The FLpor2 simulation has five layers defined within it where each layer corresponds to one of the hydrostratigraphic units identified by Barrash and Clemo (2002). A cross section of this model is seen in Figure 43. The hydrogeologic properties of this model are listed in Table 8. This simulation used the complex boundaries framework. Flow was implemented through the Hydrogeologic Unit Flow package of SEAWAT 2000. Pumping and injection were defined in the pumping zone of well B6, injection zone of well A1, and in all of the sampling zones of well A1 and in the B wells

through the Well package of SEAWAT 2000. Well bores and packers were defined in the injection zone of well B3 and in the pumping zone of well B6. The effective porosities of this simulation were increased by 20% of the porosities reported by Barrash and Clemo (2002), or 20% of those listed in Table 1. The effective porosities are input through the Basic Transport package of SEAWAT 2000.

FLpor3

The FLpor3 simulation has five layers defined within it where each layer corresponds to one of the hydrostratigraphic units identified by Barrash and Clemo (2002). A cross section of this model is seen in Figure 43. The hydrogeologic properties of this model are listed in Table 8. This simulation used the complex boundaries framework. Flow was implemented through the Hydrogeologic Unit Flow package of SEAWAT 2000. Pumping and injection were defined in the pumping zone of well B6, injection zone of well A1, and in all of the sampling zones of well A1 and in the B wells through the Well package of SEAWAT 2000. Well bores and packers were defined in the injection zone of well B3 and in the pumping zone of well B6. The effective porosities of this simulation were increased by 30% of the porosities reported by Barrash and Clemo (2002), or 30% of those listed in Table 1. The effective porosities are input through the Basic Transport package of SEAWAT 2000.

MLhp

The MLhp simulation has five layers defined within it where each layer corresponds to one of the hydrostratigraphic units identified by Barrash and Clemo (2002). A cross section of this model is seen in Figure 43. Unit 2 has further zonation within it as determined from matching highs and lows in the modified Kozeny-Carman hydraulic conductivity estimates within wells as seen in Figure 44. The hydrogeologic properties of this model are listed in Table 8. This simulation used the complex boundaries framework. Flow was implemented through the Hydrogeologic Unit Flow package of SEAWAT 2000. Pumping and injection were defined in the pumping zone of well B6, injection zone of well A1, and in all of the sampling zones of well A1 and in the B wells through the Well package of SEAWAT 2000. Well bores and packers were defined in the injection zone of well B3 and in the pumping zone of well B6.

MLsb

The MLsb simulation has five layers defined within it where each layer corresponds to one of the hydrostratigraphic units identified by Barrash and Clemo (2002). A cross section of this model is seen in Figure 43. Unit 2 has further zonation within it as determined from matching highs and lows in the modified Kozeny-Carman hydraulic conductivity estimates within wells as seen in Figure 44. The hydrogeologic properties of this model are listed in Table 8. This simulation used the complex boundaries framework. Flow was implemented through the Hydrogeologic Unit Flow package of SEAWAT 2000. Pumping and injection were defined in the pumping zone of

well B6, injection zone of well A1, and in all of the sampling zones of well A1 and in the B wells through the Well package of SEAWAT 2000. Well bores were defined in all of the screened sections of wells B3, A1, and B6. Packers were also define in the injection zone of well B3 and in the pumping zone of well B6.

MLsbS

The MLsbS simulation has five layers defined within it where each layer corresponds to one of the hydrostratigraphic units identified by Barrash and Clemo (2002). A cross section of this model is seen in Figure 43. Unit 2 has further zonation within it as determined from matching highs and lows in the modified Kozeny-Carman hydraulic conductivity estimates within wells as seen in Figure 44. The hydrogeologic properties of this model are listed in Table 8. This simulation used the complex boundaries framework. Flow was implemented through the Hydrogeologic Unit Flow package of SEAWAT 2000. Pumping and injection were defined in the pumping zone of well B6, injection zone of well A1, and in all of the sampling zones of well A1 and in the B wells through the Well package of SEAWAT 2000. Well bores were defined in all of the screened sections of wells B3, A1, and B6. Packers were also define in the injection zone of well B3 and in the pumping zone of well B6. Well bore skin as reported by Fox (2006) and Barrash et al. (2006) for both the pumping and injection wells (B3 and B6) were defined in the simulation using the Horizontal Flow Barrier package of SEAWAT 2000.

MLsba2S

The MLsba2S simulation has five layers defined within it where each layer corresponds to one of the hydrostratigraphic units identified by Barrash and Clemo (2002). A cross section of this model is seen in Figure 43. Unit 2 has further zonation within it as determined from matching highs and lows in the modified Kozeny-Carman hydraulic conductivity estimates within wells as seen in Figure 44. The hydrogeologic properties of this model are listed in Table 8. This simulation used the complex boundaries framework. Flow was implemented through the Hydrogeologic Unit Flow package of SEAWAT 2000. Pumping and injection were defined in the pumping zone of well B6, injection zone of well A1, and in all of the sampling zones of well A1 and in the B wells through the Well package of SEAWAT 2000. Well bores were defined in all of the screened sections of wells B3, A1, and B6. Packers were also define in the injection zone of well B3 and in the pumping zone of well B6. For this simulation the longitudinal dispersivity was raised to 0.2 meters in the Dispersion package of SEAWAT 2000. Well bore skin as reported by Fox (2006) and Barrash et al. (2006) for both the pumping and injection wells (B3 and B6) were defined in the simulation using the Horizontal Flow Barrier package of SEAWAT 2000.

MLsbV15a2S

The MLsb15a2S simulation has five layers defined within it where each layer corresponds to one of the hydrostratigraphic units identified by Barrash and Clemo (2002). A cross section of this model is seen in Figure 43. Unit 2 has further zonation

within it as determined from matching highs and lows in the modified Kozeny-Carman hydraulic conductivity estimates within wells as seen in Figure 44. The hydrogeologic properties of this model are listed in Table 8. This simulation used the complex boundaries framework. Flow was implemented through the Hydrogeologic Unit Flow package of SEAWAT 2000. Pumping and injection were defined in the pumping zone of well B6, injection zone of well A1, and in all of the sampling zones of well A1 and in the B wells through the Well package of SEAWAT 2000. Well bores were defined in all of the screened sections of wells B3, A1, and B6. Packers were also define in the injection zone of well B3 and in the pumping zone of well B6. For this simulation the longitudinal dispersivity was raised to 0.2 meters in the Dispersion package of SEAWAT 2000. Well bore skin as reported by Fox (2006) and Barrash et al. (2006) for both the pumping and injection wells (B3 and B6) were defined in the simulation using the Horizontal Flow Barrier package of SEAWAT 2000. This simulation has vertical hydraulic conductivity anisotropy raised from 1 to 1.5. The vertical hydraulic conductivity anisotropy is input through the Hydrogeologic Unit Flow package.

MLsbV2a2S

The MLsbV2a2S simulation has five layers defined within it where each layer corresponds to one of the hydrostratigraphic units identified by Barrash and Clemo (2002). A cross section of this model is seen in Figure 43. Unit 2 has further zonation within it as determined from matching highs and lows in the modified Kozeny-Carman hydraulic conductivity estimates within wells as seen in Figure 44. The hydrogeologic

properties of this model are listed in Table 8. This simulation used the complex boundaries framework. Flow was implemented through the Hydrogeologic Unit Flow package of SEAWAT 2000. Pumping and injection were defined in the pumping zone of well B6, injection zone of well A1, and in all of the sampling zones of well A1 and in the B wells through the Well package of SEAWAT 2000. Well bores were defined in all of the screened sections of wells B3, A1, and B6. Packers were also define in the injection zone of well B3 and in the pumping zone of well B6. For this simulation the longitudinal dispersivity was raised to 0.2 meters in the Dispersion package of SEAWAT 2000. Well bore skin as reported by Fox (2006) and Barrash et al. (2006) for both the pumping and injection wells (B3 and B6) were defined in the simulation using the Horizontal Flow Barrier package of SEAWAT 2000. This simulation has vertical hydraulic conductivity anisotropy raised from 1 to 2. The vertical hydraulic conductivity anisotropy is input through the Hydrogeologic Unit Flow package.

MLsbV3a2S

The MLsbV3a2S simulation has five layers defined within it where each layer corresponds to one of the hydrostratigraphic units identified by Barrash and Clemo (2002). A cross section of this model is seen in Figure 43. Unit 2 has further zonation within it as determined from matching highs and lows in the modified Kozeny-Carman hydraulic conductivity estimates within wells as seen in Figure 44. The hydrogeologic properties of this model are listed in Table 8. This simulation used the complex boundaries framework. Flow was implemented through the Hydrogeologic Unit Flow

package of SEAWAT 2000. Pumping and injection were defined in the pumping zone of well B6, injection zone of well A1, and in all of the sampling zones of well A1 and in the B wells through the Well package of SEAWAT 2000. Well bores were defined in all of the screened sections of wells B3, A1, and B6. Packers were also define in the injection zone of well B3 and in the pumping zone of well B6. For this simulation the longitudinal dispersivity was raised to 0.2 meters in the Dispersion package of SEAWAT 2000. Well bore skin as reported by Fox (2006) and Barrash et al. (2006) for both the pumping and injection wells (B3 and B6) were defined in the simulation using the Horizontal Flow Barrier package of SEAWAT 2000. This simulation has vertical hydraulic conductivity anisotropy raised from 1 to 3. The vertical hydraulic conductivity anisotropy is input through the Hydrogeologic Unit Flow package.

MLsbV4a2S

The MLsbV4a2S simulation has five layers defined within it where each layer corresponds to one of the hydrostratigraphic units identified by Barrash and Clemo (2002). A cross section of this model is seen in Figure 43. Unit 2 has further zonation within it as determined from matching highs and lows in the modified Kozeny-Carman hydraulic conductivity estimates within wells as seen in Figure 44. The hydrogeologic properties of this model are listed in Table 8. This simulation used the complex boundaries framework. Flow was implemented through the Hydrogeologic Unit Flow package of SEAWAT 2000. Pumping and injection were defined in the pumping zone of well B6, injection zone of well A1, and in all of the sampling zones of well A1 and in the

B wells through the Well package of SEAWAT 2000. Well bores were defined in all of the screened sections of wells B3, A1, and B6. Packers were also define in the injection zone of well B3 and in the pumping zone of well B6. For this simulation the longitudinal dispersivity was raised to 0.2 meters in the Dispersion package of SEAWAT 2000. Well bore skin as reported by Fox (2006) and Barrash et al. (2006) for both the pumping and injection wells (B3 and B6) were defined in the simulation using the Horizontal Flow Barrier package of SEAWAT 2000. This simulation has vertical hydraulic conductivity anisotropy raised from 1 to 4. The vertical hydraulic conductivity anisotropy is input through the Hydrogeologic Unit Flow package.

DP

The DP simulation has five layers defined within it where each layer corresponds to one of the hydrostratigraphic units identified by Barrash and Clemo (2002). A cross section of this model is seen in Figure 43. The hydrogeologic properties of this model are listed in Table 9. The effective porosities of this simulation are distributed within each hydrostratigraphic unit using the geostatistics listed in Table 9 and then each unit is spliced together. This simulation used the complex boundaries framework. Flow was implemented through the Layer Property Flow package of SEAWAT 2000. Pumping and injection were defined in the pumping zone of well B6, injection zone of well A1, and in all of the sampling zones of well A1 and in the B wells through the Well package of SEAWAT 2000. Well bores were defined in all of the screened sections of wells B3, A1,

and B6. Packers were also define in the injection zone of well B3 and in the pumping zone of well B6.

DK

The DK simulation has five layers defined within it where each layer corresponds to one of the hydrostratigraphic units identified by Barrash and Clemo (2002). A cross section of this model is seen in Figure 43. The hydrogeologic properties of this model are listed in Table 8. The horizontal hydraulic conductivities of this simulation are distributed within each hydrostratigraphic unit using the geostatistics listed in Table 9 and then each unit is spliced together. This simulation used the complex boundaries framework. Flow was implemented through the Layer Property Flow package of SEAWAT 2000. Pumping and injection were defined in the pumping zone of well B6, injection zone of well A1, and in all of the sampling zones of well A1 and in the B wells through the Well package of SEAWAT 2000. Well bores were defined in all of the screened sections of wells B3, A1, and B6. Packers were also define in the injection zone of well B3 and in the pumping zone of well B6.

DKP

The DKP simulation has five layers defined within it where each layer corresponds to one of the hydrostratigraphic units identified by Barrash and Clemo (2002). A cross section of this model is seen in Figure 43. The hydrogeologic properties of this model are listed in Table 8. The horizontal hydraulic conductivities and the

effective porosities of this simulation are distributed within each hydrostratigraphic unit using the geostatistics listed in Table 9 and then each unit is spliced together. This simulation used the complex boundaries framework. Flow was implemented through the Layer Property Flow package of SEAWAT 2000. Pumping and injection were defined in the pumping zone of well B6, injection zone of well A1, and in all of the sampling zones of well A1 and in the B wells through the Well package of SEAWAT 2000. Well bores were defined in all of the screened sections of wells B3, A1, and B6. Packers were also define in the injection zone of well B3 and in the pumping zone of well B6.